UNIVERSITY OF THESSALY
POLYTECHNIC SCHOOL
DEPATRMENT OF MECHANICAL ENGINEERING

Diploma Thesis

Experimental Determination of the Adhesion of Hard CAPVD Coatings

By

Konstantinos Fountas

Supervisor

Anna Zervaki

Submitted for the Partial Fulfillment
of the requirements for the degree of
Diploma in Mechanical Engineering

2016

The approval of the Diploma Thesis by the Department of Mechanical Engineering of the University of Thessaly does not imply acceptance of the author's opinions. (Law 5343/32, article 202, paragraph 2).

Certified by the members of the Thesis Committee:

First Examiner (Supervisor)	Dr. Anna Zervaki Lab Teaching Staff, Department of Mechanical Engineering, University of Thessaly
Second Examiner	Dr. Gregory Haidemenopoulos Professor, Department of Mechanical Engineering, University of Thessaly
Third Examiner	Dr. Alexios Kermanidis Assistant Professor, Department of Mechanical Engineering, University of Thessaly

Acknowledgments

This project is accomplished in the scope of partial fulfilment of the requirement for the degree of Diploma in Mechanical Engineering at University of Thessaly.

For the completion of this Thesis, I would like to thank my thesis supervisor, Dr. Anna Zervaki whose expertise, valuable suggestions, comments, guidance and patience added considerably to my knowledge and for the tremendous support over this semester.

Furthermore, very special thanks go to Professor Gregory Haidemenopoulos and Assistant Professor Alexios Kermanidis for accepting to be the referees of this work.

I would also like to thank the PhD student Gülşah Aktaş as well as the Professors Şeyda Polat and Hakan Atapek from Kocaeli University, for giving me the idea of the current Thesis and preparing the specimens in order to conduct the experiments.

I would also like to express my very great appreciation to EBETAM S.A., specially to Mr. Stamou and Mrs. Papadimitriou for providing us the Scratch Tester Unit.

Thanks also extended to the Instructor Dr. Eleni Kamoutsi for her crucial contribution in the conduction of SEM as well as AFM analysis.

I wish to acknowledge the help provided by Associate Professor Eleni Pavlidou from Aristotle University of Thessaloniki for the conduction of the EDX analyses.

I would also like to extend my thanks to Mr. Anastasios Dafereras for his help in setting up the Scratch Tester Unit.

Last but not least, special recognition goes to my family for their continuous support and encouragement during this study.

Konstantinos Fountas

Abstract

Hard coatings are extensively used in various applications, such as machining tools, die components, turbine blades etc. Along with other improvements, these coatings provide significant enhancement in the mechanical reliability of the components as well as in their wear resistance. A vital role to the substrate/coating system performance plays the adhesion of the coating which characterizes its capability to remain intact over all the substrate surface when the substrate/coatimg system is subjected to tensile or shear stresses during service.

The current thesis focuses on the characterization of the adhesion of specific hard coatings on the surface of a hot work tool steel used typically as a die in metal extrusion process. The technique selected to evaluate the adhesion to the substrate of the thin hard coatings, was the "scratch test" which-according to the literature-is the the only one that has led consistently to meaningful results and which is applicable also to quality control in the production of large numbers of parts.

To that purpose, various combinations of single or double layer coatings (i.e. CrN, AlTiN, CrN/AlTiN) were deposited on the surface of a hot work tool steel, either directly or after surface nitriding, by CAPVD process (this part of the work was performed by Kocaeli University in Turkey). The experimental work carried out at the University of Thessaly, included the scratch tests as well as the characterization of the failure modes of the coatings evolved during the tests. Stereo-Optical microscopy, SEM/EDX as well as AFM were employed in the evaluation process.

The critical load where the coating failure occurred was determined for each sample allowing a ranking of the samples based on the coating adhesion measurements. The double layer coating (Nitriding+AlTiN+CrN) exhibited the better adhesion values, over all the tested samples. Both adhesive as well as cohesive failure modes were found, while the coating failure pattern evolved during the scratch tests was also determined for each case providing useful conclusions on the coating's behavior under specific loading conditions.

The results are in good agreement with the reported values found in the open literature.

Περίληψη

Οι σκληρές επικαλύψεις χρησιμοποιούνται ευρέως σε διάφορες εφαρμογές, όπως σε εργαλεία κατεργασίας μετάλλων, σε μήτρες εξώθησης σε κατεργασίες διαμορφώσεων, σε πτερύγια τουρμπινών κ.α. Πέρα από τη συνεισφορά τους στην αύξηση του χρόνου ζωής, οι σκληρές επικαλύψεις προσφέρουν αυξημένη αξιοπιστία αλλά και αντίσταση σε φθορά στα μηχανολιγικά στοιχεία που εφαρμόζονται. Σημαντικό ρόλο στις επιδόσεις του συστήματος υποστρώματος-επικάλυψης παίζει η πρόσφυση της επικάλυψης, μια έννοια η οποία χαρακτηρίζει την ικανότητα της επίστρωσης να παραμένει άθικτη στην επιφάνεια του υποστρώματος, όταν αυτό υπόκειται σε εφελκυστικές αλλά και διατμητικές τάσεις κατά τη λειτουργία του.

Η παρούσα διπλωματική επικεντρώνεται στον χαρακτηρισμό της πρόσφυσης συγκεκριμένων επιστρώσεων στην επιφάνεια εργαλειοχάλυβα, ο οποίος χρησιμοποιείται στην κατασκευή μητρών εξώθησης σε κατεργασίες διέλασης κραμάτων αλουμινίου. Η μέθοδος που χρησιμοποιήθηκε με σκοπό να μετρηθεί η πρόσφυση των σκληρών επικαλύψεων στο υπόστρωμα του χάλυβα ονομάζεται ‘’scratch test’’, το οποίο σύμφωνα με τη βιβλιογραφία είναι το μόνο που παρέχει αξιόπιστα αποτελέσματα, ενώ χρησιμοποιείται και κατά τον έλεγχο ποιότητας στην παραγωγή μεγάλου αριθμού αντικειμένων.

Γι’ αυτό το σκοπό, ποικίλοι συνδυασμοί από απλές και σύνθετες επιστρώσεις, όπως οι CrN, AlTiN, CrN/AlTiN εναποτέθηκαν στην επιφάνεια του εργαλειοχάλυβα, είτε απευθείας είτε μετά από την εναζώτωσή του, μέσω της μεθόδου CAPVD (η εργασία αυτή εκπονήθηκε από το πανεπιστήμιο Kocaeli στην Τουρκία). Η πειραματική διαδικασία έλαβε χώρα στο Πανεπιστήμιο Θεσσαλίας, και συμπεριελάμβανε τα scratch tests καθώς και την αξιολόγηση των τρόπων αστοχίας των επικαλύψεων κατά τη διάρκεια των μετρήσεων. Ο χαρακτηρισμός πραγματοποιήθηκε μέσω της παρατήρησης των δοκιμίων σε στερεοσκόπιο, ηλεκτρονικό μικροσκόπιο σάρωσης (SEM) καθώς και μικροσκόπιο ατομικής δύναμης (AFM).

Το κρίσιμο φορτίο κατά το οποίο εμφανίστηκε η πρώτη αστοχία της επίστρωσης προσδιορίστηκε για κάθε ένα από τα δοκίμια, γεγονός που οδήγησε στην κατάταξη των παραπάνω δοκιμίων σύμφωνα με τις μετρήσεις πρόσφυσης της επικάλυψης. Το διπλής επίστρωσης (CrN/AlTiN) και εναζωτωμένο δοκίμιο παρουσίασε την καλύτερη πρόσφυση συγκριτικά με όλα τα υπόλοιπα δοκίμια. Κατά τη διάρκεια του ελέγχου των χαραγών, παρατηρήθηκαν τόσο αστοχίες πρόσφυσης (adhesive failure) όσο και συνοχής (cohesive failure) της επικάλυψης, ενώ καταγράφηκε η σειρά με την οποία αυτές εμφανίστηκαν. Το παραπάνω έχει ως αποτέλεσμα να αντληθούν χρήσιμα συμπεράσματα για τη συμπεριφορά των επιστρώσεων υπό την επιβολή φορτίων.

Τα αποτελέσματα των δοκιμών πρόσφυσης καθώς και οι τρόποι αστοχίας που προτείνονται, συμφωνούν με αντίστοιχα αποτελέσματα που αναφέρονται στη βιβλιογραφία.

Table of Contents

Experimental Determination of the Adhesion of Hard CAPVD Coatings i
Acknowledgments iv
Abstract v
Περίληψη vi
List of Figures ix
List of Tables xii
Chapter 1: Introduction 1
1.1 Aim and Structure of the Diploma Thesis 1
1.2 Definition of Tribology 2
1.3 Die Wear in Metal Extrusion Method 3
1.4 High Temperature Wear of Extrusion Dies 5
Chapter 2: Literature Review 6
2.1 Adhesion of Hard Coatings 6
2.2 Scratch Test: A Review on the Method 7
2.2 Failure modes in hard coatings 8
2.2.1 Adhesion failure analysis 9
2.3 Properties of hard coatings 11
2.3.1 CrN 11
2.3.2 AlTiN 11
2.3.3 CrN/AlTiN 11
Chapter 3: Experimental Procedure 12
3.1: Preparation of Specimens 12
3.2 Scratch Tests 15
3.3 Stereoscopy 16
3.4 SEM Analysis 16
3.5 EDX Analysis 16
3.6 AFM Analysis 16
Chapter 4: Experimental Results 18
4.1 Scratch Tests 18
4.1.1 Sample 9101 (AlTiN) 18
4.1.2 Sample 9102 (CrN) 19
4.1.3 Sample 9103 (AlTiN+CrN) 20

4.1.4 Sample 9151 (Nitrided+AlTiN) 21
4.1.5 Sample 9152 (Nitrided+CrN) 22
4.1.6 Sample 9153 (Nitrided+AlTiN+CrN) 23
4.2 SEM Analysis 24
4.2.1 Sample 9101 (AlTiN) 24
4.2.2 Sample 9102 (CrN) 27
4.2.3 Sample 9103 (AlTiN+CrN) 29
4.2.4 Sample 9151(Nitrided+AlTiN) 32
4.2.5 Sample 9152 (Nitrided+CrN) 34
4.2.6 Sample 9153 (Nitrided+AlTiN+CrN) 36
4.3 EDX Analysis 37
4.3.1 Sample 9101 (AlTiN coated) 37
4.3.2 Sample 9102 (CrN) 39
4.3.3 Sample 9103 (AlTiN+CrN) 42
4.3.4 Sample 9151 (Nitrided+AlTiN) 45
4.3.5 Sample 9152 (Nitrided+CrN) 47
4.3.6 Sample 9153 (Nitrided+AlTiN+CrN) 49
4.4 AFM Analysis 51
Chapter 5: Conclusions & Discussion 58
5.1 Coating Failure Analysis 58
5.2 The influence of Gas Nitriding 58
5.3 Future Work Recommendations 60
References 61
Appendix: Acoustic Emission to Load Charts 63
A: Sample 9101 63
B: Sample 9102 64
C: Sample 9103 64
D: Sample 9151 65
E: Sample 9152 65
F: Sample 9153 66

List of Figures

Fig. 1: Definition of tribology [2] 2
Fig. 2: Economic savings through tribology on the U.K (1966, £millions) [3] 3
Fig. 3: Metal extrusion process and die wear defects [4] 3
Fig. 4: A series of processes needed to improve an extrusion die's performance [4] 4
Fig. 5: Tribologically important properties in different zones of the coated surface [1] 7
Fig. 6: Equipment layout of a scratch tester [1] 8
Fig. 7: The surface cracks generated in a scratch test track can be classified as: (a) angular cracks, (b) parallel cracks, (c) transverse semicircular cracks, (d) coating chipping, (e) coating spalling and (f) coating breakthrough [13] 9
Fig. 8: Coating failure modes [1] 10
Fig. 9: Main scratch test failure modes in terms of substrate and coating hardness [14] 10
Fig. 10: CSM Revetest Scratch Test Connected with CSM Scratch Test Control Unit equipped with an ABB SE-790 XY plotter 15
Fig. 11: Specimen #9101. The scratches can be seen macroscopically on the surface 18
Fig. 12: Acoustic emission vs. load diagram for sample 9101 18
Fig. 13: Acoustic emission vs. load diagram for sample 9102 19
Fig. 14: Acoustic emission vs. load diagram for sample 9103 20
Fig. 15: Acoustic emission vs. load diagram for sample 9151 21
Fig. 16: Acoustic emission vs. load diagram for sample 9152 22
Fig. 17: Acoustic emission vs. load diagram for sample 9153 23
Fig. 18: The initial stage of the crack 25
Fig. 19: The area where the first acoustic emission peak was recorded 25
Fig. 20: Microcracks appearance 26
Fig. 21: End of the scratch path 26
Fig. 22: Formation of the scratch path 27
Fig. 23: Appearance of angular cracks 27
Fig. 24: Appearance of semicircular cracks 28
Fig. 25: Coating buckling 28
Fig. 26: Coating chipping associated with microcracks 29
Fig. 27: Formation of angular microcracks 29
Fig. 28: Coating buckling and chipping 30
Fig. 29: Recovery spallation of the coating 30
Fig. 30: Coating adhesion failure by recovery spallation 31

Fig. 31: The endpoint of the scratch 31
Fig. 32: The initial stage of the scratch track 32
Fig. 33: Formation of angular microcracks 32
Fig. 34: Formation of semicircular microcracks 33
Fig. 35: The endpoint of the scratch 33
Fig. 36: Formation of angular microckracks during the initial stages of the scratch 34
Fig. 37: Formation of semicircular microcracks 34
Fig. 38: The endpoint of the scratch 35
Fig. 39: Growth of semicircular microcracks 35
Fig. 40: The initial phase of the scratch path 36
Fig. 41: Formation of semicircular microcracks 36
Fig. 42: Coating buckling and chipping at the end of the scratch track 37
Fig. 43: Line scan transverse to the scratch track 38
Fig. 44: Line scan parallel to the scratch track 38
Fig. 45: Spot chemical analysis at the end of the scratch track 39
Fig. 46: Line scan transverse to the scratch track 40
Fig. 47: Line scan on microcracks 40
Fig. 48: Line scan on porous surface 41
Fig. 49: Spot chemical analysis at the end of the scratch track 42
Fig. 50: Spot chemical analysis in the area of first coating failure 42
Fig. 51: Line scan parallel to the scratch track 43
Fig. 52: Line scan transverse to the scratch track 43
Fig. 53: Line scan at the end of the scratch track 44
Fig. 54: Spot chemical analysis at the end of the scratch 45
Fig. 55: Line scan transverse to the scratch track 45
Fig. 56: Line scan parallel to the scratch track 46
Fig. 57: Line scan at the end of the scratch track 46
Fig. 58: Line scan transverse to the scratch track 47
Fig. 59: Line scan on porous surface 47
Fig. 60: Line scan on microcrack 48
Fig. 61: Line scan at the end of the scratch track 48
Fig. 62: Line scan transverse to the scratch track 49
Fig. 63: Line scan parallel to the scratch track 49
Fig. 64: Spot analysis at the end of the scratch track 50

Fig. 65: Line scan at the end of the scratch track 51
Fig. 66: The area before the point where the first coating failure occurred 51
Fig. 67: Line scan measurements before the first coating failure occurred 52
Fig. 68: The area where the first coating failure occurred 52
Fig. 69: Line scan measurements in the area where the first coating failure occurred 53
Fig. 70: The area after the appearance of the first coating failure 53
Fig. 71: Line scan measurements in the area after the appearance of the first coating failure 54
Fig. 72: The area before the point where the first coating failure occurred 54
Fig. 73: Line scan measurements before the first coating failure occurred 55
Fig. 74: The area where the first coating failure occurred 55
Fig. 75: Line scan measurements in the area where the first coating failure occurred 56
Fig. 76: The area after the appearance of the first coating failure 56
Fig. 77: Line scan measurements in the area after the appearance of the first coating failure 57
Fig. 78: Critical loads of AlTiN coated specimens 59
Fig. 79: Critical loads of CrN coated specimens 59
Fig. 80: Critical loads of the AlTiN+CrN coated specimens 60
Fig. 81: Acoustic emission to load charts for tests no. 1-5 63
Fig. 82: Acoustic emission to load chart for test no. 6 63
Fig. 83: Acoustic emission to load charts for tests no. 1-5 64
Fig. 84: Acoustic emission to load charts for tests no. 1-5 64
Fig. 85: Acoustic emission to load charts for tests no. 1-3 65
Fig. 86: Acoustic emission to load charts for tests no. 1-4 65
Fig. 87: Acoustic emission to load chart for test no. 1 66
Fig. 88: Acoustic emission to load charts for tests no. 2,3 66
Fig. 89: Acoustic emission to load chart for test no. 4 67
Fig. 90: Acoustic emission to load chart for test no. 5 67
Fig. 91: Acoustic emission to load chart for test no. 6 68

List of Tables

Table 1: The standard chemical composition of DIN 1.2999 hot work tool steel (wt. %) [17] 12
Table 2: The heat treatment conditions applied on experimental steels before surface treatment [4] 12
Table 3: The gas nitriding conditions applied on experimental steels [4] 12
Table 4: The parameters used for coatings in CAPVD process [4] 12
Table 5: The list of specimens [4] 13
Table 6: Surface hardness values of experimental steels [4] 13
Table 7: SEM micrographs and EDX analysis of coated steels [4] 14
Table 8: Sample 9101: Experimental results per scratch 19
Table 9: Sample 9102: Experimental results per scratch 19
Table 10: Sample 9103: Experimental results per scratch 20
Table 11: Sample 9151: Experimental results per scratch 21
Table 12: Sample 9152: Experimental results per scratch 22
Table 13: Sample 9153: Experimental results per scratch 23
Table 14: Mean and standard deviation Lc values of coated samples 24
Table 15: Evolution of the coatings' failure pattern of each specimen 58

Chapter 1: Introduction

1.1 Aim and Structure of the Diploma Thesis

The aim of this work is to measure the adhesion of six selected coated specimens by conducting scratch tests, as well as the analysis of the failure modes occurred during the tests, that allow the classification of the coatings according to their performance.

The thesis is divided in five chapters, which are briefly presented hereinafter.

In *Chapter One*, general aspects of tribology are reviewed while the motivation of the current work is discussed.

In *Chapter Two*, the literature review is presented. The review presents the different materials that were used in the present thesis combined with their properties. In addition, the failure modes that may occur during the conduction of a scratch test are analyzed.

In *Chapter Three*, the experimental procedure is provided.

In *Chapter Four*, the results including scratch tests, optical and stereo microscopy results, SEM/EDX studies as well as selected AFM tests are presented in detail for each one of the specimens examined.

In *Chapter Five*, a discussion about the above results and the failure modes of the specimens is provided alongside with future work recommendations.

1.2 Definition of Tribology

It is well known that when two different surfaces contact each other, friction force is produced. In most cases, friction is an undesirable phenomenon which causes the deterioration of contacting surfaces, a situation also called wear. Tribology is the field of engineering that deals with the above situation and in recent years is becoming a more complex discipline, including a great number of sciences such as chemistry, physics, metallurgy and engineering (Fig. 1).

Tribology plays a significant role in the technological evolution of industrialized societies since it contributes to the reduction of the friction forces. Advanced Tribology could offer numerous benefits, such as reduced costs for maintenance of the machinery (in-service failure, maintenance downtime), energy saving and the amelioration of working conditions by improving safety. As a result, scientists nowadays focus their research on the surface properties that need to be improved (hardness, fracture toughness, adhesion). The research on this field has led to the development of numerous coatings which offer a wide range of properties and enhance the performance of mechanical components. In parallel, coating deposition techniques were developed allowing the deposition of thin solid with superior tribological properties [1].

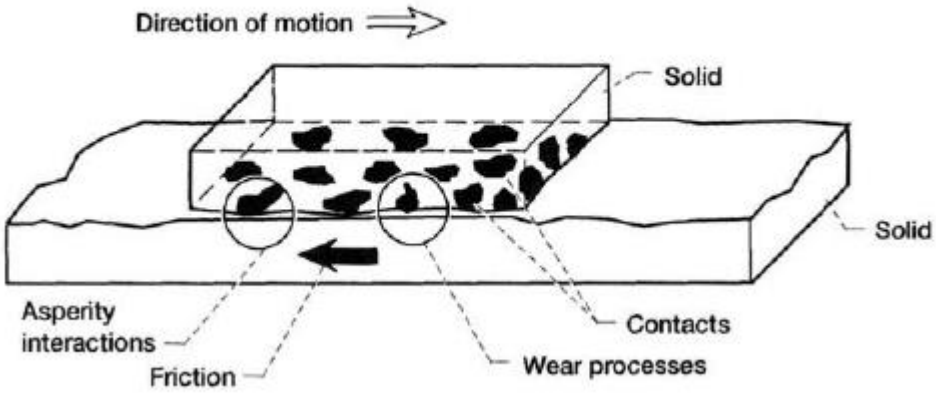

Fig. 1: Definition of tribology [2]

It is obvious that tribology has a significant social and, thus, economic impact. In particular, large amounts of money have been lost per year due to friction and wear problems. In the United States of America, material losses due to tribology are estimated at about $100 billion per year, fact that highlights the importance of improving the tribological properties of moving components [2]. As it concerns the United Kingdom [3], £515 million could be saved annually by ameliorating tribology conditions, as it is demonstrated in Fig. 2.

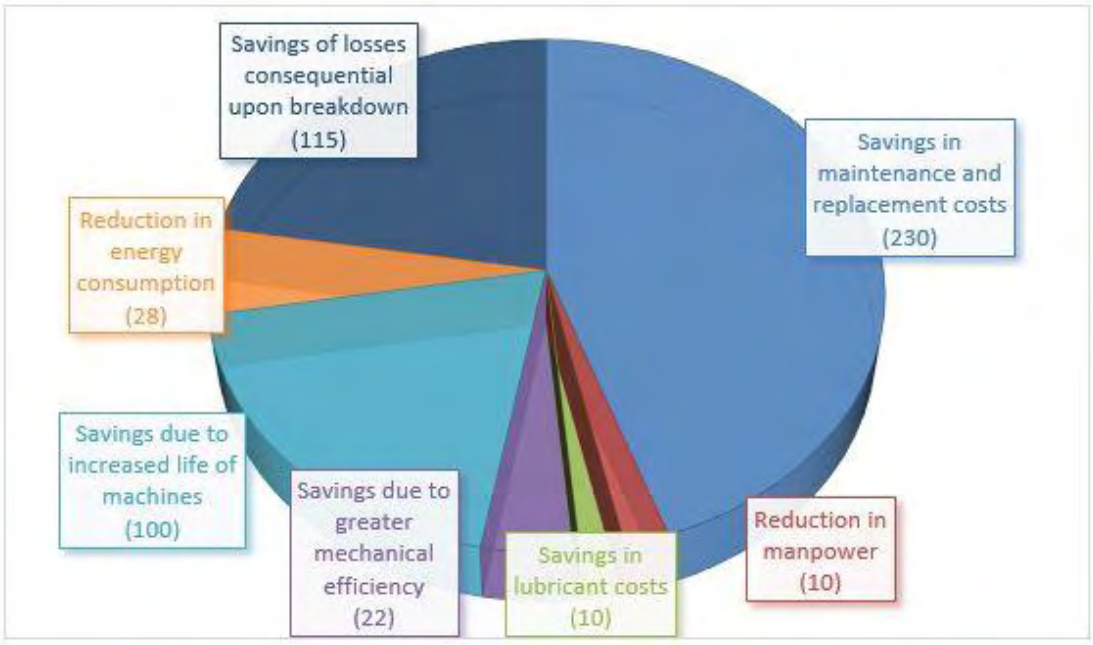

Fig. 2: Economic savings through tribology on the U.K (1966, £millions) [3]

1.3 Die Wear in Metal Extrusion Method

The current thesis focuses on the characterization of the adhesion of hard coatings on the surface of a specific tool steel used typically as a die in metal extrusion process. The tool suffers from high temperature wear and thus research is conducting in developing hard coating to minimize the problem. In metal extrusion processes, a cross section of material is reduced by passing it through a die opening, which has a desired shape, by means of a compressive force, as it is schematically demonstrated in Fig. 3.

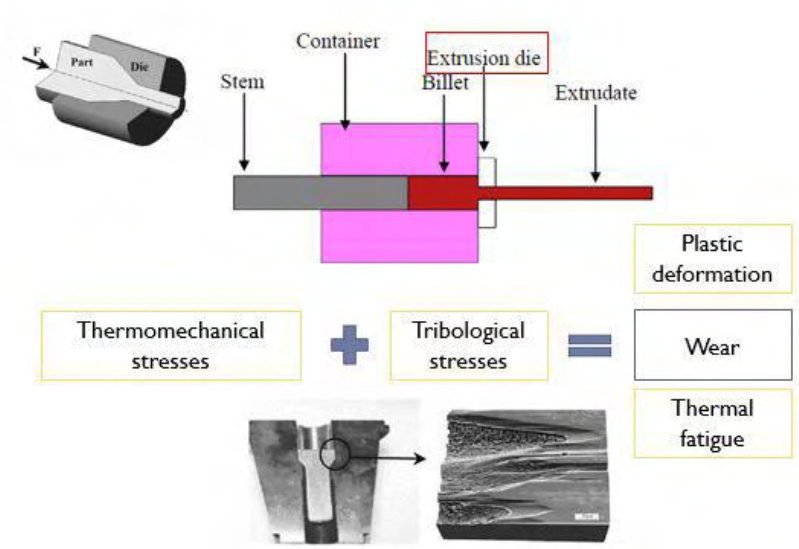

Fig. 3: Metal extrusion process and die wear defects [4]

In order to have improved performance, extrusion dies need to possess a number of fundamental properties, such as high hardness, sufficient toughness, resistance to deformation, resistance to shock and resistance to high temperature wear (Fig. 4). This may be achieved via the following steps:

1. *Alloy design:* Improved performance of extrusion dies is achieved by controlling the alloying elements that impart the ideal properties to the metal.
2. *Heat treatments:* In most cases, the metal needs to undergo a number of heat treatments (i.e. austenization, tempering, gas nitriding etc.) so that it will not fail during die process.
3. *Surface treatments*: A crucial factor for an extrusion die is to have improved properties on the surface, as it suffers from high temperature and stress loads. For this reason, a great number of surface treatment techniques have been developed and surface coating is one of them.

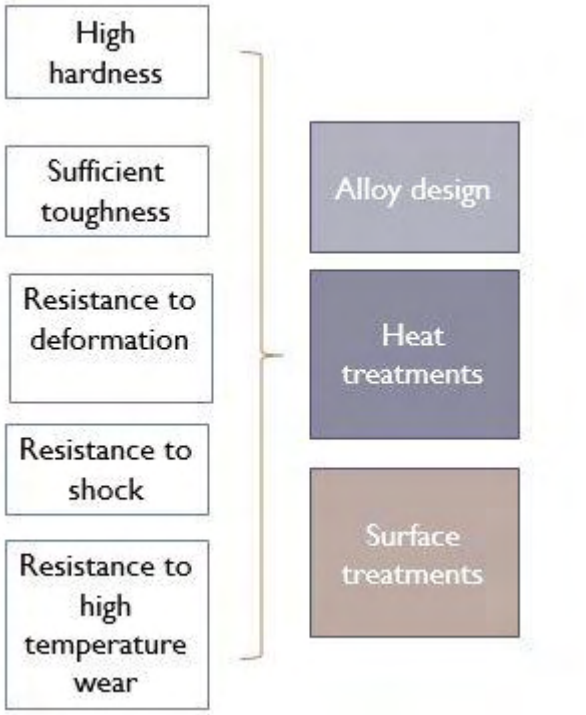

Fig. 4: A series of processes needed to improve an extrusion die's performance [4]

The die of extrusion processes is exposed to strong tribological loads by high contact normal pressure and sliding friction.

The cost of forming tools usually covers a significant amount of the total manufacturing cost. Additionally, unexpected tool changes due to excessive wear are causing down times of the manufacturing process. In extrusion, high temperature wear is the main failure mechanism. High temperature wear occurs when metallic components slide against each other under high pressure and temperature. The heat generated due to friction causes micro welds to form between the sliding surfaces. Methodologies currently used are based mainly on designer intuition and experience, which are not the most adequate when considering the complexity of the problem. Quantitative approach to tool wear analysis would improve service life, leading to an important reduction of manufacturing costs [5].

The importance of specific surface treatments on a hot work tool steel will be examined in the current work.

More specifically, various combinations of single or multilayer CAPVD coatings in combination to the traditional gas nitriding technique will be evaluated in relation to their adhesion in order to rank their performance.

1.4 High Temperature Wear of Extrusion Dies

In extrusion process, dies are considered the most critical component of tooling due to their complex design, high tolerance requirements, critical processing conditions and complex state of stress that acts on them during extrusion [6]. Previous investigations on aluminum extrusion dies showed that the three most common failure mechanisms are wear, fracture and plastic deformation [7]. More specifically, the wear of extrusion dies is much accelerated, while adhesive wear occurs. Since aluminum has a strong tendency to adhere on the steel surface, there will be development of the adhesive layer on the die bearing. The development of an adhesive layer on the die bearing surface is dependent on many factors:

- Temperature developed in the die bearing,
- Speed of extrusion,
- Shape and geometry of the die,
- Die bearing length,
- Surface roughness parameters of the die bearing,
- Hardness of the bearing surface.

Among the above factors, the most important are temperature and speed of the process. Extrusion speed and temperature rise on the die bearing are directly related to each other. For the same billet temperature, temperature rise on the die bearing is greater at higher speeds due to increase in strain rate and increase in shear deformation (sticking friction) on the die bearing. When the temperature on the die bearing increases, the tendency for the development of an adhesive layer increases. Due to the increase of temperature, the adhesive layer begins to develop, and with the increase of press cycles, the adhesive layer slowly may cover the complete bearing area and become a thicker layer. The repetitive adhesive layers' buildup, and detachment leads to die wear and contaminates in the extrusion [8]. Coatings with adequate adhesion may withstand to these phenomena extending the life time of the die.

Chapter 2: Literature Review

2.1 Adhesion of Hard Coatings

Adhesion means the property and capability of a coating to remain intact over all the substrate surface when the composite is subjected to tensile or shear stresses. The adhesion therefore characterizes the rupture strength of the interface or of the transition zone between the coating and the substrate. Among the various techniques proposed for testing the adhesion to the substrate of thin hard films, the only one which has led consistently to meaningful results and which is applicable also to quality control in the production of large numbers of parts is the so-called “scratch test”, first proposed by Heavens [9] and introduced by Benjamin and Weaver [10]. As it concerns the coating deposition, it can be divided into four generic groups: gaseous, solution, molten and solid, depending on the state of the depositing phase [11]. More specifically, the coatings that we shall consider will be those deposited by plasma – assisted techniques, such as the CAPVD method, since those can provide excellent adhesion to the substrate and dense coating structural morphology, properties needed for tribological applications. To meet the desired wear and friction requirements, the coated surface must possess a suitable combination of properties. As shown in Fig. 5, we can distinguish between four different areas, each with different properties which must be taken under consideration. The properties required by the substrate and by the coating involve material strength and thermal attributes determined by their composition and microstructure as well as the porosity and homogeneity of the material. At the interface between them, the adhesion and shear strength of the junction is important. At the surface of the coating the chemical reactivity and the roughness must be considered in addition to the shear strength. A primary problem in surface design is that many desired properties, such as good adhesion at the coating/substrate interface and no surface interactions with the counterface, or high hardness and high toughness of the coating, cannot easily be obtained simultaneously. Increased hardness and strength is often concomitant with decreasing toughness and adherence. For this reason, the final coating design is always a compromise between many different technical requirements on the properties of the coating system and the economical requirements on the deposition of the coating on to products.

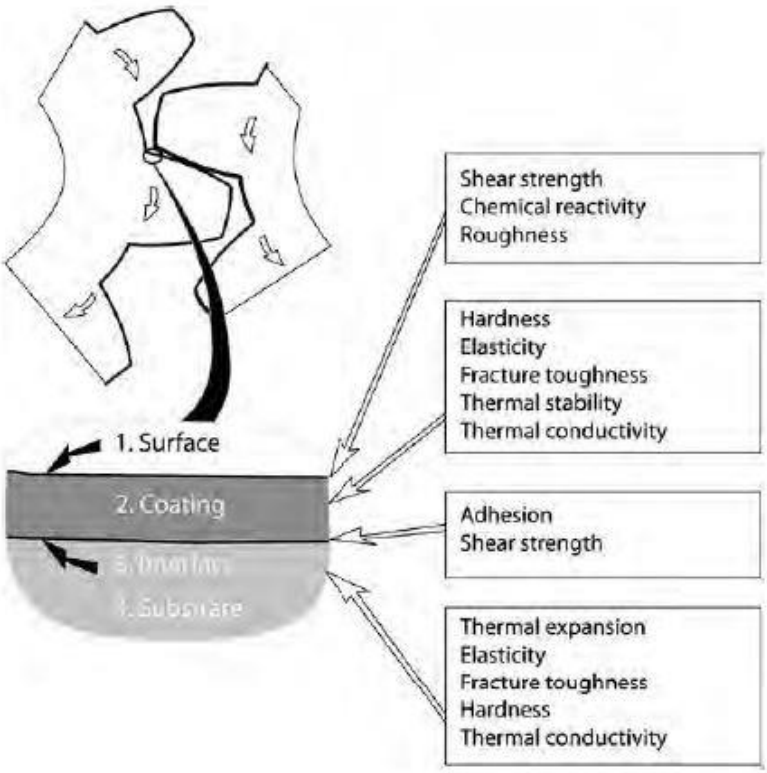

Fig. 5: Tribologically important properties in different zones of the coated surface [1]

This work focuses on the determination of values which correspond to the interfacial bond between the coating and the substrate. The interfacial bond strength or adhesion of the coating to the substrate is a very important property of thin, hard coatings. Poor adhesion leads to "flaking" (adhesive failure), whereas poor cohesion causes chipping (cohesive failure). Adhesion can be evaluated by various techniques some of which, however, have serious limitations. Among them, the "scratch test" is applicable as a quality control tool in the production of large numbers of coated parts.

2.2 Scratch Test: A Review on the Method

The term *Scratch Test* refers to a widespread accepted scientific and industrial technique which aim to measure the coating's adhesion. The technique involves a controlled scratch on a selected area. The tip material (normally diamond) is drawn across the coated surface under constant, incremental or progressive load. At a certain critical load, the coating will start to fail. The critical load data is used to quantify the adhesive properties of different film - substrate combinations. A typical scratch tester is equipped with an acoustic emission detector and image capture & measurement system.

In scratch testing, stresses are introduced at the coating/substrate interface by deforming the surface with a moving diamond tip (r = 200 µm, angle 120^0). The applied load is increased stepwise or continuously until the deformation causes stresses which result in flaking or

chipping of the coating. The smallest load at which the coating cracks (cohesive failure) or is detached (adhesive failure) is called the critical load and is determined by optical or electron microscopy, as well as by acoustic emission (AE). Usually, the onset of AE signal and the microscopical observation of the first damage occurring in the coating correlate quite well. With the CSM Revetest, the scratches are made at constant speed and either constant or linearly increasing load with automatic recording of an AE-normal loading graph. The load corresponding to failure provides information about the adhesion strength and is referred to as the critical load (L_c) [1]. The most widely used version involves a diamond stylus with a 200μm radius spherical tip (Fig. 6). The type of coating failure exhibits microcracks ahead or behind the tip, coating spalling and chipping or production of a scratch in which the whole coating is pulled off. The factors that affect the type of coating failure are presented below:

- The ductility of the film,
- The coating/substrate hardness ratio. Generally, a low ratio leads to superior adhesive strength while on the other hand high coating to substrate hardness ratio values mean failure at lower loads, [12]
- The thickness, geometry and surface condition of the coating,
- The indenter material.

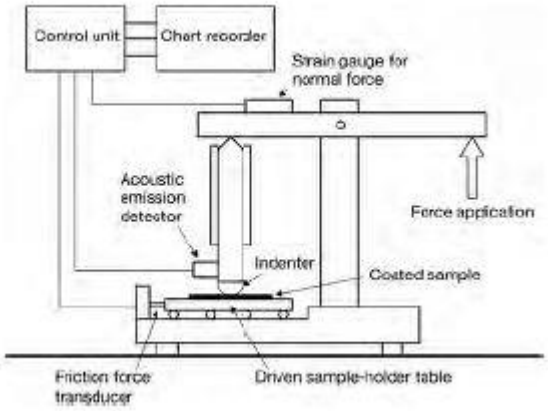

Fig. 6: Equipment layout of a scratch tester [1]

2.2 Failure modes in hard coatings

The load where failure occurs alongside with the type of failure during the scratch test are the main criteria in order to evaluate the adhesion.

The continuous, progressive loading of a hard coated surface leads to the appearance of microcracks, which then multiply and merge. The appearance and growth of the cracks during the scratch test follows a basic pattern: Initially, angular cracks are formed at the edges of the scratch at the same time that parallel to the scratch cracks appear. Then, the pre-existing cracks are growing and merging to semicircular transverse cracks. As the load increases

progressively, some areas of the coating are spalled off, fact that finally leads to a complete coating removal from the surface of the base metal, as it is depicted on Fig. 7 [13].

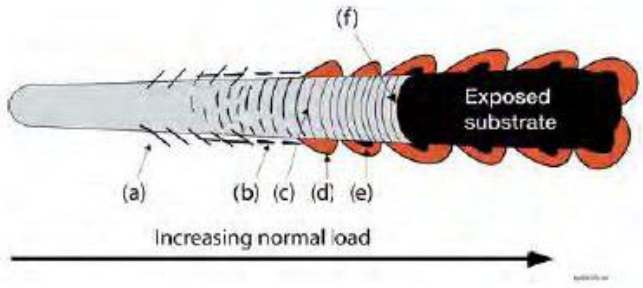

Fig. 7: The surface cracks generated in a scratch test track can be classified as: (a) angular cracks, (b) parallel cracks, (c) transverse semicircular cracks, (d) coating chipping, (e) coating spalling and (f) coating breakthrough [13]

2.2.1 Adhesion failure analysis

The adhesion failure modes are classified into three main categories:

1. Buckling and spallation:

    - *Buckling:* This is the most common failure mode in thin coatings. Buckling occurs as a result of compressive stresses generated in front of the diamond tip. Regions with interfacial cracks lead to buckling while the tip produces stresses to the coated surface.
    - *Wedge Spallation:* When the critical thickness is exceeded, through-thickness angular cracks are formed instead of buckling, which leads to adhesion failure between the coating and the metal. Rarely, regional coating spallation as well as dramatic increase of scratch width and depth are observed.
    - *Recovery Spallation:* This type of adhesion failure is the result of the elastic recovery during the conduction of a scratch test and depends on the properties of the base metal and the through thickness cracks that may pre-exist. The residual stresses combined with through thickness cracks lead to the spallation of the coating on both sides of the scratch. Recovery spallation is observed for hard coatings combined with hard substrates.
2. Chipping: As the diamond tip moves forward and previous buckling or spallation failures have already appeared, chipping of the coating is observed. As a result, the coating is deposited laterally to the crack.
3. Conformal and tensile cracking: This type of failure takes place in case that the coating remains attached to the substrate, despite the increasing load. Conformal cracking appears in front of the diamond tip while the tensile cracking behind it. It should also be highlighted that the cracks in front of the tip may change their shape during the conduction of the scratch test [14] (Fig. 8).

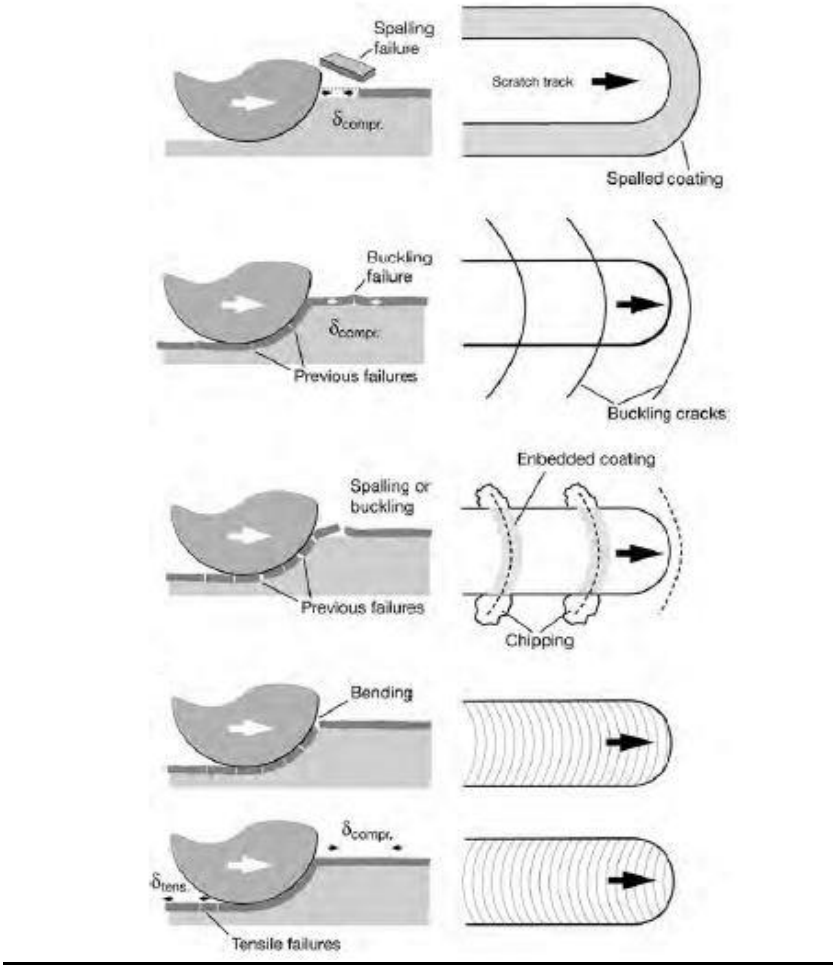

Fig. 8: Coating failure modes [1]

S.J. Bull [14] created a general map in which the above coating failure modes are gathered and compared to the coating and substrate hardness (Fig. 9).

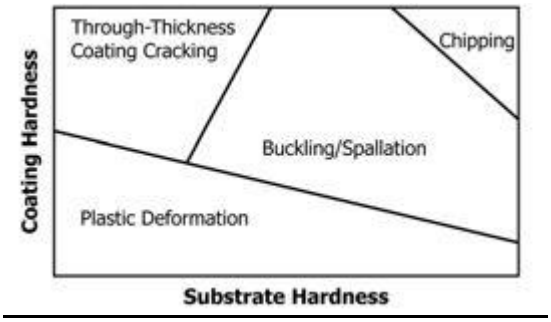

Fig. 9: Main scratch test failure modes in terms of substrate and coating hardness [14]

According to this map, higher hardness values of both the substrate and the coating lead to chipping, while for lower substrate hardness values in combination to high coating hardness lead to through thickness coating cracking.

2.3 Properties of hard coatings

The advantages of the application of hard coatings are well known for forming and cutting tools where anti-wear properties are required in order to enhance the tool's life time. For this purpose, a wide range of coatings and methods of application to various substrates have been studied. The current thesis is focused on the study of CrN, AlTiN and CrN/AlTiN coatings, deposited by CAPVD (Cathodic Arc Physical Vapor Deposition) on a DIN 1.2999 tool steel. This method provides high levels of ionization, which leads to denser structure [13]. At the same time, CAPVD method offers the ability to create thin of the order of 1μm thick. A short overview of the properties is given hereinafter:

2.3.1 CrN

CrN coating is widely used in industrial applications, such as cutting applications, cold metal forming and protecting molds from corrosion and wear. This coating is usually combined with soft substrates (stainless steel, aluminum and copper alloys) that are not able to support, more brittle coatings. Generally, CrN coatings are characterized by a fine-grained microstructure and low residual stresses, which allows their implementation in large thicknesses (more than 10-25 μm). Furthermore, these coatings offer low friction coefficient, protection against oxidation at high temperatures but they do not reach high hardness values [15].

2.3.2 AlTiN

This is another widely used type of coating. AlTiN coating offers high resistance to high temperature oxidation, high resistance to stress conditions and slightly improved hardness values in comparison with CrN coating [16]. In combination with the above features, AlTiN coating is characterized by low friction coefficient as well as low thermal conductivity. The properties of the above coating resulted from a thin, protective Al_2O_3 layer that formed at the surface, preventing substrate oxidation and coating wear during high temperature treatment. In particular, is seems that the amount of Al also affects the hardness of the coating due to the generation of Al_2O_3 oxide. All the above properties make AlTiN coating ideal for applications such as drilling and milling [15].

2.3.3 CrN/AlTiN

This is a double layer coating, which actually combines the previous two coatings. Each one of the CrN and AlTiN coatings offer high performance as it concerns their resistance to oxidation but at the same time the elastic and plastic deformation that the substrate shows under stress conditions lead to the deterioration of its properties and finally leads to failure.

A proposed solution to this undesirable behavior, is the two-layer coatings, which combine the properties of each single coating, for improved performance [15]. Using the double layer coating in conjunction to the prior nitriding of the substrate, it is expected to create a new, reinforced AlTiN/CrN coating, which will offer increased adhesion to the substrate.

In this case, the CrN coating becomes the ''missing link'' between the substrate and the AlTiN coating [16].

Chapter 3: Experimental Procedure

3.1: Preparation of Specimens

The specimens' preparation was carried out by Kocaeli University [4]. The substrate, i.e. DIN 1.2999 hot work tool steel [17] was heat treated (Table 1) and three of the specimens were then coated by the CAPVD process (Tables 2,4). The experimental conditions of the heat treatment as well as the surface treatments are presented in Tables 2,3. Each coating had a 2μm thickness while the double layer coatings consisted of a 1+1 μm CrN + AlTiN.

Three specimens were subjected to nitriding (Table 3) and then they were coated under the same conditions to the above-non nitrided-specimens. Two specimens, the first consisted of the DIN 1.2999 tool steel without any treatment and the other consisted of the above steel including the gas nitriding process were provided as reference.

A material code was assigned to each specimen in order to be easily discriminated (Table 5).

Table 1: The standard chemical composition of DIN 1.2999 hot work tool steel (wt. %) [17]

C	Mn	Si	Cr	Mo	V	Fe
0.45	0.30	0.30	3.00	5.00	1.00	balance

Table 2: The heat treatment conditions applied on experimental steels before surface treatment [4]

Preheating 1	Preheating 2	Austenization	Tempering
600-650 °C, 60 min	800-850 °C, 60 min	1030 °C, 30 min	585°C, 120min 560°C, 120min 560°C, 120min

Table 3: The gas nitriding conditions applied on experimental steels [4]

Nitriding temperature	Nitriding time	Cooling
585 °C	6 h	1.1 bar air

Table 4: The parameters used for coatings in CAPVD process [4]

Coating type	Cathodic arc current (A)	Bias voltage (V)	Coating time (min)	Nitrogen partial pressure (mTorr)
CrN	60	110	70	6.5
AlTiN	50	200	30	8
CrN/AlTiN	80/60	120/100	60/60	6.5/7

Table 5: The list of specimens [4]

Material code	Treatments
9100	Heat treated
9101	Heat treated + AlTiN
9102	Heat treated + CrN
9103	Heat treated + CrN + AlTiN
9150	Heat treated + Nitrided
9151	Heat treated + Nitrided + AlTiN
9152	Heat treated + Nitrided + CrN
9153	Heat treated + Nitrided + CrN + AlTiN

Surface hardness measurements were conducted by Kocaeli University in order to provide sufficient information about the properties of each coating/substrate combination (Table 6).

Table 6: Surface hardness values of experimental steels [4]

Material code	Hardness ($HV_{0.01}$)
9100	504±2
9101	1782±4
9102	1739±2
9103	1940±3
9150	755±3
9151	2167±2
9152	2018±2
9153	2272±1

The coated specimens were studied at the SEM microscope in order to ensure that the coating procedure had led to the desired structure. At the same time, every sample was characterized by EDX analysis, a technique that provides useful information about the chemical composition for both the coatings and the substrate (Table 7).

Table 7: SEM micrographs and EDX analysis of coated steels [4]

<table>
<tr><th>Material code</th><th>SEM micrograph</th><th>EDX analysis</th></tr>
<tr><td>9101</td><td> 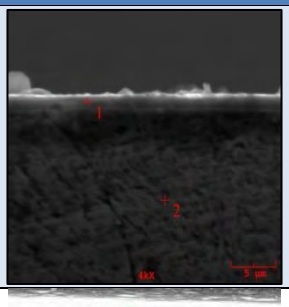 </td><td>
<table>
<tr><th>Elt.</th><th>1</th><th>2</th><th>Units</th></tr>
<tr><td>Al</td><td>35,655</td><td>-</td><td>wt.%</td></tr>
<tr><td>Ti</td><td>23,026</td><td>-</td><td>wt.%</td></tr>
<tr><td>N</td><td>35,655</td><td>-</td><td>wt.%</td></tr>
<tr><td>Fe</td><td>-</td><td>91,220</td><td>wt.%</td></tr>
<tr><td>Other elements</td><td>5,664</td><td>8,788</td><td>wt.%</td></tr>
</table>
</td></tr>
<tr><td>9102</td><td> 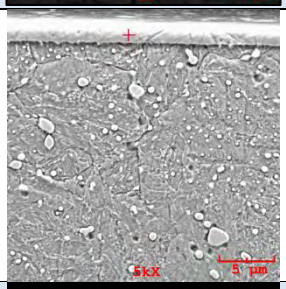 </td><td>
<table>
<tr><th>Elt.</th><th>Conc</th><th>Units</th></tr>
<tr><td>N</td><td>16,685</td><td>wt.%</td></tr>
<tr><td>Cr</td><td>83,315</td><td>wt.%</td></tr>
<tr><td></td><td>100,000</td><td>wt.%</td></tr>
</table>
</td></tr>
<tr><td>9103</td><td> 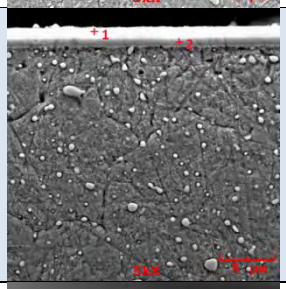 </td><td>
<table>
<tr><th>Elt.</th><th>1</th><th>2</th><th>Units</th></tr>
<tr><td>Al</td><td>35,655</td><td>-</td><td>wt.%</td></tr>
<tr><td>Ti</td><td>23,026</td><td>-</td><td>wt.%</td></tr>
<tr><td>N</td><td>35,655</td><td>-</td><td>wt.%</td></tr>
<tr><td>Fe</td><td>-</td><td>91,220</td><td>wt.%</td></tr>
<tr><td>Other elements</td><td>5,664</td><td>8,788</td><td>wt.%</td></tr>
</table>
</td></tr>
<tr><td>9151</td><td> 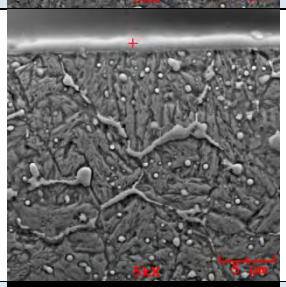 </td><td>
<table>
<tr><th>Elt.</th><th>1</th><th>Units</th></tr>
<tr><td>Al</td><td>39,080</td><td>wt.%</td></tr>
<tr><td>Ti</td><td>25,473</td><td>wt.%</td></tr>
<tr><td>N</td><td>35,447</td><td>wt.%</td></tr>
<tr><td>Fe</td><td>-</td><td>wt.%</td></tr>
<tr><td>Other elements</td><td>-</td><td>wt.%</td></tr>
</table>
</td></tr>
<tr><td>9152</td><td> 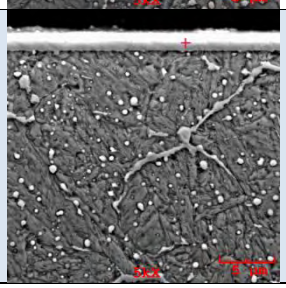 </td><td>
<table>
<tr><th>Elt.</th><th>Conc</th><th>Units</th></tr>
<tr><td>Cr</td><td>75,197</td><td>wt.%</td></tr>
<tr><td>N</td><td>24,803</td><td>wt.%</td></tr>
</table>
</td></tr>
<tr><td>9153</td><td> 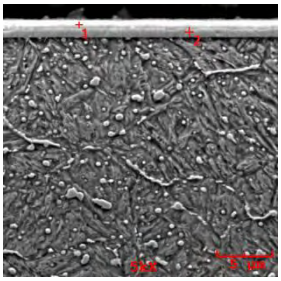 </td><td>
<table>
<tr><th>Elt.</th><th>1</th><th>2</th><th>Units</th></tr>
<tr><td>Al</td><td>37,577</td><td>5,584</td><td>wt.%</td></tr>
<tr><td>Ti</td><td>22,781</td><td>1,239</td><td>wt.%</td></tr>
<tr><td>N</td><td>34,983</td><td>16,165</td><td>wt.%</td></tr>
<tr><td>Cr</td><td>4,659</td><td>66,726</td><td>wt.%</td></tr>
<tr><td>Fe</td><td>-</td><td>9,186</td><td>wt.%</td></tr>
<tr><td>Other elements</td><td>-</td><td>1,100</td><td>wt.%</td></tr>
</table>
</td></tr>
</table>

3.2 Scratch Tests

CSM Revetest Scratch Tester was used for the experiments. The parameters of the scratch tests were set by the CSM Scratch Test Control Unit, while the acoustic emission to load diagrams were recorded by the ABB SE-790 XY plotter (Fig. 10).

As far as all the prerequisite information about the coated specimens are gathered, several scratch tests were conducted in order to determine the critical load, L_c where the first coating failure occurs. The standard scratch test parameters were:

1. Travel speed: 10 mm/min,
2. Loading rate: 100 N/min.

Progressively increasing load was applied to every measurement since it is suitable for rapid assessment and quality assurance of the coating, while it is the most popular method reported in the literature [18].

Another standard experimental parameter for scratch tests was the maximum load applied to the samples. During the first tests this value was set to 60 N. This fixed value allowed the determination of the specimen's L_c and then the minimum and maximum loads applied.

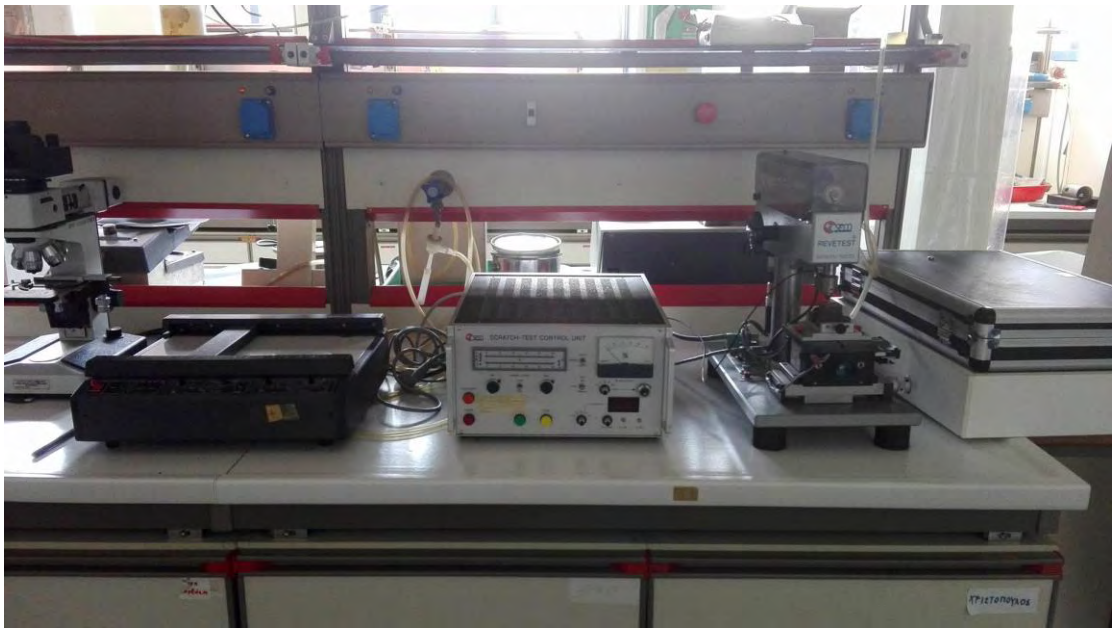

Fig. 10: CSM Revetest Scratch Test Connected with CSM Scratch Test Control Unit equipped with an ABB SE-790 XY plotter

3.3 Stereoscopy

The worn surfaces were initially examined by using a stereoscope in order to observe any macroscale failure on the scratch paths. A Leica Wilz M3Z stereoscope was employed for this work.

3.4 SEM Analysis

All specimens were examined in a Scanning Electron Microscope (SEM). The analysis was focused on the classification of the failure occurred during the scratch tests. A Jeol JSM-5310 SEM in the secondary electron mode with an accelerating voltage of 30 KV was used. The scope of this work was to investigate every scratched specimen in order to determine the mode of failure. For the observation in SEM it is essential that the conductivity of specimens during observation is ensured, therefore the specimens were affixed on the special specimen holder with graphite paste. Then they are placed in the vacuum chamber of the microscope for the observation.

3.5 EDX Analysis

The specimens were further examined by energy-dispersive X-ray spectroscopy (EDX). Line scans and local chemical analysis contributed to the identification of the failure patterns. The EDX analyses were conducted at the Department of Physics, Aristotle University of Thessaloniki, Greece.

3.6 AFM Analysis

Use of AFM (Atomic Force Microscopy) constitutes the most modern methodology for the study of surfaces of all types of materials (metals, ceramics, and complex materials). It provides the possibility of studying surfaces with dimensions up to 1mm x 1mm, with magnifications of their topographic configuration up to x300.000. The acquisition of three-dimensional images of the examined surfaces is possible with the help of a computer.
The AFM senses repulsive contact forces between a fixed flexible micro cantilever and the surface of the sample. The *Z* motion of a silicon nitride tip is monitored in height mode by mounting the sample on an *X–Y–Z* piezoelectric tube scanner. The tip of the sensor is placed on an isolated cantilever, which has a low spring constant (0.1-1 N/m) and diverts as a reaction to the forces exercised between the tip of the cantilever and the specimen. The AFM microscope uses the technique of beam laser reflection for the control of force. As AFM allows

the depiction of conductible and not conductible surfaces directly in laboratory atmosphere, the preparation of surfaces is a relatively easy work.

AFM topographies were acquired with a Topometrix Explorer Atomic Force Microscope, equipped with a hardware-linearized 100µm, X-Y scanner (z-range 10µm) or an X-Y scanner 2µm (z-range 0,8µm). Pyramidal tips made of silicon nitride (Topometrix, 1520-00) and silicon (Topometrix, 1660-00) was used in the non-contact mode. Different areas of every specimen were scanned. The images were captured and section analysis data for each image was obtained. These data provided essential information on the surface morphology, i.e. accurate measurements of the scratched area and scratching depth.

Chapter 4: Experimental Results

4.1 Scratch Tests

The scratch tests parameters for each specimen are shown in Tables 8-13 while the acoustic emission to load diagrams are depicted in Figures 12-17.

4.1.1 Sample 9101 (AlTiN)

A typical specimen after conducting the scratch tests is shown in Fig. 11 where all the scratches can be seen:

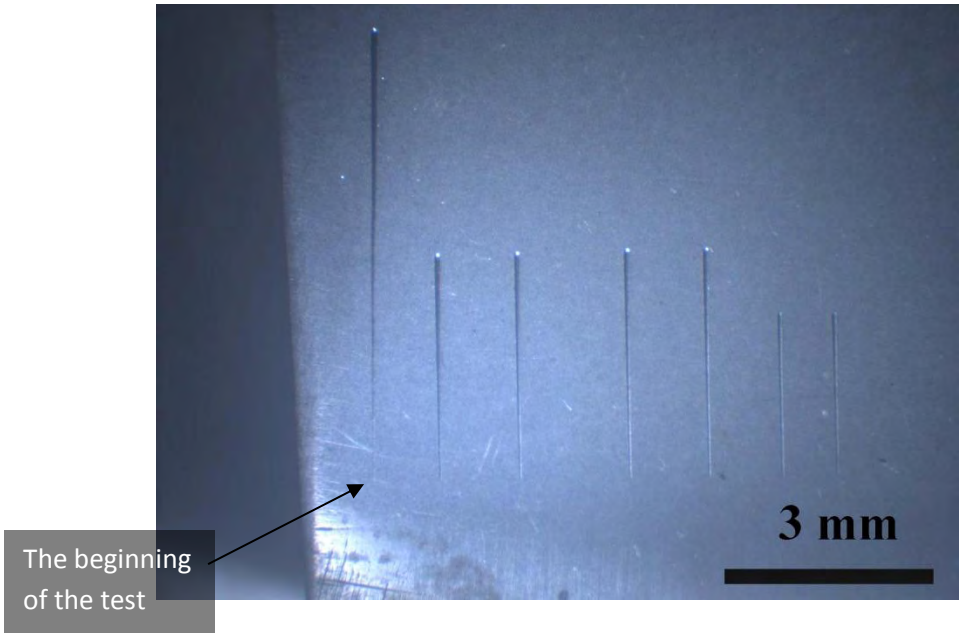

Fig. 11: Specimen #9101. The scratches can be seen macroscopically on the surface

A typical diagram which correlates the acoustic emission signal to the load where the first coating failure occurs is depicted in Fig. 12:

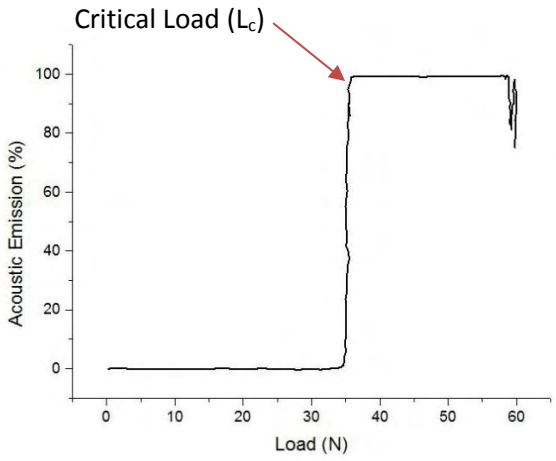

Fig. 12: Acoustic emission vs. load diagram for sample 9101

Six scratch test experiments were carried out for #9101 and all the results are summarized in Table 8 below. Besides the recorded critical load (Lc), the selected min and max load in N, and the length of the scratch are also given. It is worth noting that the critical load appears to be independent on the load range and the selected scratch length.

Table 8: Sample 9101: Experimental results per scratch

Test No.	Min. Load – Max. Load (N)	L_c (N)	Scratch Length (mm)
1	0-60	21	10
2	10-40	17.4	4.5
3	10-40	15.7	4.5
4	10-40	17.3	4.5
5	10-40	14.6	4.5
6	10-25	16.7	3.9

4.1.2 Sample 9102 (CrN)

A typical representative diagram which correlates the acoustic emission signal to the load where the first coating failure occurs is depicted in Fig. 13:

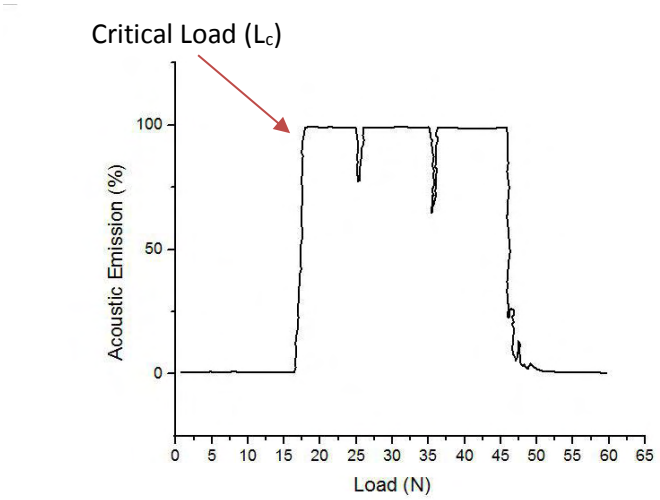

Fig. 13: Acoustic emission vs. load diagram for sample 9102

Five scratch test experiments were carried out for #9102 and the results are summarized in Table 9 below. Besides the recorded critical load (Lc), the selected min and max load in N, and the length of the scratch are also provided. It is worth noting that the critical load appears to be independent on the load range and the scratch length.

Table 9: Sample 9102: Experimental results per scratch

Test No.	Min. Load – Max. Load (N)	L_c (N)	Scratch Length (mm)
1	0-60	8.7	10
2	0-20	18	6
3	0-20	11.8	6
4	0-20	11.5	6
5	0-20	11.5	6

4.1.3 Sample 9103 (AlTiN+CrN)

A typical representative diagram which correlates the acoustic emission signal to the load where the first coating failure occurs is depicted in Fig. 14:

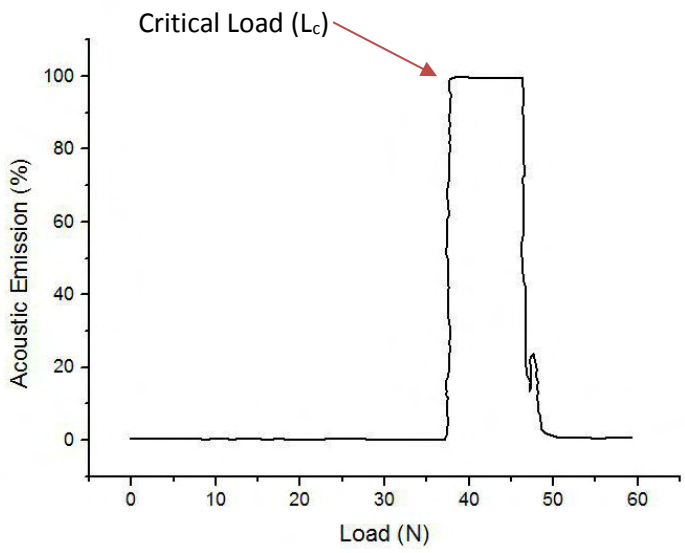

Fig. 14: Acoustic emission vs. load diagram for sample 9103

Five scratch test experiments were carried out for #9103 and the results are summarized in Table 10 below. Besides the recorded critical load (Lc), the selected min and max load in N, and the length of the scratch are also depicted. It is worth noting that the critical load appears to be independent on the load range and the scratch length.

Table 10: Sample 9103: Experimental results per scratch

Test No.	Min. Load – Max. Load (N)	L_c (N)	Scratch Length (mm)
1	0-60	25.1	10
2	10-40	21.5	4.5
3	10-40	17.8	4.5
4	10-40	18.6	4.5
5	10-40	20.2	4.5

4.1.4 Sample 9151 (Nitrided+AlTiN)

A typical representative diagram which correlates the acoustic emission signal to the load where the first coating failure occurs is depicted in Fig. 15:

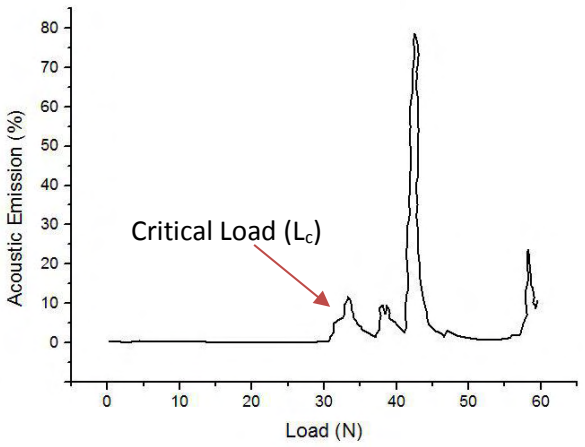

Fig. 15: Acoustic emission vs. load diagram for sample 9151

Three scratch test experiments were carried out for #9151 and the results are summarized in Table 11 below. Besides the recorded critical load (Lc), the selected min and max load in N, and the length of the scratch are also given. Similarly to the above cases, the critical load appears to be independent on the load range and the scratch length.

Table 11: Sample 9151: Experimental results per scratch

Test No.	Min. Load – Max. Load (N)	L_c (N)	Scratch Length (mm)
1	0-60	20.1	10
2	0-60	14.6	10
3	0-60	10.1	10

4.1.5 Sample 9152 (Nitrided+CrN)

A typical representative diagram which correlates the acoustic emission signal to the load where the first coating failure occurs is depicted in Fig. 16:

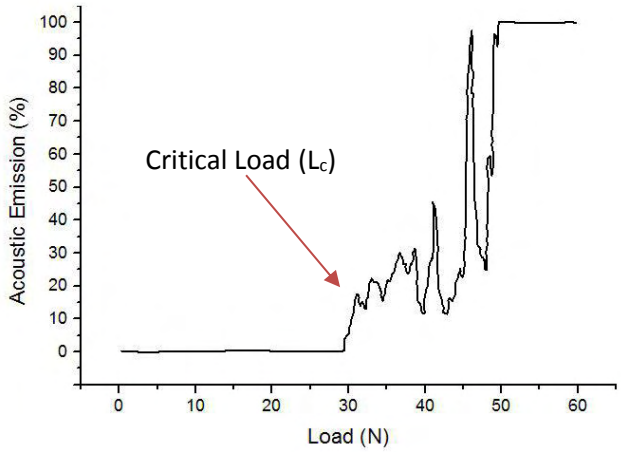

Fig. 16: Acoustic emission vs. load diagram for sample 9152

Three scratch test experiments were carried out for #9152 and the results are summarized in Table 12 below. Besides the recorded critical load (Lc), the selected min and max load in N, and the length of the scratch are also given. Also for this case, the critical load appears to be independent on the load range and the scratch length.

Table 12: Sample 9152: Experimental results per scratch

Test No.	Min. Load – Max. Load (N)	L_c (N)	Scratch Length (mm)
1	0-60	16.5	10
2	0-60	15	10
3	0-60	30	10
4	0-60	28.8	10

4.1.6 Sample 9153 (Nitrided+AlTiN+CrN)

A typical representative diagram which correlates the acoustic emission signal to the load where the first coating failure occurs is depicted in Fig. 17:

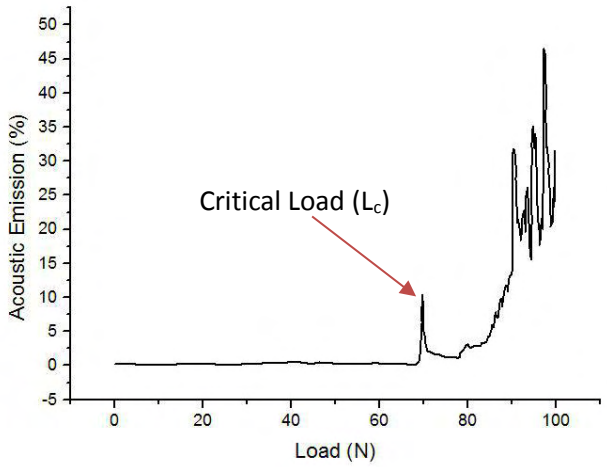

Fig. 17: Acoustic emission vs. load diagram for sample 9153

Nine scratch test experiments were performed for #9153 and the results are summarized in Table 13 below. The differences observed in the critical load of this sample, may be attributed to the most complex combination of the overlay coatings that may trigger different failure modes. It is worth noting that the critical load appears to be independent on the load range and the scratch length, while three tests did not record L_c values.

Table 13: Sample 9153: Experimental results per scratch

Test No.	Min. Load – Max. Load (N)	L_c (N)	Scratch Length (mm)
1	0-60	27.4	10
2	10-40	-	4.5
3	0-90	18.1	13.5
4	0-80	-	12.5
5	0-90	-	13.5
6	0-90	26.8	13.5
7	0-120	31	14
8	0-140	51.2	14.5
9	0-100	73	13.75

Table 14 summarizes the results from all tests, in terms of the mean value of the critical load and the standard deviation per sample:

Table 14: Mean and standard deviation Lc values of coated samples

Material code	Treatment	Mean L_c value (N)	L_c standard deviation (N)
9101	AlTiN coated	17.12	1.99
9102	CrN coated	12.30	3.06
9103	AlTiN+CrN coted	20.64	2.53
9151	Nitrided+AlTiN coated	14.93	4.09
9152	Nitrided+CrN coated	22.57	6.86
9153	Nitrided+AlTiN+CrN coated	37.91	18.63

Based on the above results, a first comment is that the measured L_c values of AlTiN and CrN coated specimen have shown low deviation from the respective L_c values reported in the literature [15], [19]. Another observation is that the nitrided samples have exhibited enhanced adhesion, with the exception of the AlTiN coated specimens.

More specifically, the sample 9151 had slightly decreased L_c values compared to the non-nitrided sample (9101). Another factor that plays a vital role in scratch resistance is the coating type. Specimens 9103 and 9153 have shown improved resistance than the other nitrided and non-nitrided samples respectively. In general, sample 9153 reached the highest mean L_c value while the sample 9102 the lowest one. As it concerns the standard deviation of the L_c, it is observed that the nitrided specimens exhibited higher values of standard deviation compared to the non-nitrided ones. More specifically, the sample 9153 reached the highest L_c standard deviation value while the sample 9101 the lowest one. Consequently, the information gathered by the scratch tests provided useful information about the gas nitriding process as well as about the double CrN/AlTiN coating.

4.2 SEM Analysis

Each specimen was examined at the scanning electron microscope in order to characterize the coating failure mode.

4.2.1 Sample 9101 (AlTiN)

During the initial stages of the scratch test, the scratch path is starting to form. As the diamond tip moves forward, it seems that buckling as well as coating chipping appear at low scale, despite the fact that the applied force is lower than the L_c. Fig. 18 shows the scratch before the first acoustic emission peak recorded. Buckling and coating chipping phenomena are initially observed:

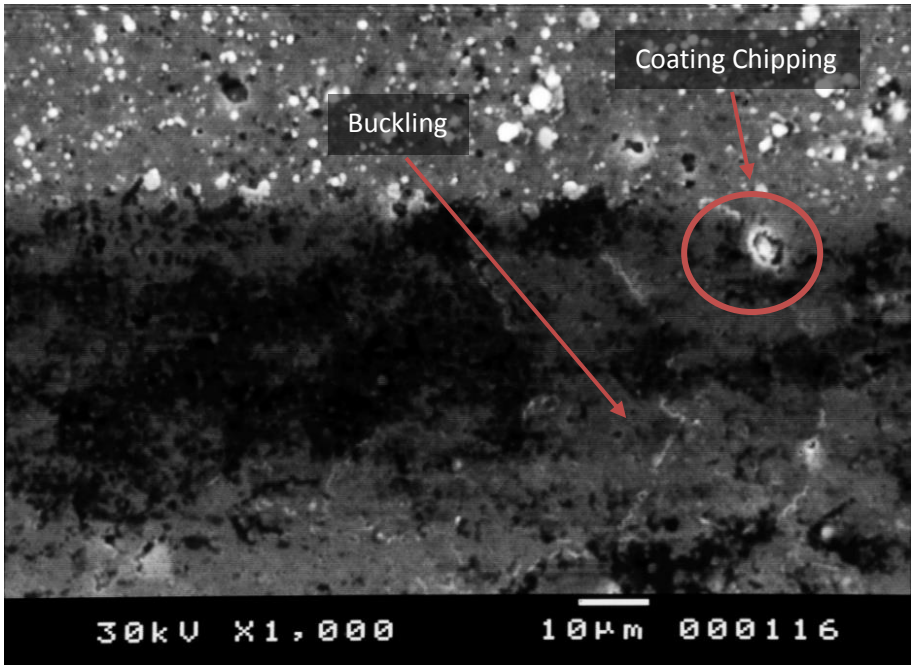

Fig. 18: The initial stage of the crack

The applied force progressively increases and reaches the L_c value. The buckling and chipping phenomena are more pronounced at this stage of analysis, as it is demonstrated in Fig. 19:

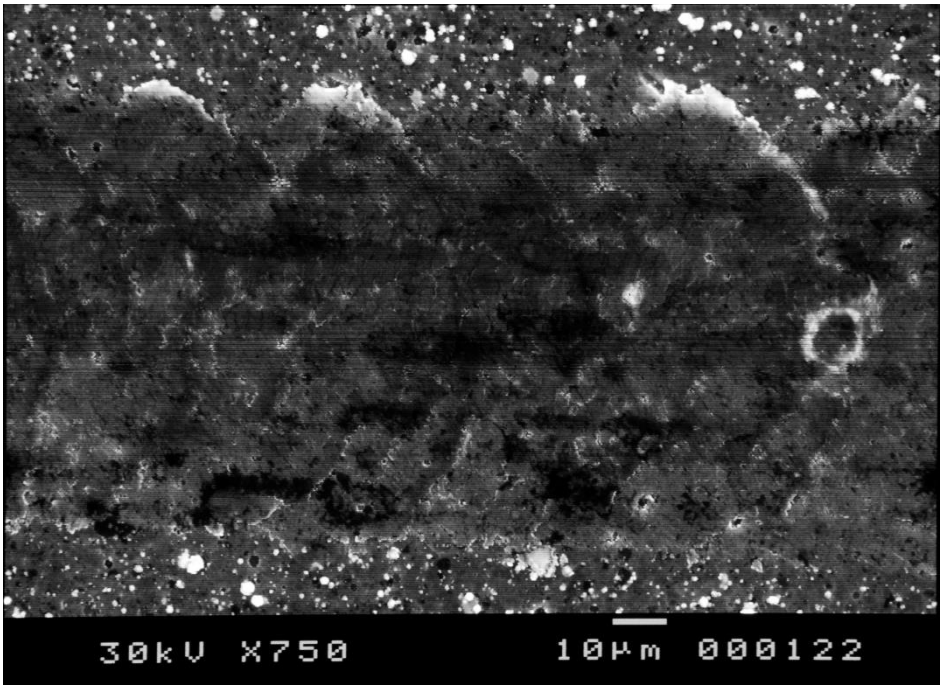

Fig. 19: The area where the first acoustic emission peak was recorded

In higher magnification, it is obvious that the microcracks formed into the scratch path and become denser as the applied load is increasing (Fig. 20).

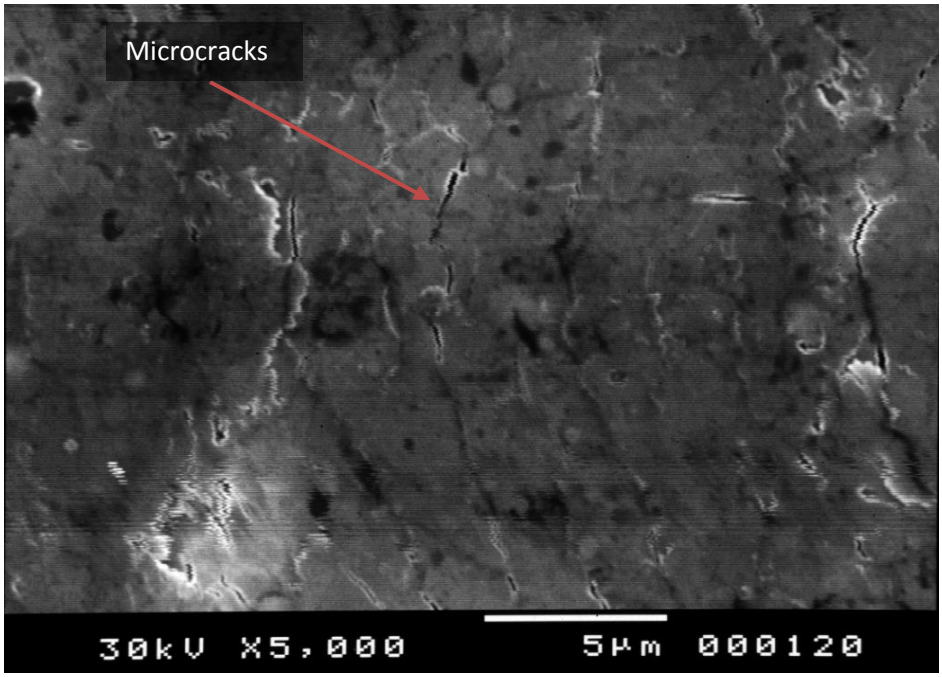

Fig. 20: Microcracks appearance

During the last stage of the scratch test, the vertical load reaches its highest value. It is observed that buckling and chipping become more intense than in previous stages of the test. Furthermore, microcracks grow intensively while the coating is deposited laterally to the scratch trace (Fig. 21).

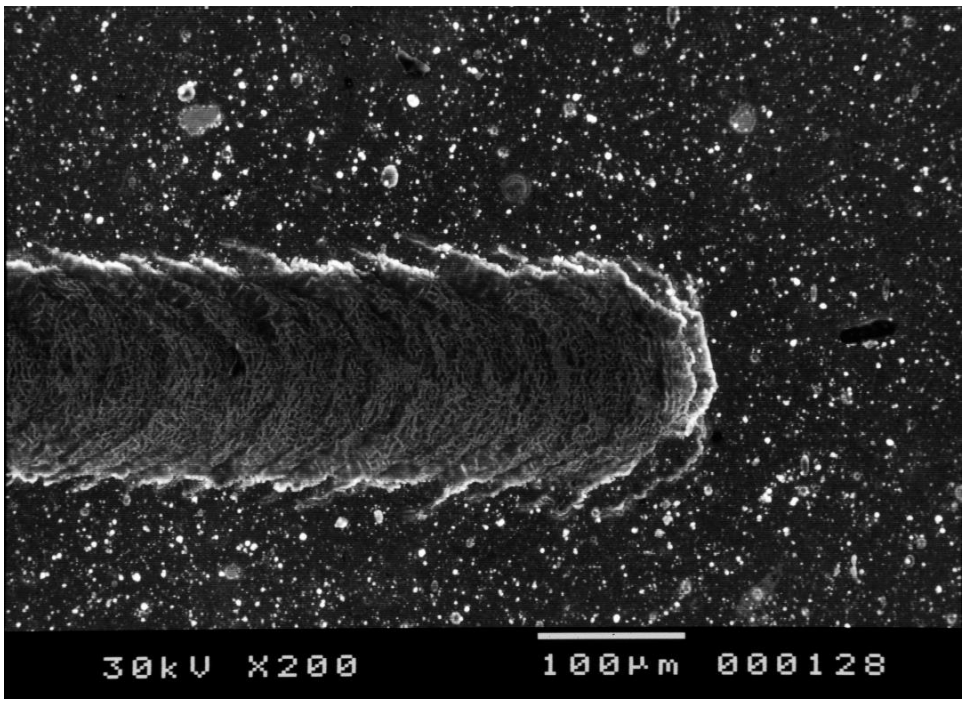

Fig. 21: End of the scratch path

4.2.2 Sample 9102 (CrN)

Initially, the scratch surface seems to be intact from the test, while the spherical tip moves on (Fig. 22):

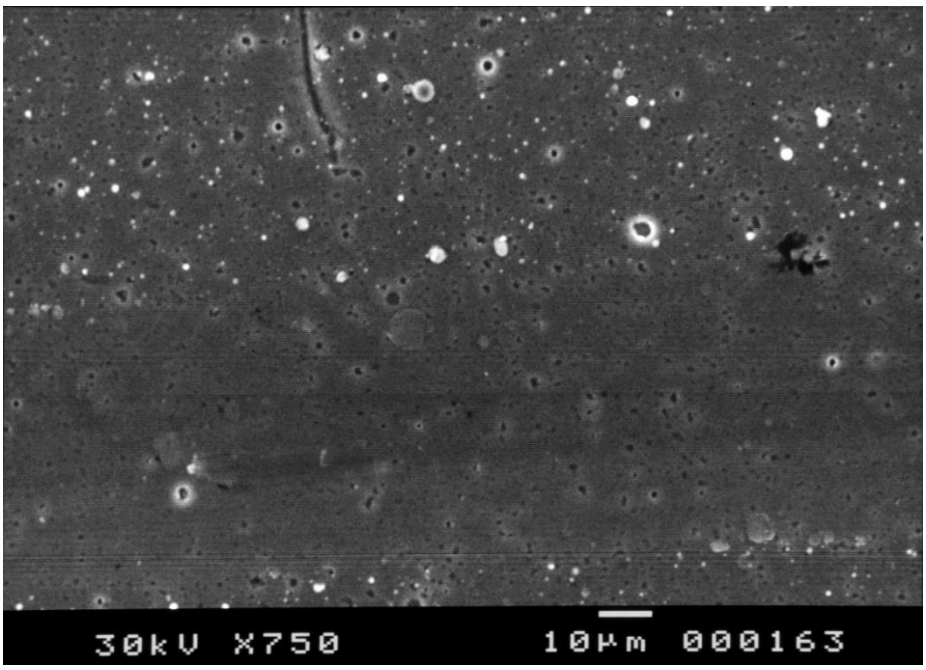

Fig. 22: Formation of the scratch path

The increasing force leads to the occurrence of the first acoustic emission peak. In the above stage, angular cracks are forming at the edges of the scratch, as it is shown in Fig. 23:

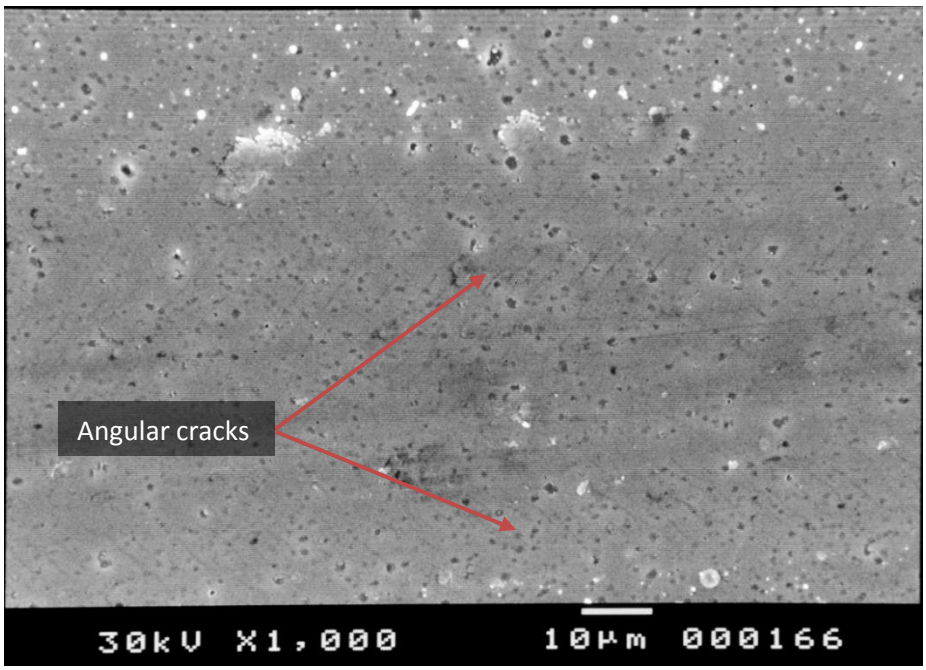

Fig. 23: Appearance of angular cracks

As the tip moves forward, the pre-existing microcracks grow and become denser while forming semicircular microcracks which extend in the whole scratch width (Fig. 24).

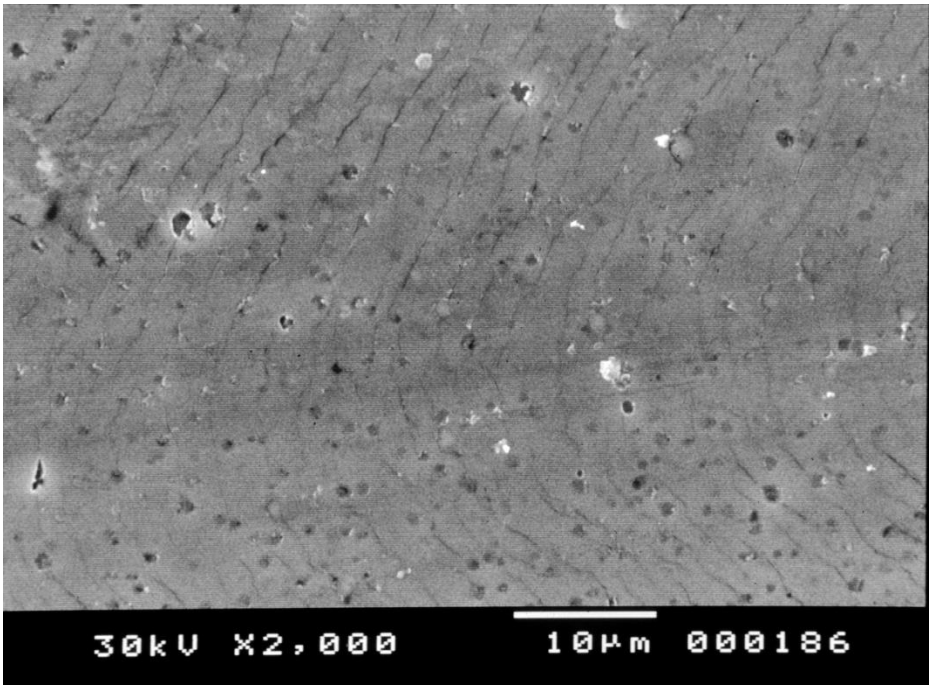

Fig. 24: Appearance of semicircular cracks

At the end of the scratch, the semicircular microcracks coexist with buckling and chipping phenomena, as it is shown in Figs. 25, 26:

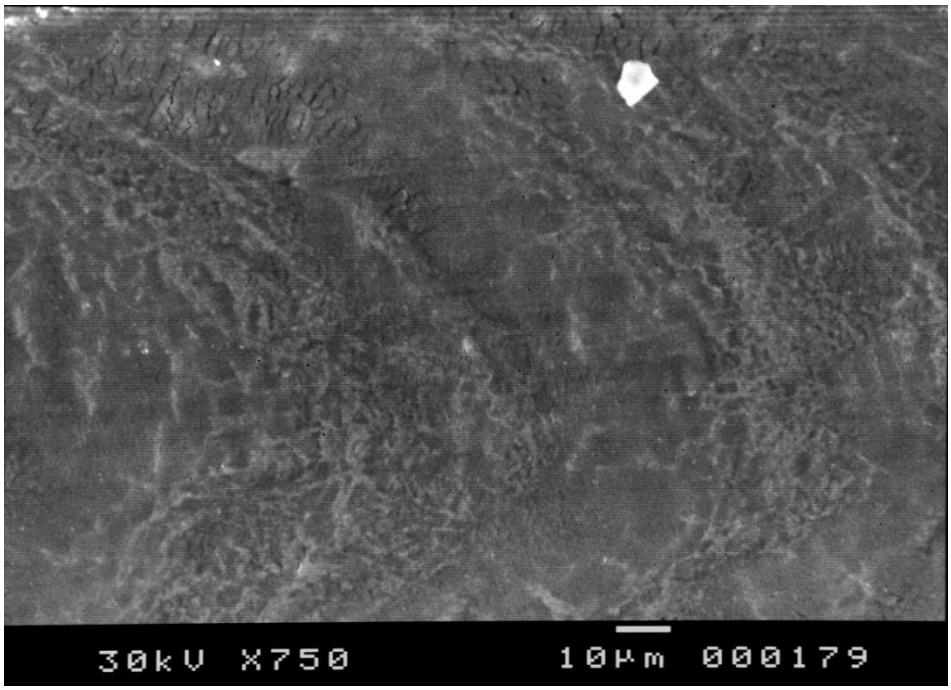

Fig. 25: Coating buckling

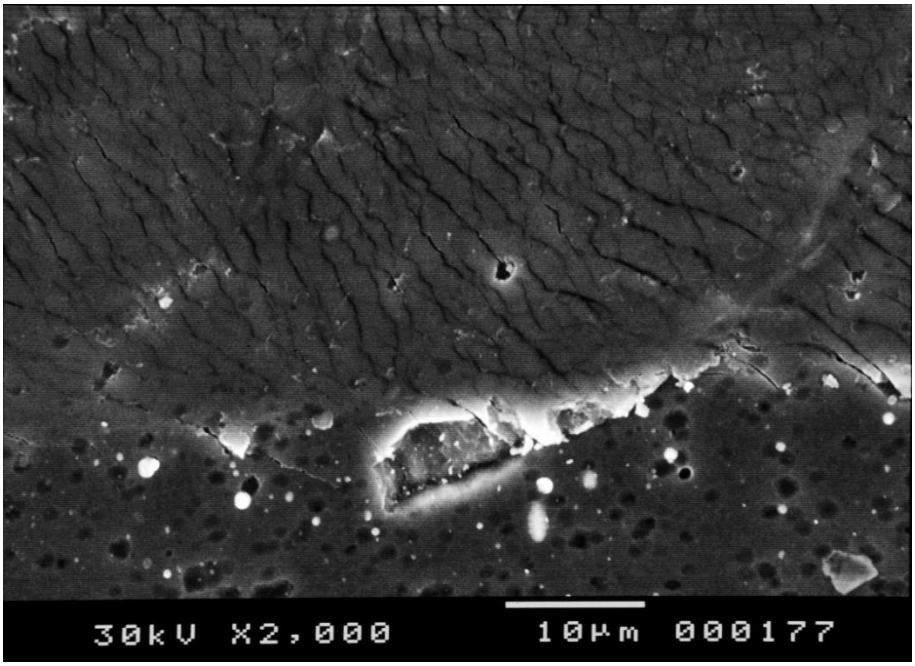

Fig. 26: Coating chipping associated with microcracks

4.2.3 Sample 9103 (AlTiN+CrN)

During the early stages of the scratch track, angular microcracks are formed on both the edges of the scratch (Fig. 27):

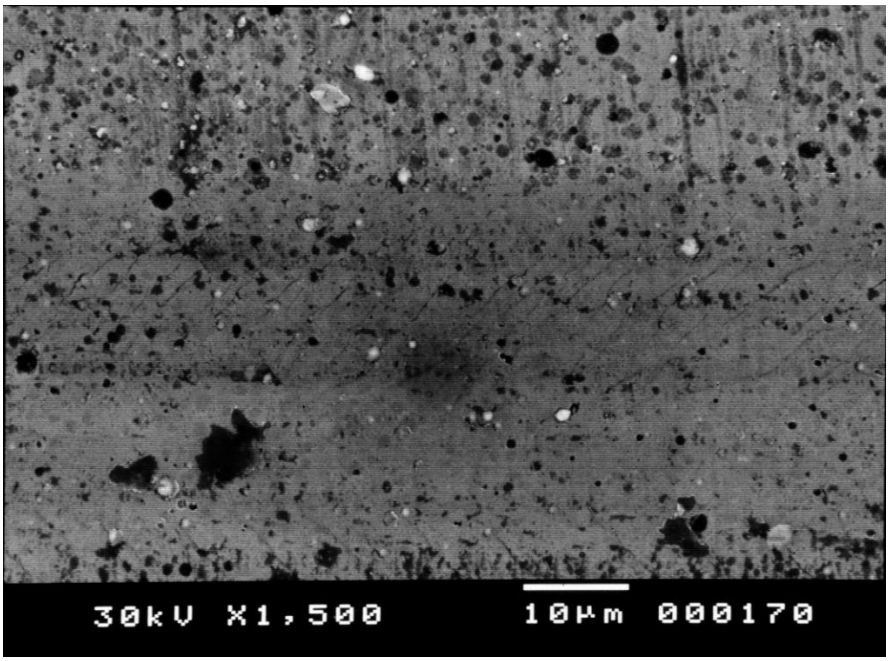

Fig. 27: Formation of angular microcracks

As the applied load increases progressively and reaches values below the L_c, coating buckling and chipping are observed, while the angular cracks are connected, forming semicircular cracks (Fig. 28):

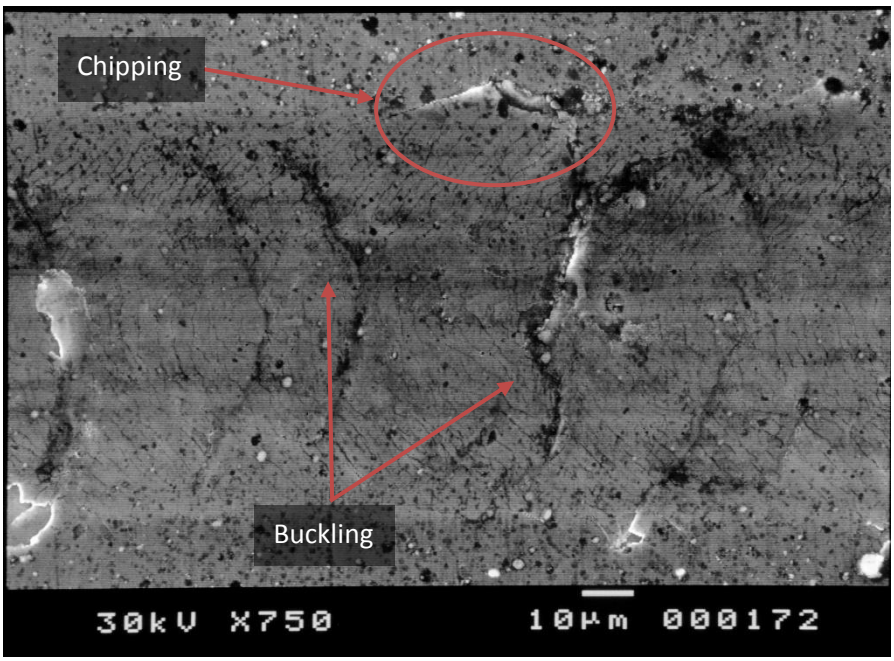

Fig. 28: Coating buckling and chipping

When the applied load reaches the Lc value, recovery spallation is observed (Fig. 29). This type of adhesion failure is the result that depends on the properties of the substrate combined with the pre-existing through thickness microcracks. The spallation of the coating takes place on both sides of the scratch. At the same time, the network of the microcracks become denser and buckling coexists with recovery spallation.

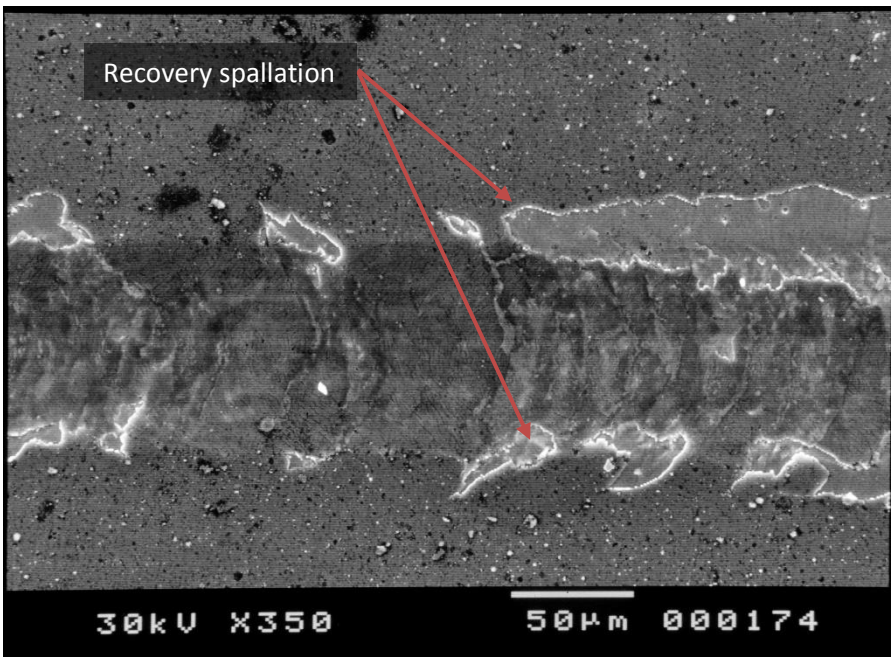

Fig. 29: Recovery spallation of the coating

The spherical diamond tip moves forward while the applied force continues increasing. During this stage, recovery spallation occupies the edges of the scratch path. At the same time, microcracks become wider and have no specific orientation as coating buckling is more intense (Fig. 30):

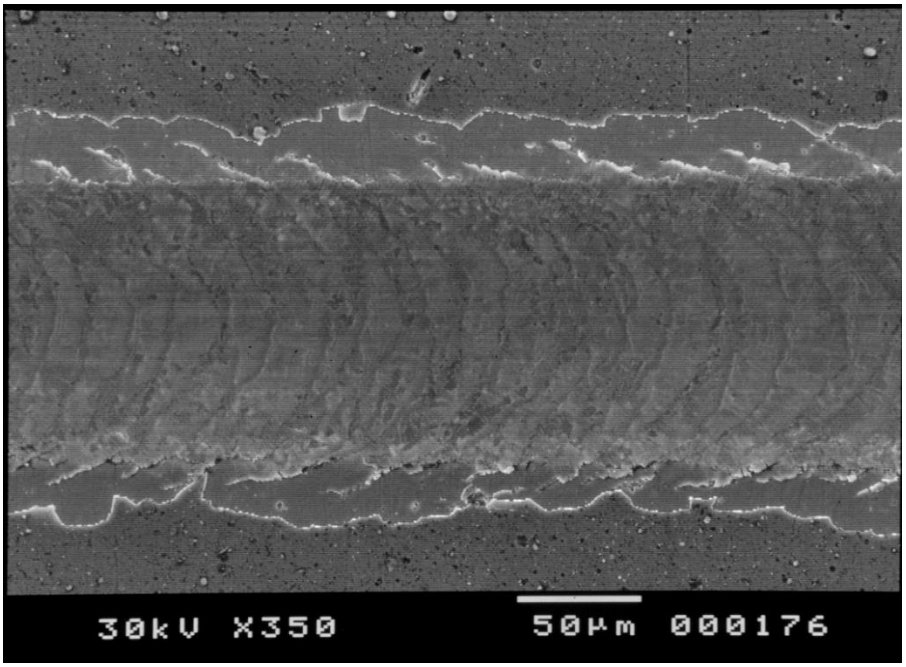

Fig. 30: Coating adhesion failure by recovery spallation

At the endpoint of the scratch path, recovery spallation as well as coating chipping coexist. The increasing force led to the deposition of the coating laterally to the crack (Fig. 31):

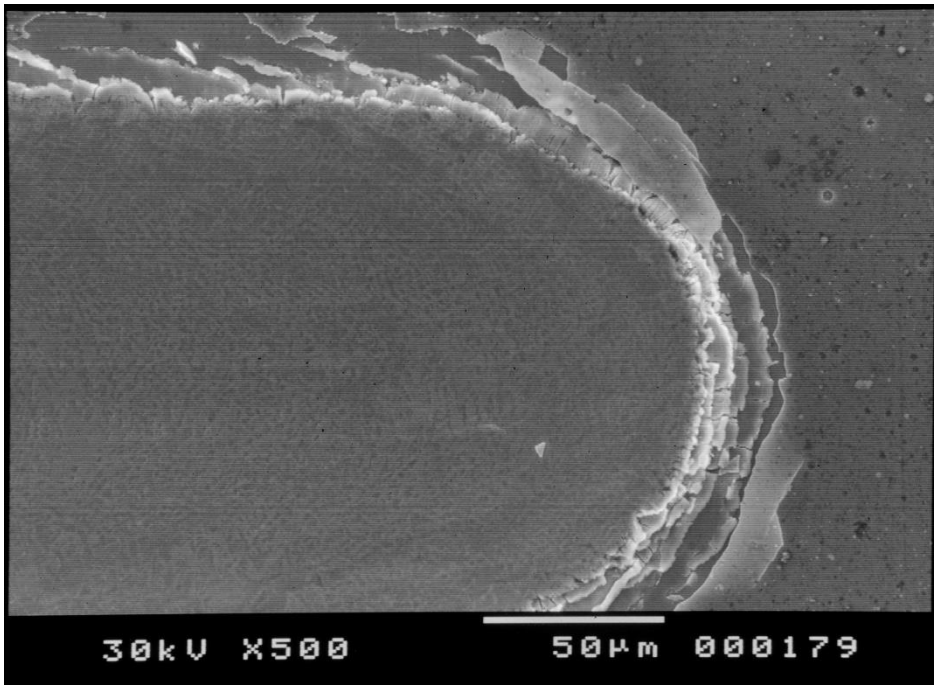

Fig. 31: The endpoint of the scratch

4.2.4 Sample 9151(Nitrided+AlTiN)

During the early stages of the observation, the scratch test track seems to have low depth and width. The coating remains intact, as it is shown in Fig. 32:

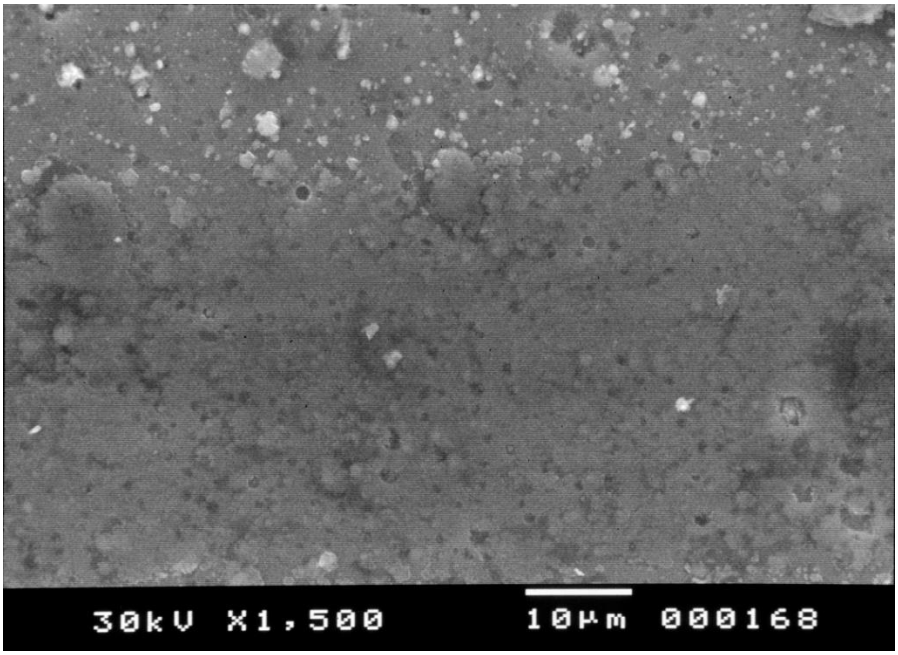

Fig. 32: The initial stage of the scratch track

When the first acoustic emission peak is recorded, angular microcracks appear to form on both the upper and the lower edges of the scratch (Fig. 33). Microcracks are visible under large magnifications.

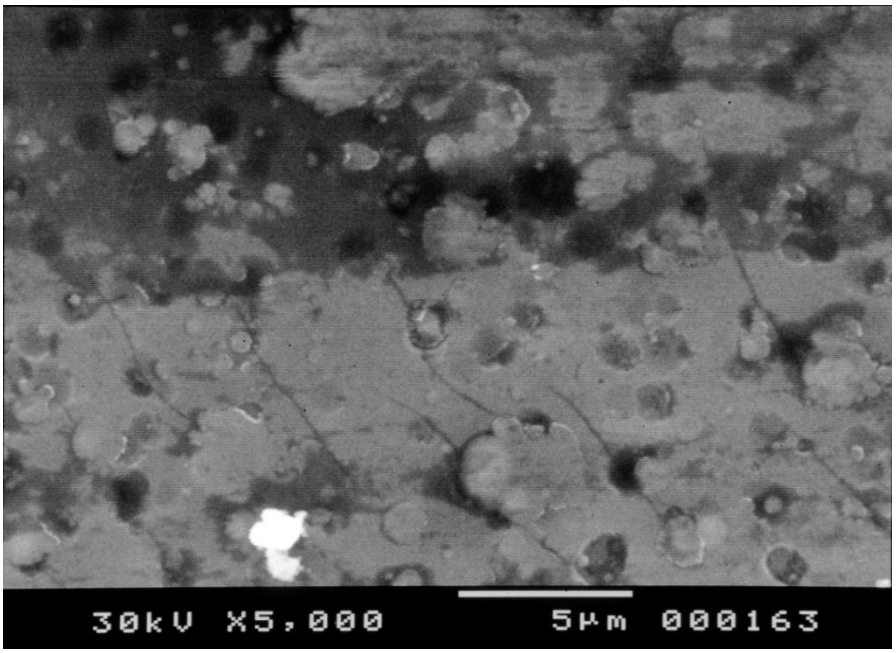

Fig. 33: Formation of angular microcracks

As the applied load increases, angular cracks are linked, forming semicircular microcracks through the entire scratch width (Fig. 34):

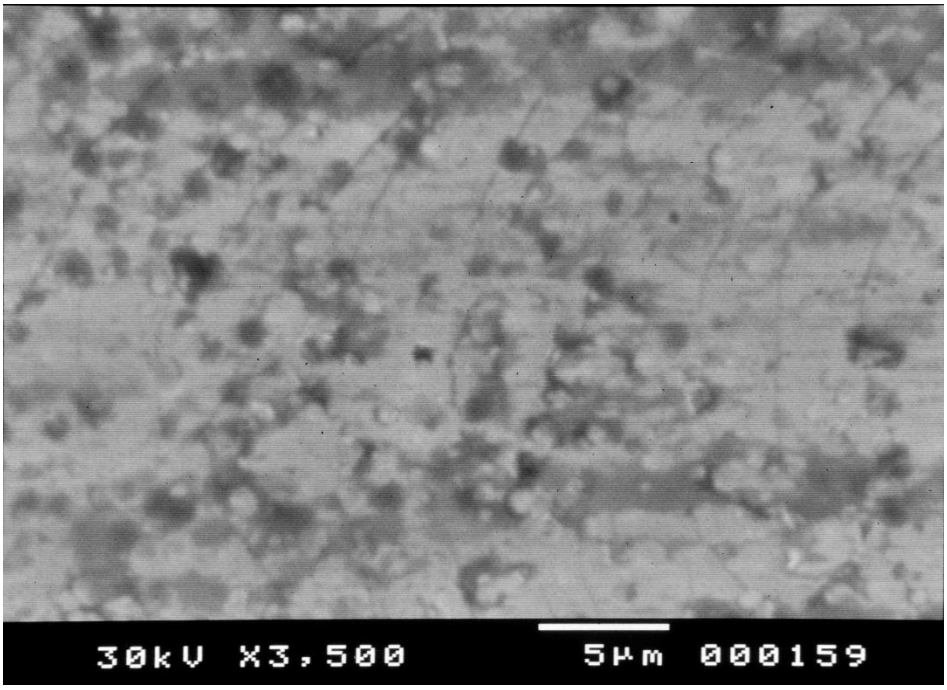

Fig. 34: Formation of semicircular microcracks

At the endpoint of the scratch track, coating chipping appears. The diamond tip deposits the coating laterally to the crack (Fig. 35):

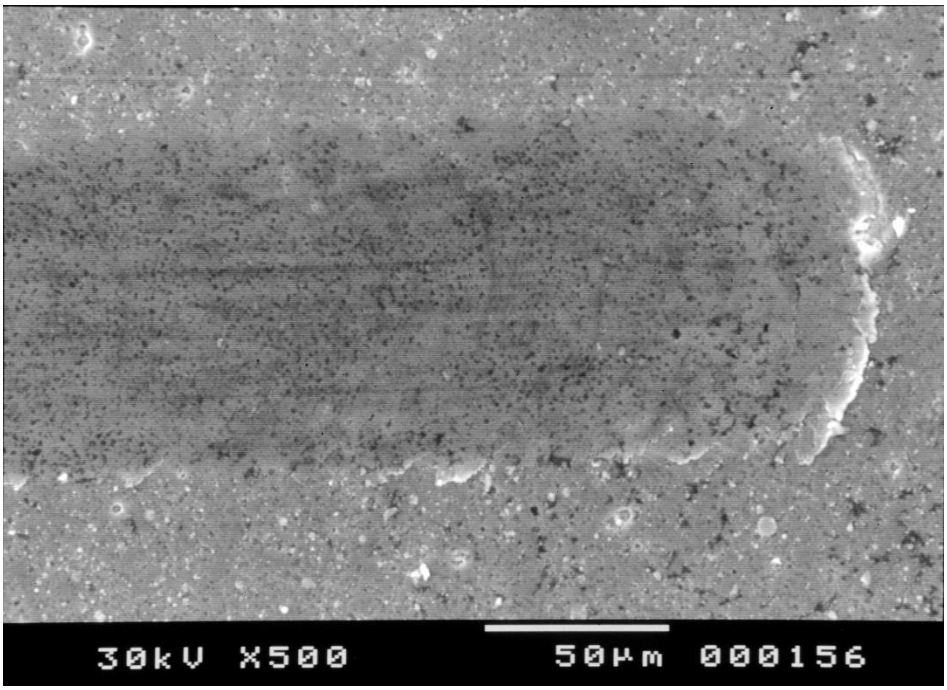

Fig. 35: The endpoint of the scratch

It is worth mentioning that the dimensions of the microcracks are low, fact that is confirmed by the high magnifications that were used in order to locate the coating failure.

4.2.5 Sample 9152 (Nitrided+CrN)

An initial observation is that the scratch track seems to have low width and depth. Despite the fact that the applied force is currently low, angular microcracks form at the scratch path boundaries (Fig. 36):

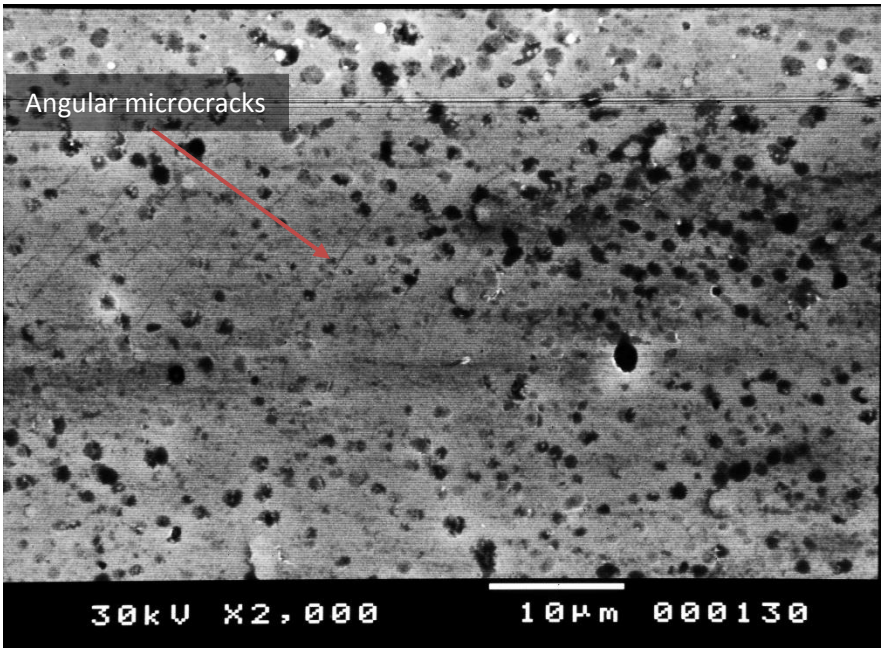

Fig. 36: Formation of angular microckracks during the initial stages of the scratch

In the area where the critical load is applied, the formation of semicircular microcracks is observed (Fig. 37).

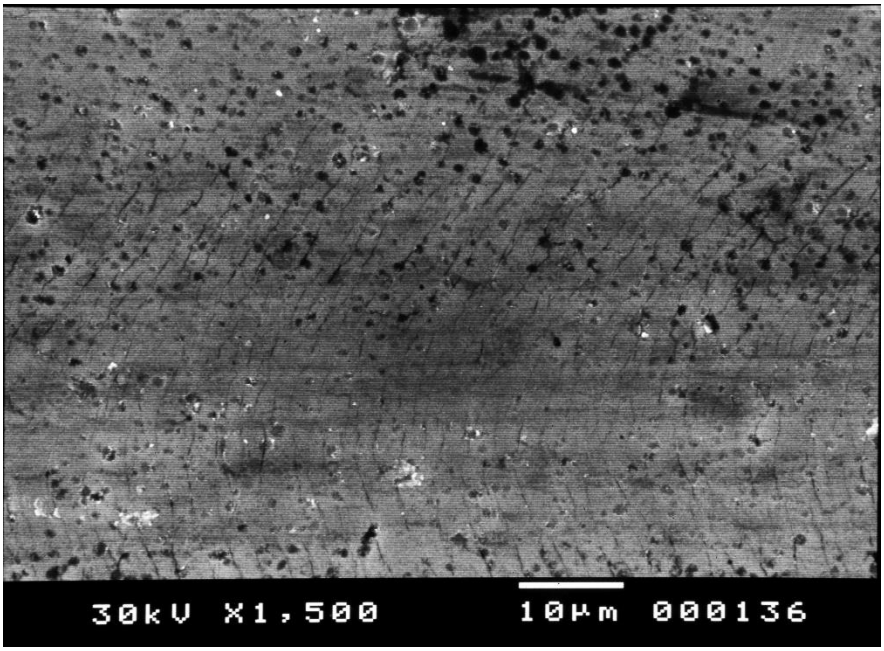

Fig. 37: Formation of semicircular microcracks

As the diamond tip reaches its final position on the specimen, the coating seems to remain attached to the substrate (Fig. 38). The dimensions of the scratch track also remain low, while semicircular cracks are continuously growing (Fig. 39):

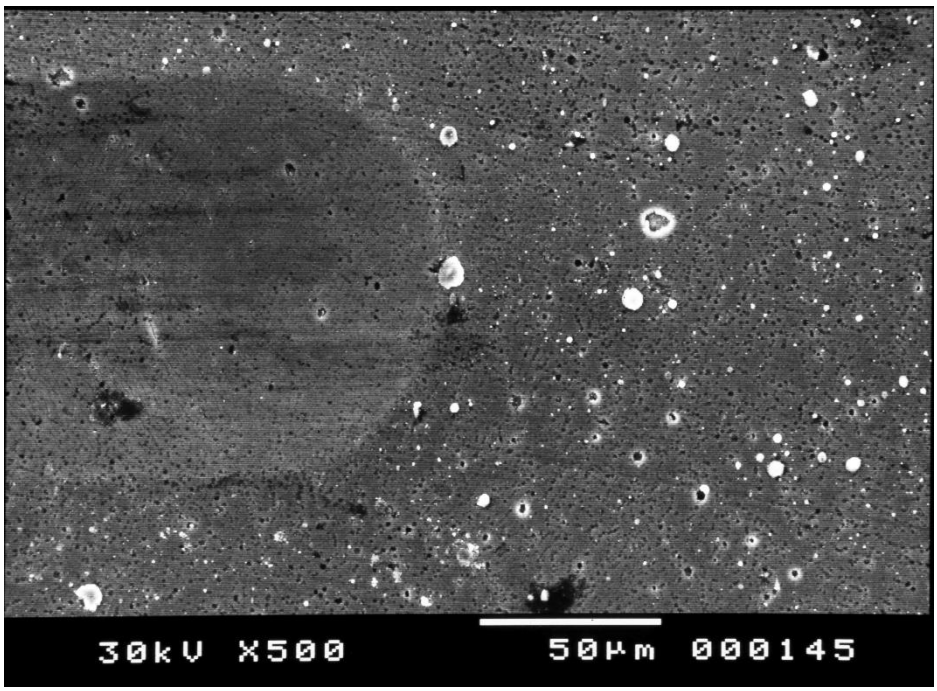

Fig. 38: The endpoint of the scratch

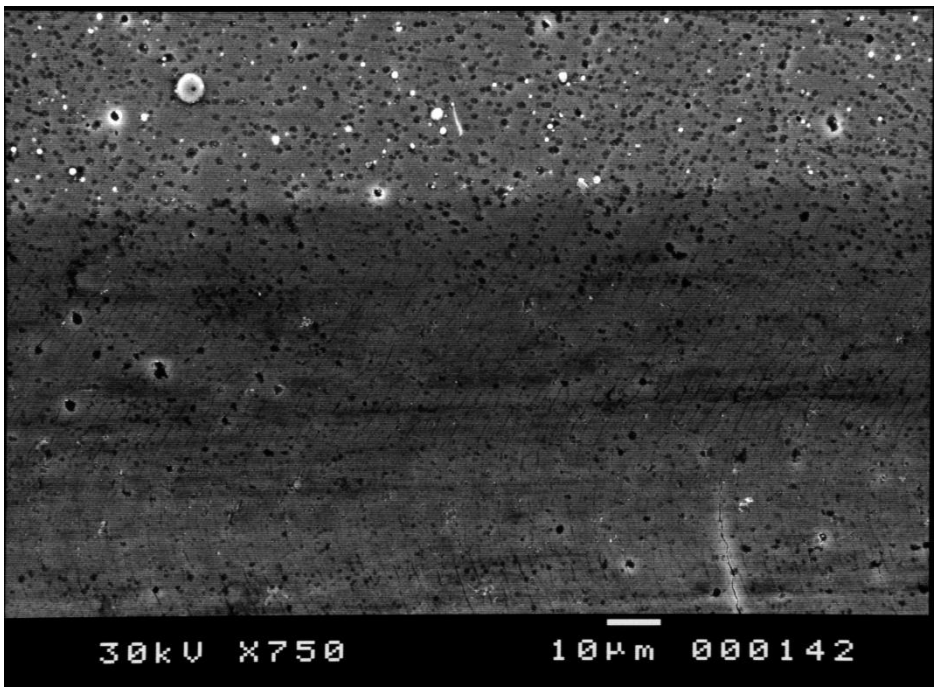

Fig. 39: Growth of semicircular microcracks

4.2.6 Sample 9153 (Nitrided+AlTiN+CrN)

The double layer coated, gas nitrided specimen, seems to have many similarities about its failure pattern as the above nitrided samples 9151 and 9152. More specifically, the surface is not damaged by the spherical tip during the initial stages of the scratch test, as it is shown in Fig. 40:

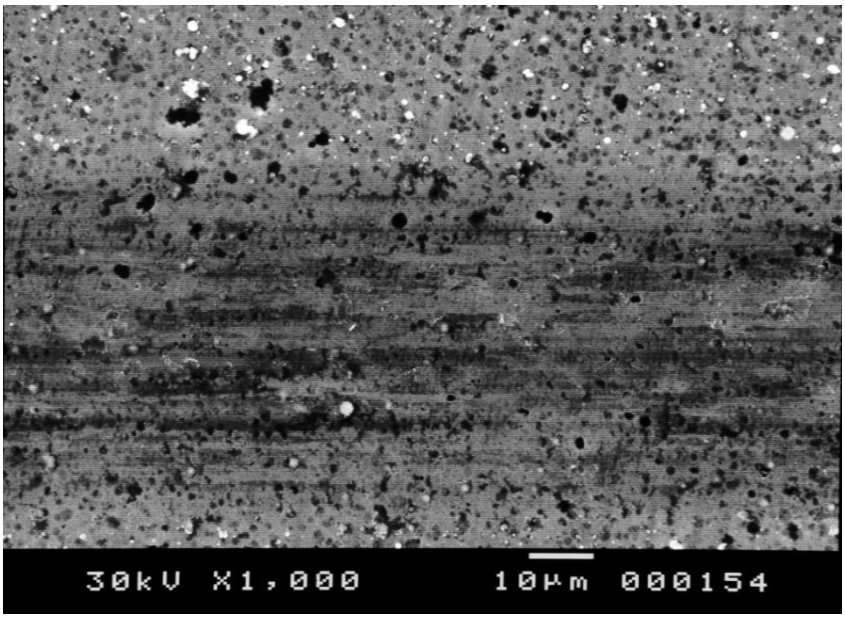

Fig. 40: The initial phase of the scratch path

When the applied force reaches the L_c value, semicircular microcracks are formed (Fig. 41). The above fact indicates that pre-existing angular cracks propagated and linked across the width of the scratch track.

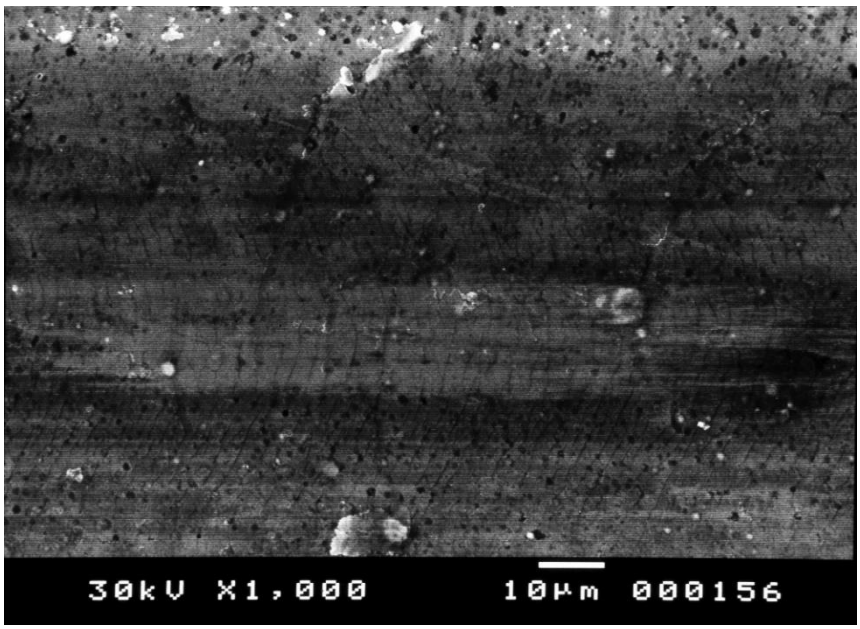

Fig. 41: Formation of semicircular microcracks

As a result of the compressive stresses generated in front of the diamond tip and of the pre-existence of interfacial cracks, buckling occurs. At the same time, coating is deposited laterally to the crack (chipping) due to previous buckling failures (Fig. 42):

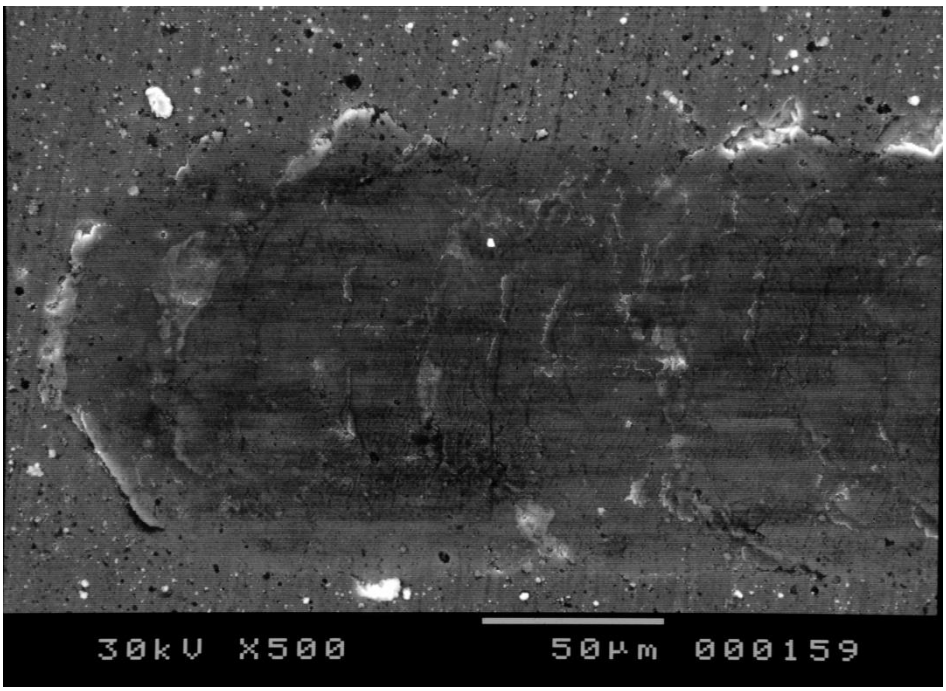

Fig. 42: Coating buckling and chipping at the end of the scratch track

4.3 EDX Analysis

Each coated specimen was examined by energy-dispersive X-ray spectroscopy in order to acquire further information about the failure modes of the coatings that occurred during the conduction of the scratch tests.

4.3.1 Sample 9101 (AlTiN coated)

- Area of first coating failure

It is observed that the Al composition by weight is slightly reduced inside the crack compared to its composition outside the crack (Fig. 43). On the contrary, the composition of Fe, the main substrate element, has elevated values inside the scratch than in the area outside it. This fact implies the partial coating removal from the spherical tip.

The results of the line scan that was acquired parallel to the scratch track (Fig. 44) depicts variations in the chemical composition of the main elements. Fe concentration increases while Al decreases. This fact leads to the conclusion that a local coating abruption took place during the test at this area.

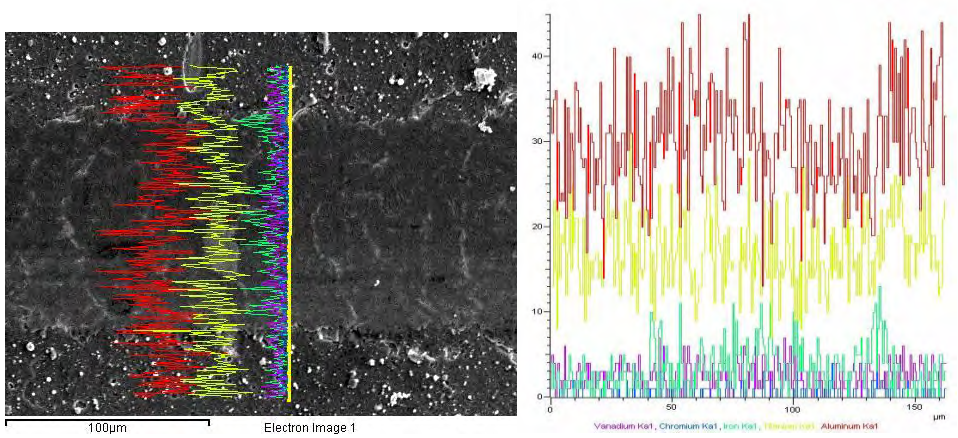

Fig. 43: Line scan transverse to the scratch track

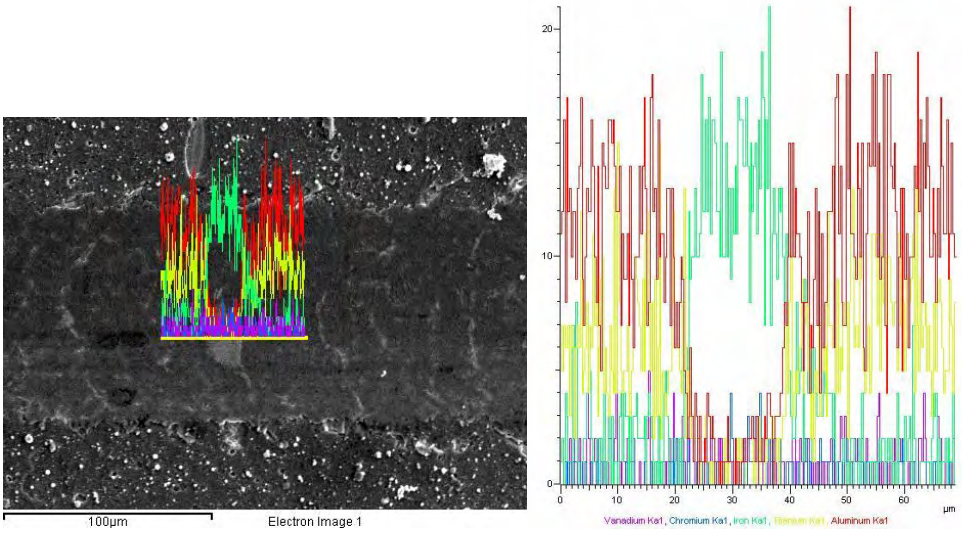

Fig. 44: Line scan parallel to the scratch track

- End of scratch

The EDX analysis results acquired at the end of the scratch are given in Fig. 45. It is worth comparing spectrums 1 and 3. Spectrum 1 provides the chemical compositions of the elements inside the scratch track while spectrum 3 outside it. In particular, the chemical compositions of Al and N are reduced by almost 50% inside the scratch while Ti is reduced more. Summarizing, the coating has been removed to a large extent, but not entirely by the diamond tip.

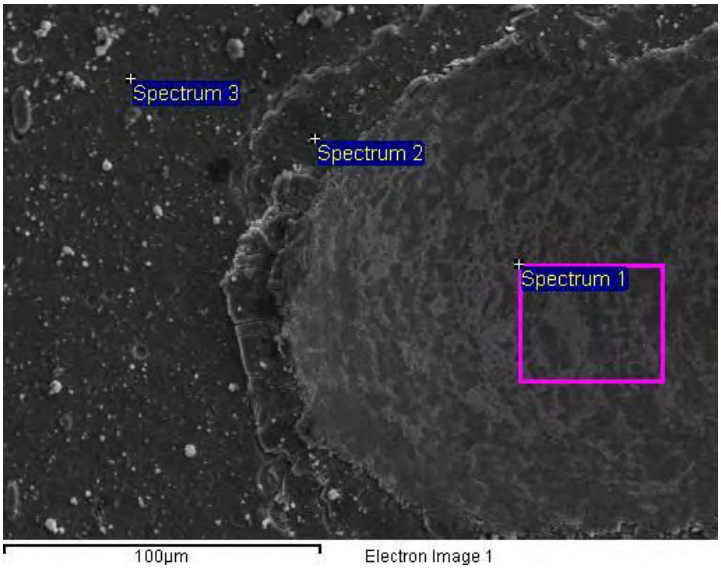

Spectrum	In stats.	N	Al	Si	Ti	V	Cr	Mn	Fe	Mo	Total
Spectrum 1	Yes	8.69	20.81	0.13	11.34	0.87	2.06	0.16	54.39	1.54	100.00
Spectrum 2	Yes	10.93	41.81	0.16	38.00	0.52	0.87	-	9.22	-	100.00
Spectrum 3	Yes	16.68	39.95	0.16	37.53	0.32	-	-	6.48	-	100.00

Fig. 45: Spot chemical analysis at the end of the scratch track

4.3.2 Sample 9102 (CrN)

- Area of first coating failure

The current line scan (shown in Fig. 46) indicates that the coating remains attached to the substrate, as the Cr composition (wt%) remains high.

It seems that the coating remains almost intact by the spherical tip (Fig. 47). Another significant clue is that the composition of Fe inside the microcracks is increased, fact that leads to the conclusion that these cracks seem to be through coating thickness.

Pores found on the surface (Fig. 48) probably created due to discontinuities of the coating. As a result, the detection of Fe, supports that the coating has partially removed from the substrate.

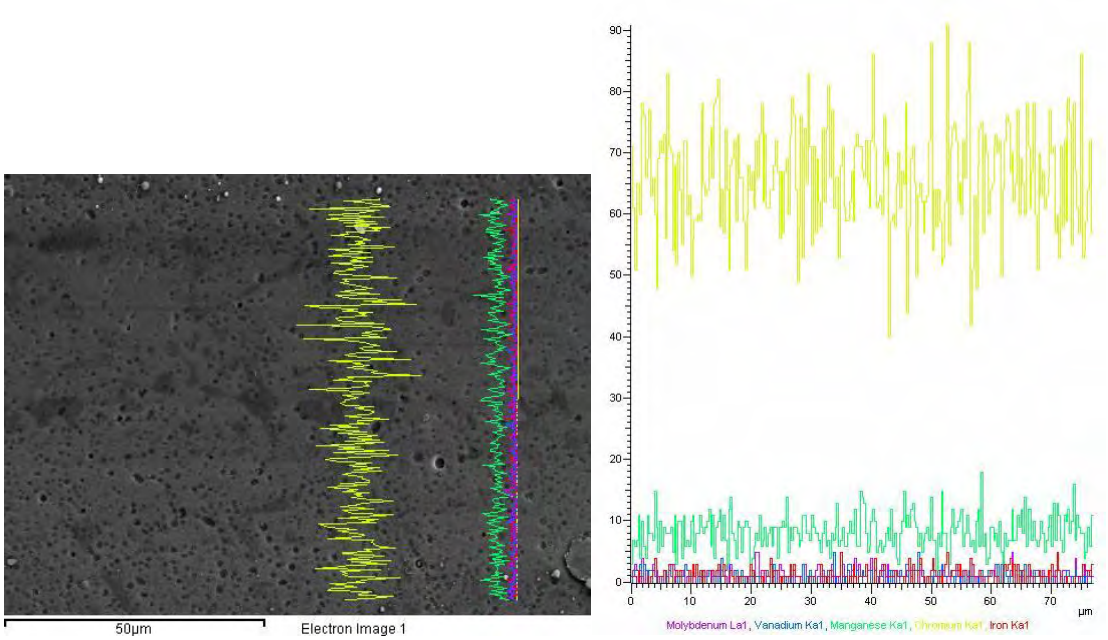

Fig. 46: Line scan transverse to the scratch track

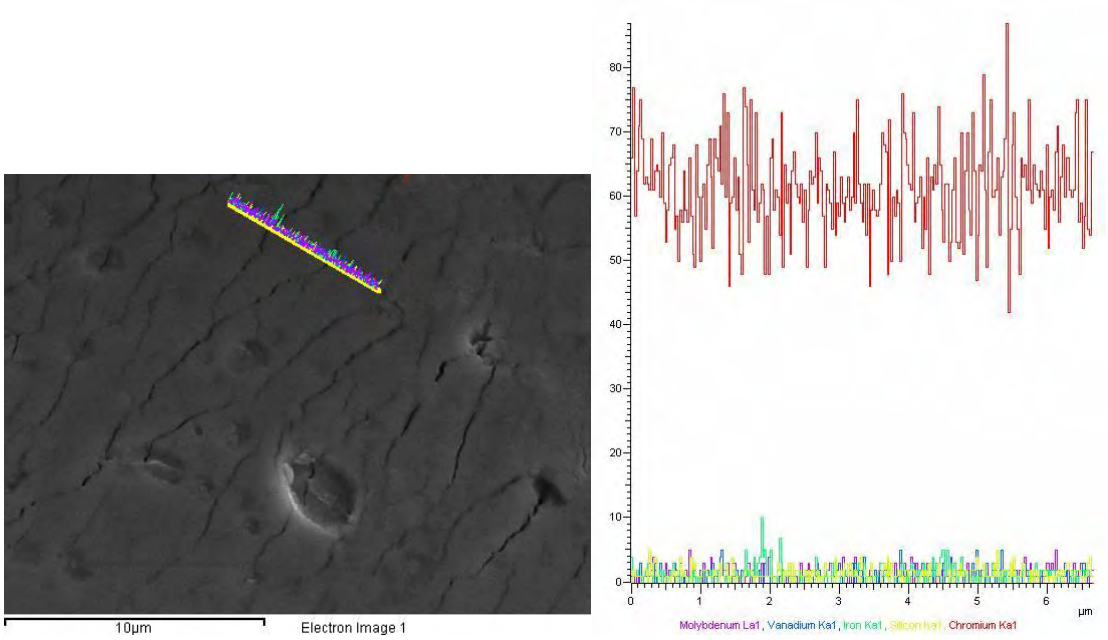

Fig. 47: Line scan on microcracks

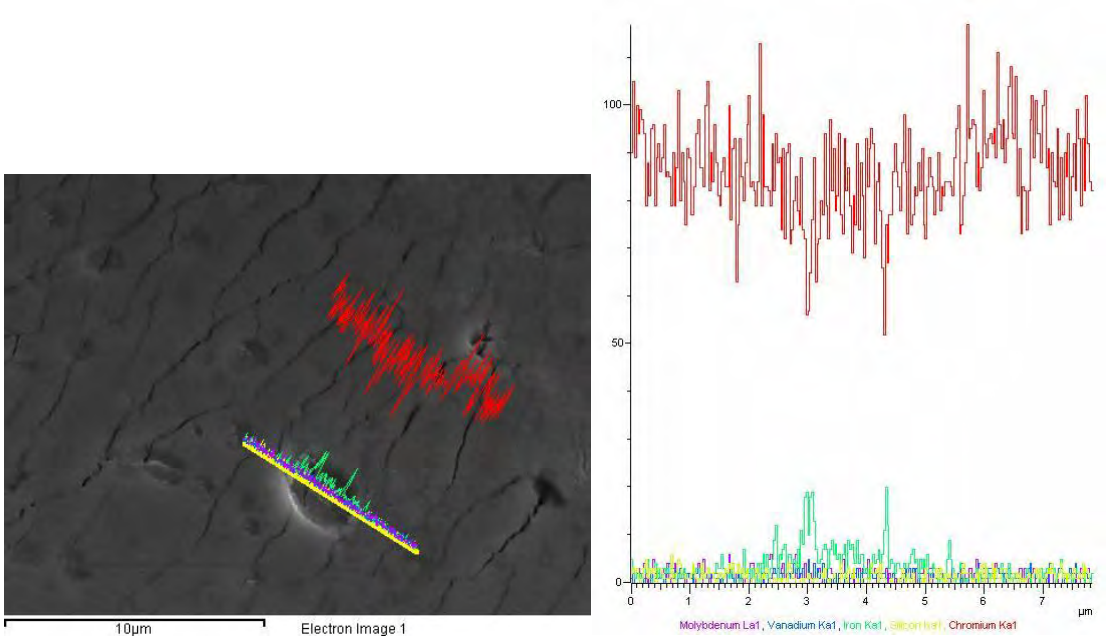

Fig. 48: Line scan on porous surface

- End of scratch

At the end of the scratch representative results are provided in Fig. 49. Inside the scratch path (Spectrum 2), the N composition is lower compared to its composition outside it. This fact means that the coating has been removed, but to a small extent (N is decreased by 8%). It is also important to note that no reliable conclusions could extracted from the chemical composition of Cr, as it constitutes an alloying element of DIN 1.2999 steel.

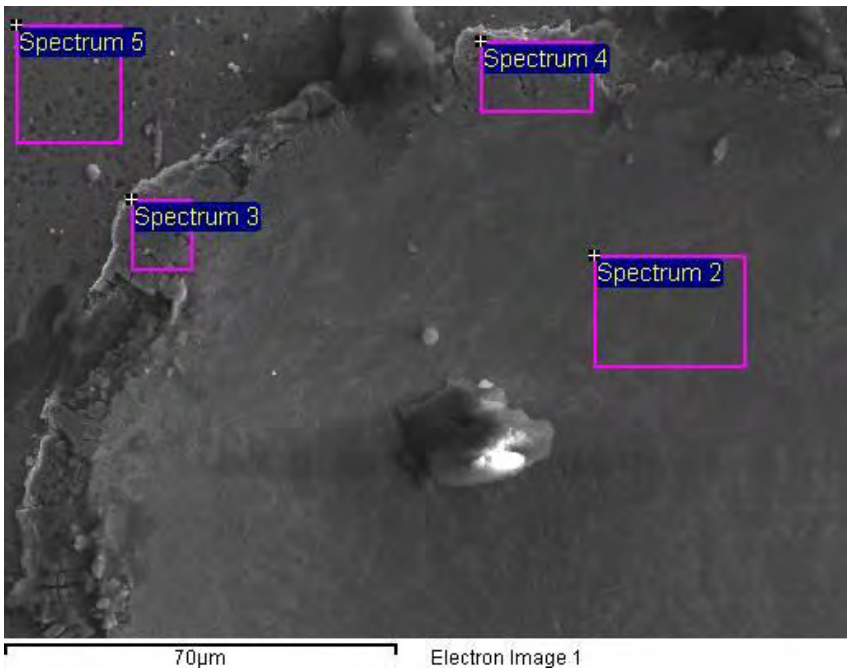

Spectrum	In stats.	C	N	Si	V	Cr	Mn	Fe	Mo	Total
Sum Spectrum	Yes	2.60	6.66	-	1.15	49.53	3.25	35.45	1.82	100.00
Spectrum 2	Yes	3.40	9.19	-	0.29	56.91	-	29.73	1.17	100.00
Spectrum 3	Yes	4.59	11.43	-	-	81.23	1.11	2.17	-	100.00
Spectrum 4	Yes	6.49	12.85	0.09	0.40	71.51	0.11	8.05	0.50	100.00
Spectrum 5	Yes	5.45	9.97	0.03	0.48	83.06	0.29	0.98	-	100.00

Fig. 49: Spot chemical analysis at the end of the scratch track

4.3.3 Sample 9103 (AlTiN+CrN)

- Area of first coating failure

Through the observation of the Al composition by weight in spectrums 2,3 (Fig. 50), it is concluded that the AlTiN coating has been almost entirely removed by the diamond tip. As a result, CrN coating was revealed. The reduction of the composition of Al reaches 97%.

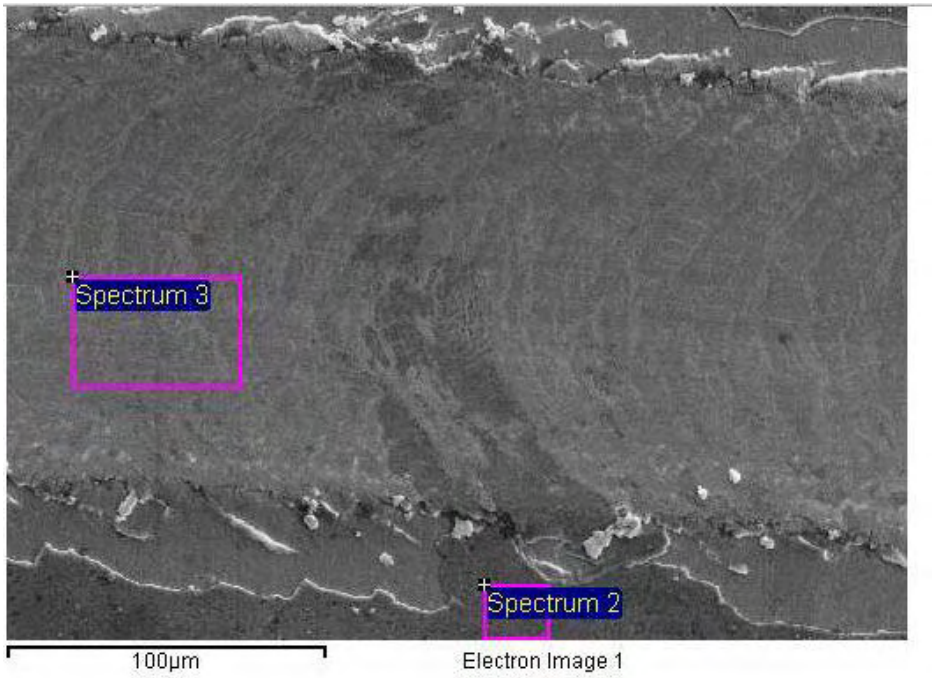

Spectrum	In stats.	Al	Si	Ti	V	Cr	Mn	Fe	Mo	Total
Sum Spectrum	Yes	13.07	0.10	5.71	0.32	51.08	0.34	27.48	1.91	100.00
Spectrum 2	Yes	32.91	0.15	19.90	-	43.77	0.55	2.80	0.25	100.00
Spectrum 3	Yes	0.98	0.63	0.32	0.57	44.67	0.93	49.34	2.55	100.00

Fig. 50: Spot chemical analysis in the area of first coating failure

In Fig. 51, two main areas are observed: a dark area where the composition by weight of Al appears to be increased while this of Cr is reduced and the areas at the limits of the line scan wherein the composition by weight of Cr is higher than this of Al. This fact leads to the conclusion that the dark area contains the AlTiN coating while the lighter one depicts the CrN coating, which was revealed after the removal of the AlTiN coating.

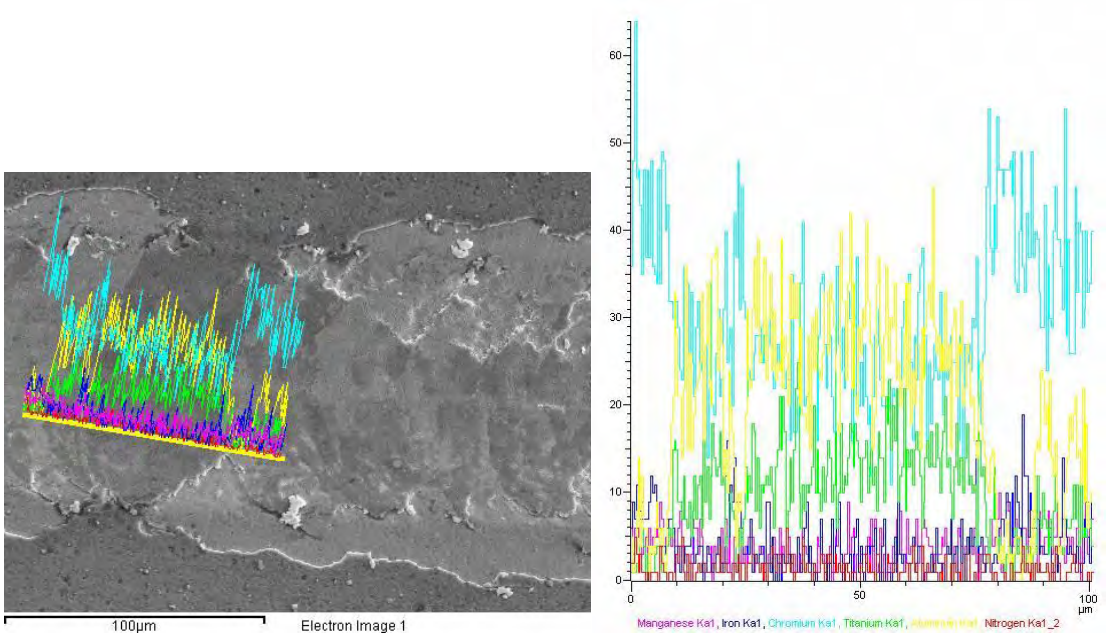

Fig. 51: Line scan parallel to the scratch track

It is obvious that the AlTiN coating was detached as the CrN coating comes off (Fig. 52). The above remark is supported by the results of the previous analysis and by the fact that the composition by weight of the Al is high outside the scratch track, while the Cr composition appears to be low.

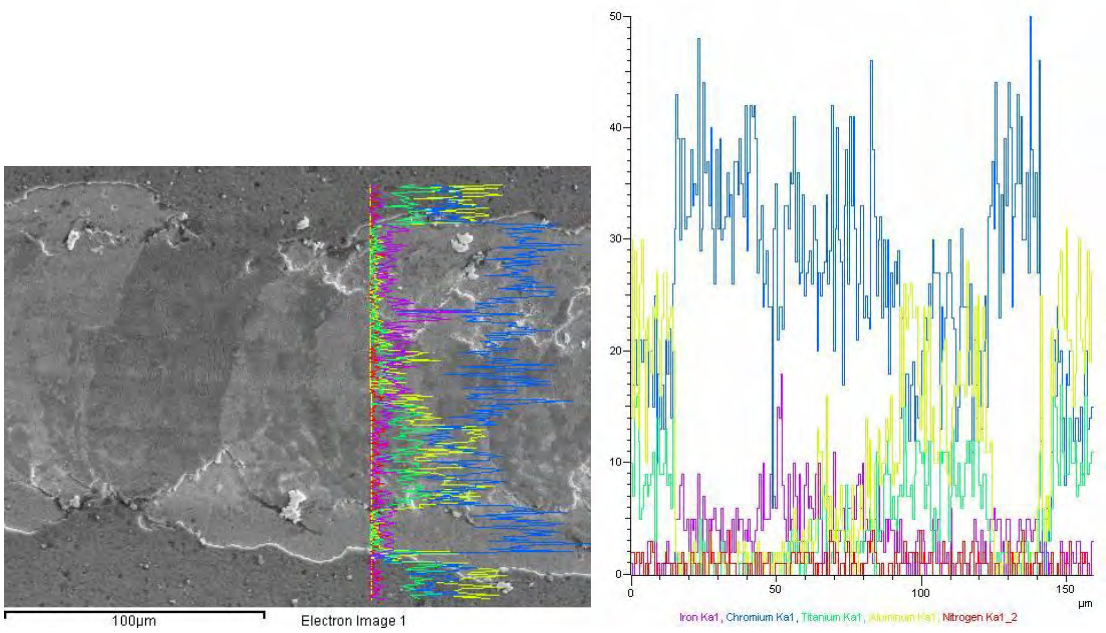

Fig. 52: Line scan transverse to the scratch track

- End of scratch

Inside the scratched area, Cr as well as Fe compositions appear to be increased (Fig. 53). The above fact means that the CrN coating is partially removed by the diamond tip, which caused the substrate revelation. As the line scan proceeds outside the scratch, the Al composition by weight is increased as expected, since the AlTiN coating is on top of the specimen.

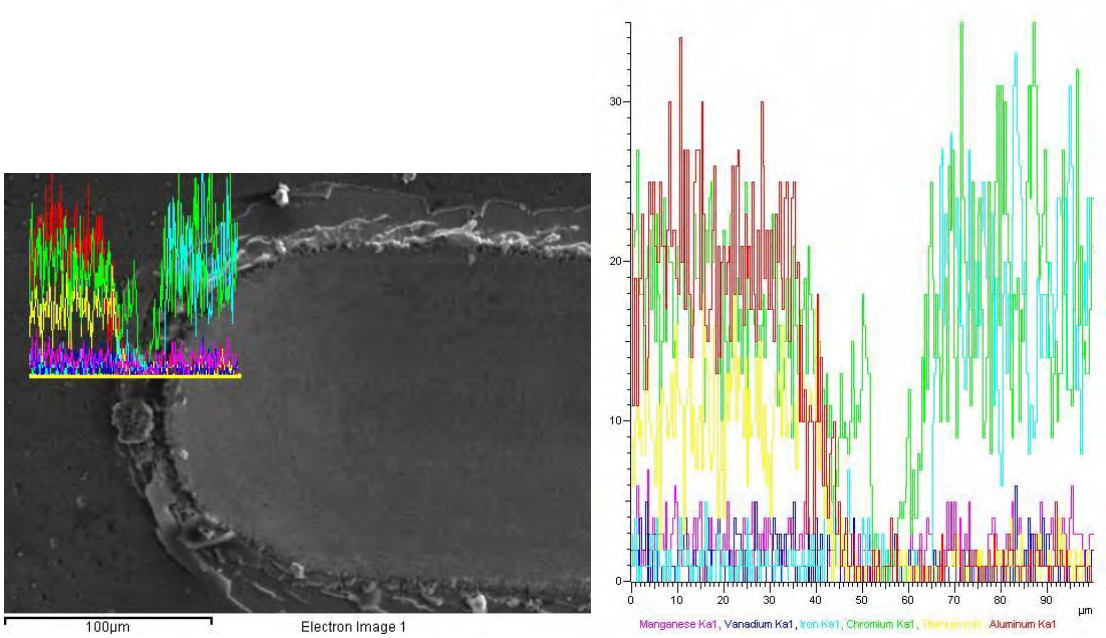

Fig. 53: Line scan at the end of the scratch track

The same conclusion is reached by the spot chemical analysis (Fig. 54). The composition by weight of Al shows a decrease of 98% inside the scratch compared to that inside the scratch. On the contrary, the composition of Fe is increased by 96% inside the scratch than outside of it.

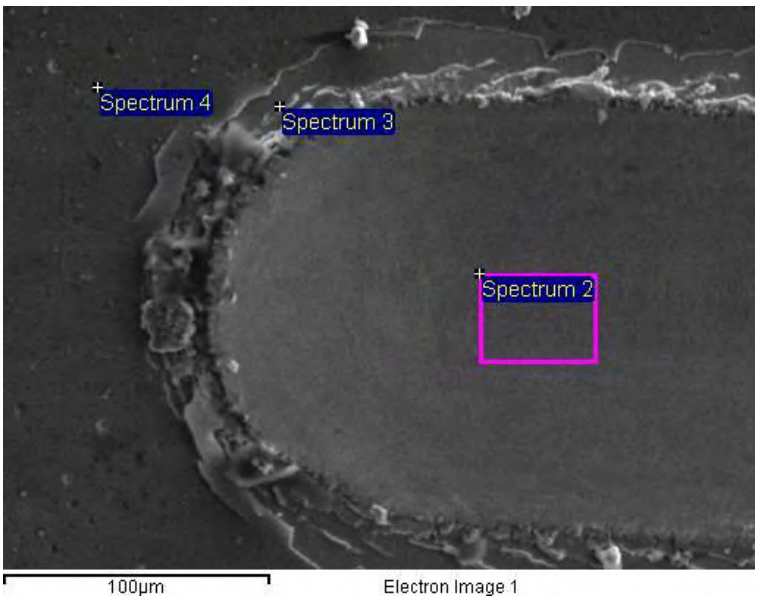

Spectrum	In stats.	Al	Si	Ti	V	Cr	Mn	Fe	Mo	Total
Sum Spectrum	Yes	17.77	0.62	9.33	0.17	42.06	0.10	28.23	1.71	100.00
Spectrum 2	Yes	0.57	0.31	0.37	0.80	26.59	0.20	67.47	3.68	100.00
Spectrum 3	Yes	1.21	0.13	0.91	-	80.26	1.32	16.22	0.18	100.00
Spectrum 4	Yes	33.53	-	19.22	0.16	44.01	0.44	2.61	0.10	100.00

Fig. 54: Spot chemical analysis at the end of the scratch

4.3.4 Sample 9151 (Nitrided+AlTiN)

- Area of first coating failure

It is observed that both the Al and the Ti composition by weight remained almost unchanged compared to the respective compositions outside the scratch path (Fig. 55). Thus, it is concluded that the AlTiN coating has been removed in a small scale by the spherical tip.

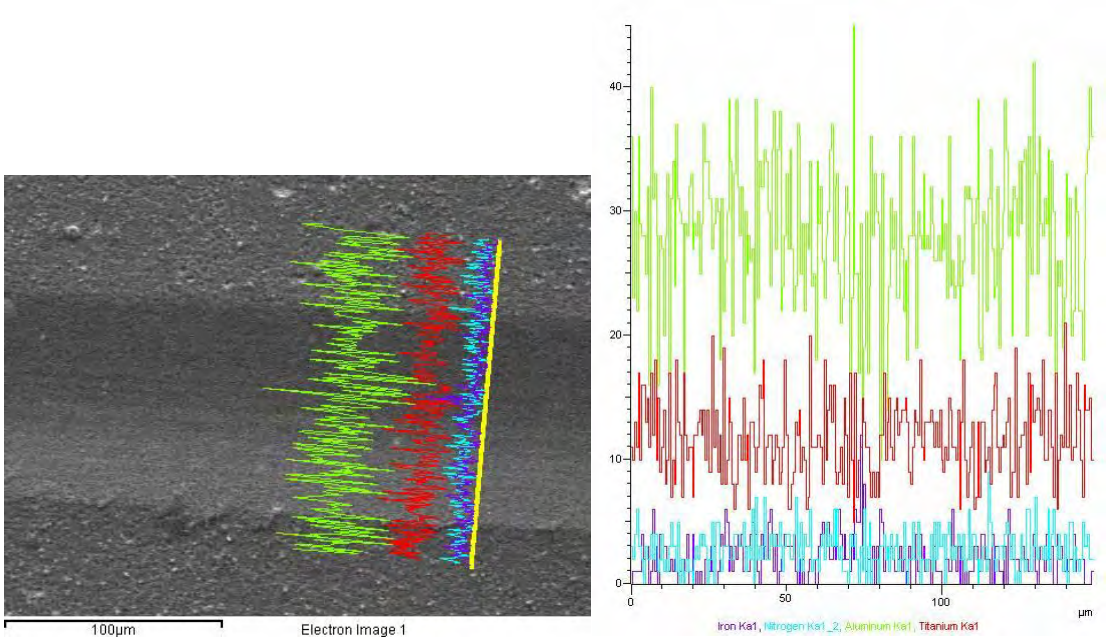

Fig. 55: Line scan transverse to the scratch track

The current illustration (Fig. 56) is similar to the above. More specifically, the compositions of Al and Ti, main components of the AlTiN coating, remained at high level, fact that leads to the conclusion that the coating is attached on the substrate while the tip moves forward.

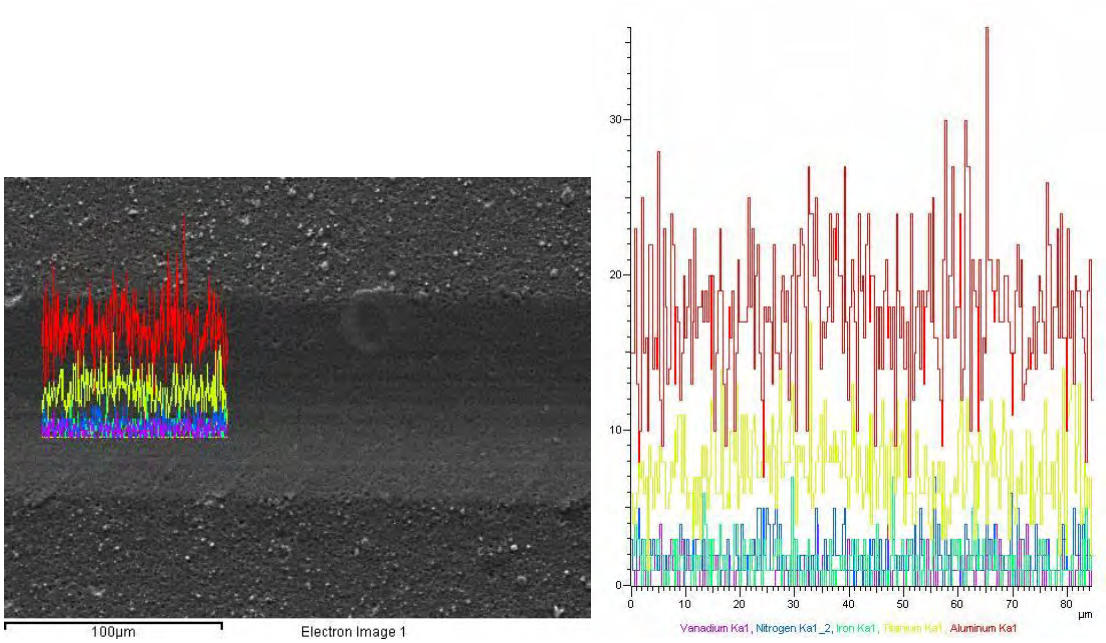

Fig. 56: Line scan parallel to the scratch track

- End of the scratch

At the end of the scratch track, the coating remains attached to the substrate, for as much as Al and Ti are detected (Fig. 57). Although, at the point where the scratch ends, it is observed that the composition of Fe increases rapidly. The above observation leads to the conclusion that the existence of Fe at the end of the scratch is due to the partial substrate drifting by the diamond tip as it moves forward to the scratch track. Fe remained at the scratch path as the tip lifted.

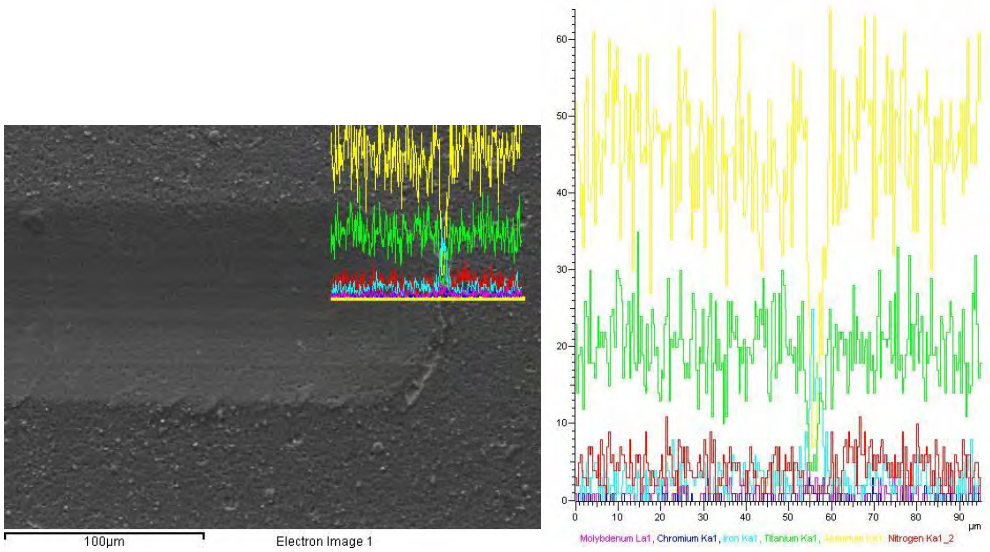

Fig. 57: Line scan at the end of the scratch track

4.3.5 Sample 9152 (Nitrided+CrN)

- Area of first coating failure

The results below (Fig. 58) demonstrate the attachment of the CrN coating on the substrate, as the Cr composition by weight remains high inside the scratch track. As a result, the coating seems to be partially removed by the spherical tip at the area where the first failure occurred.

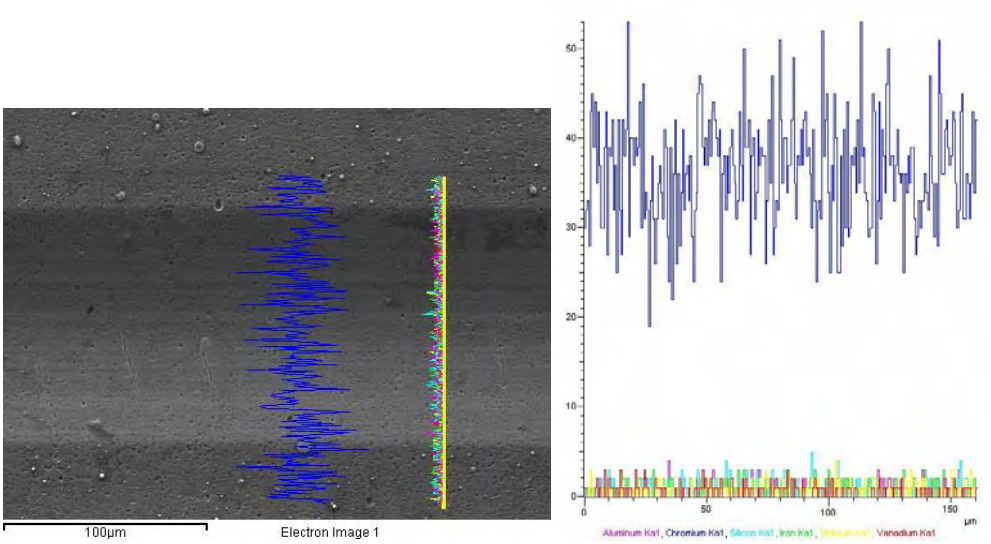

Fig. 58: Line scan transverse to the scratch track

Through the analysis below, becomes clear that inside the area of the pores, the composition of N is radically reduced while Fe is detected in increased composition values (Fig. 59). Consequently, pores are a discontinuity of the coating through which microcracks evolve under progressively increased force.

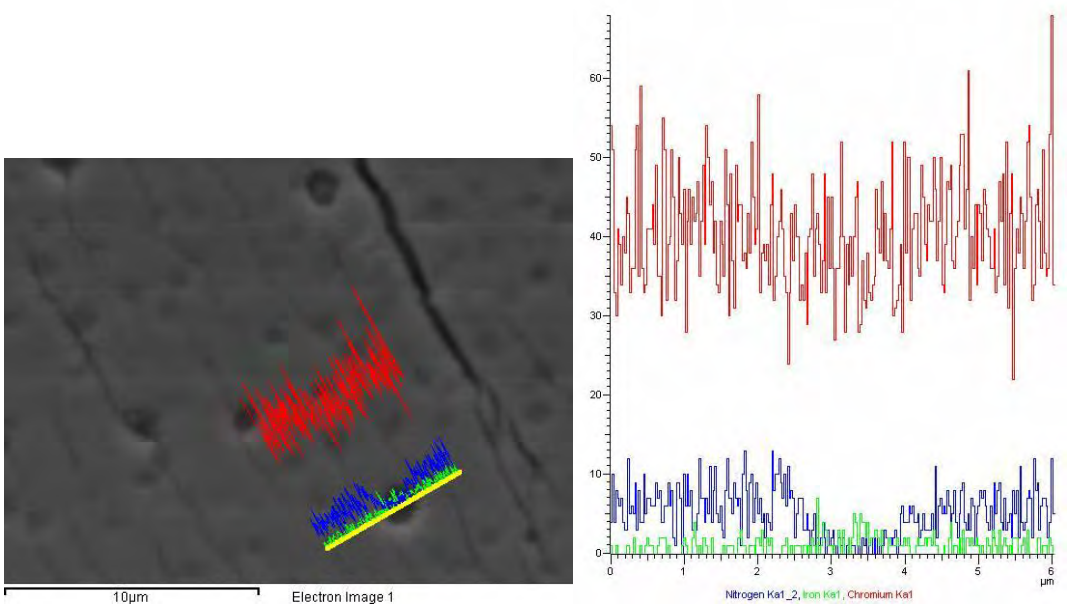

Fig. 59: Line scan on porous surface

In the current area of the scratch track, the existence of the coating is obvious, due to the presence of Cr at high chemical composition levels (Fig. 60). More specifically, inside the microcrack, the compositions by weight of both the coating components (Cr and N) are steeply reduced while Fe is detected at high values. As a result, the growth of microcracks leads to the creation of through-thickness cracks, causing the adhesive failure of the coating.

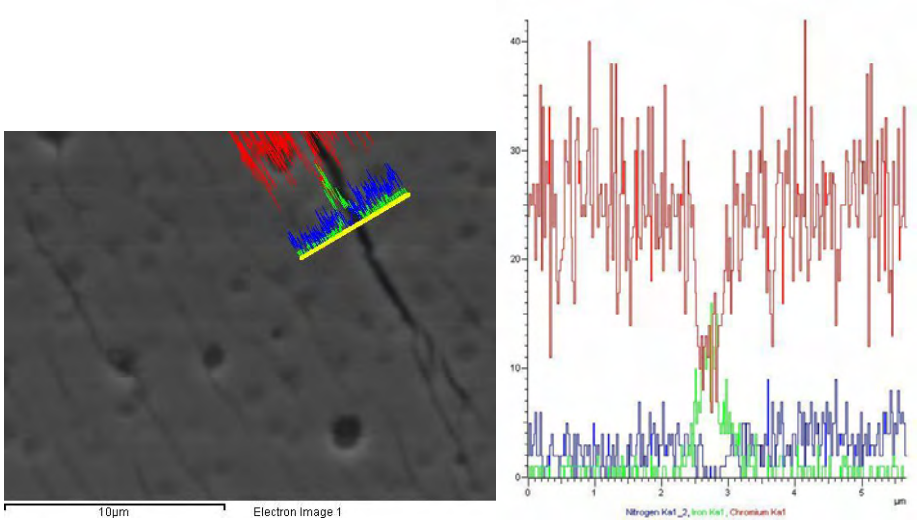

Fig. 60: Line scan on microcrack

- End of the scratch

Through the EDX analysis at the end of the scratch path, it is observed that the chemical composition by weight of Cr is slightly decreased compared to the respective composition at the area where the first coating failure occurred (Fig. 61). It should be also highlighted that Cr is one of the alloying elements of the substrate in low composition (3%). At the end of the scratch, Cr is detected at higher percentages, fact that leads to the conclusion that the CrN coating has not been entirely removed by the diamond tip.

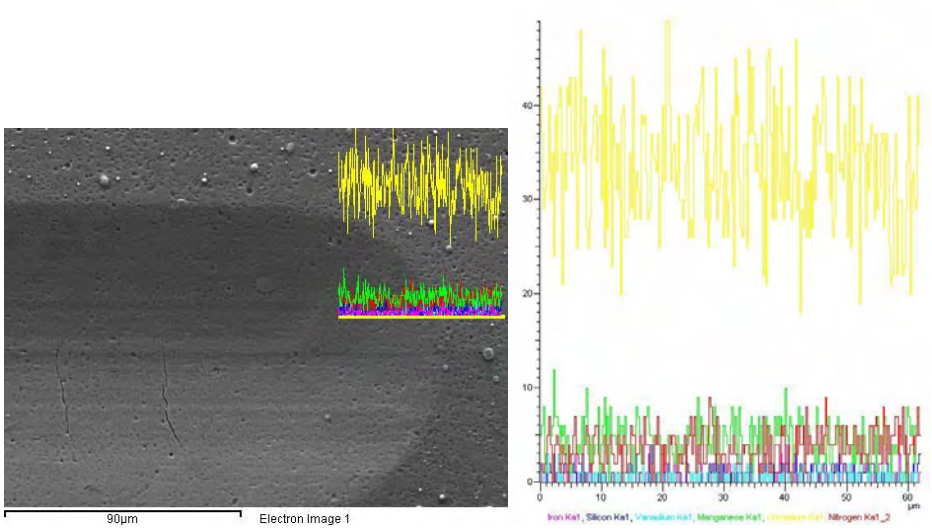

Fig. 61: Line scan at the end of the scratch track

4.3.6 Sample 9153 (Nitrided+AlTiN+CrN)

- Area of first coating failure

The EDX analysis at the area where the first coating failure occurred (Fig. 62) reveals that the chemical compositions of both Al and Ti are slightly reduced while Cr has increased composition value (Table 7). At this point, it should be mentioned that the AlTiN coating lies on top and CrN coating is between the AlTiN coating and the substrate. Thus, the simultaneous composition alternations take place due to the partial removal of the AlTiN coating by the spherical tip.

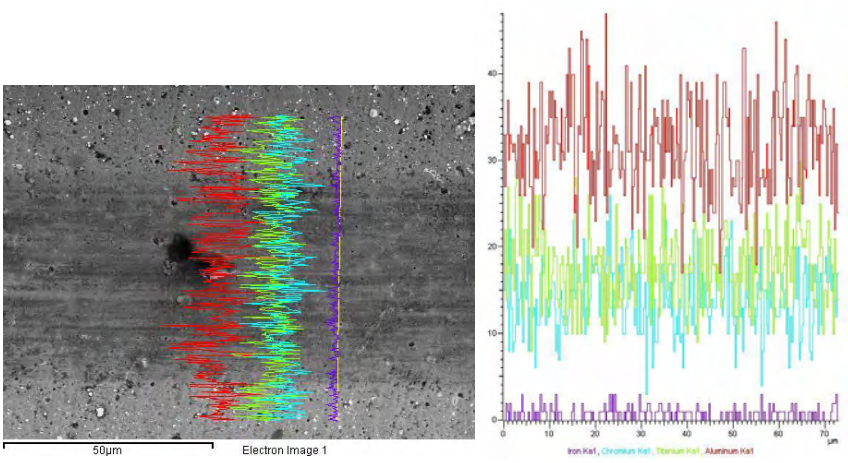

Fig. 62: Line scan transverse to the scratch track

The same conclusion is reached by the above data (Fig. 63). Al as well as Ti show decreased composition by weight values while CrN coating is partially revealed on top of the surface. As the implied load increases, AlTiN coating is being peeled off.

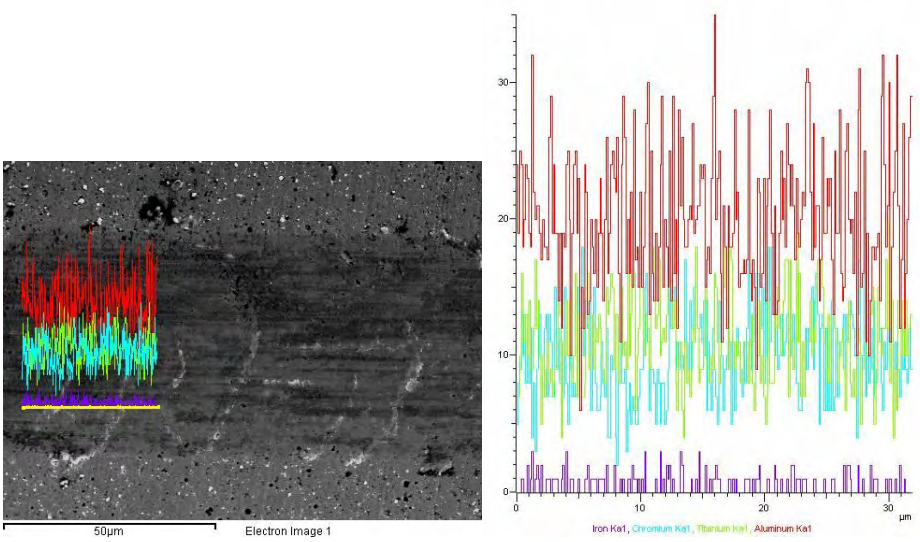

Fig. 63: Line scan parallel to the scratch track

- End of the scratch

The current illustration (Fig. 64) provides useful information in order to define the coating failure mode. It is concluded that the dark area of the scratch (spectrum 2) corresponds to the AlTiN coating while the bright area (spectrum 3) depicts the CrN coating. The above fact leads to the conclusion that the coating has not been entirely removed by the spherical tip. Furthermore, the material which has been drifted on the scratch edge mainly consists of Cr and Fe, which means that the diamond tip peeled off one part of the CrN coating as well as of the substrate during the conduction of the scratch test. Consequently, high values of Cr and Fe composition by weight were detected at the end of the scratch, mainly on the chipped material. Line scan at the end of the scratch track (Fig.65) leads to the same conclusions.

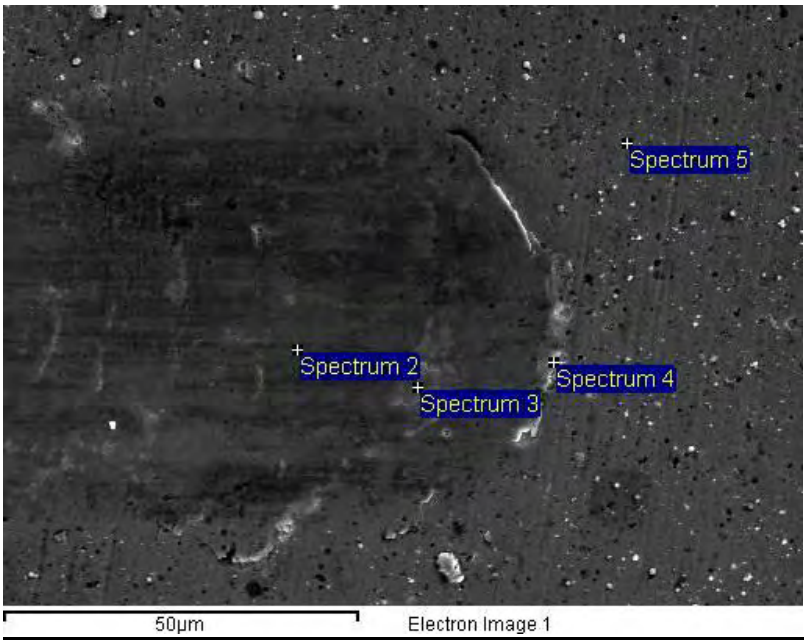

Spectrum	In stats.	Al	Si	Ti	V	Cr	Mn	Fe	Mo	Total
Sum Spectrum	Yes	33.58	0.02	25.16	0.71	37.68	0.76	1.81	0.30	100.00
Spectrum 2	Yes	38.95	0.39	29.64	0.74	28.18	0.25	1.41	0.43	100.00
Spectrum 3	Yes	5.60	0.27	2.84	-	87.04	1.01	3.41	-	100.00
Spectrum 4	Yes	1.51	0.28	0.88	0.46	42.76	-	50.81	3.36	100.00
Spectrum 5	Yes	41.31	0.23	36.16	0.13	21.28	0.10	0.89	-	100.00

Fig. 64: Spot analysis at the end of the scratch track

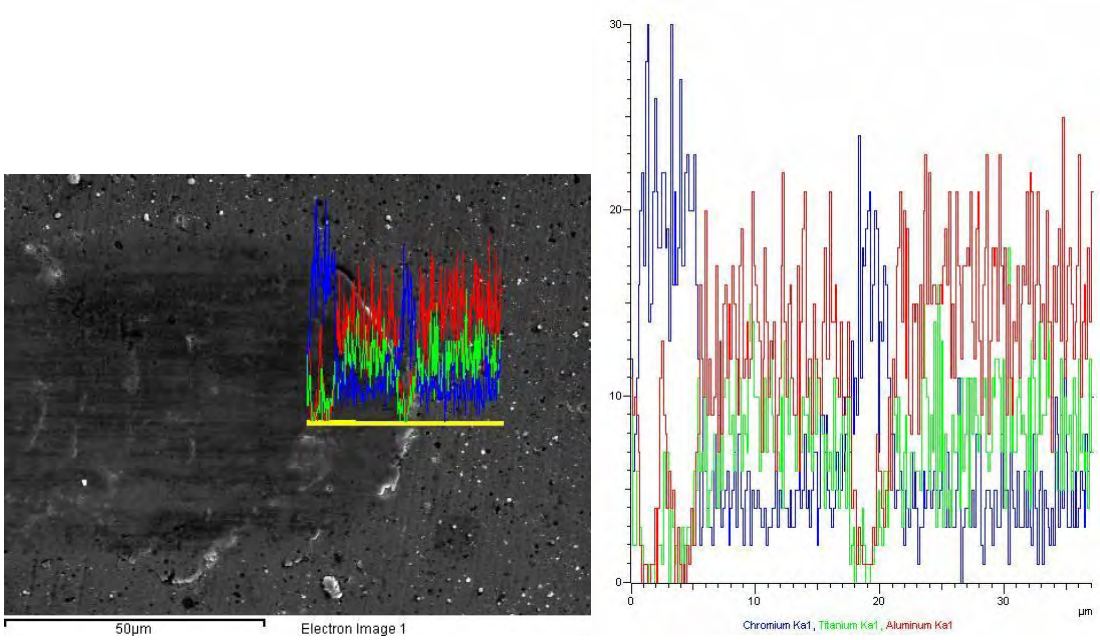

Fig. 65: Line scan at the end of the scratch track

4.4 AFM Analysis

Typical measurements were taken from the specimen's #9152 scratched surface. More specifically, the scratches corresponding to tests no. 1,2 were analyzed.

- Test no. 1

The initial stage of the analysis included a 3-D display of the scratch (Fig. 66) as well as line scan measurements (Fig. 67) before the area where the first coating failure occurred:

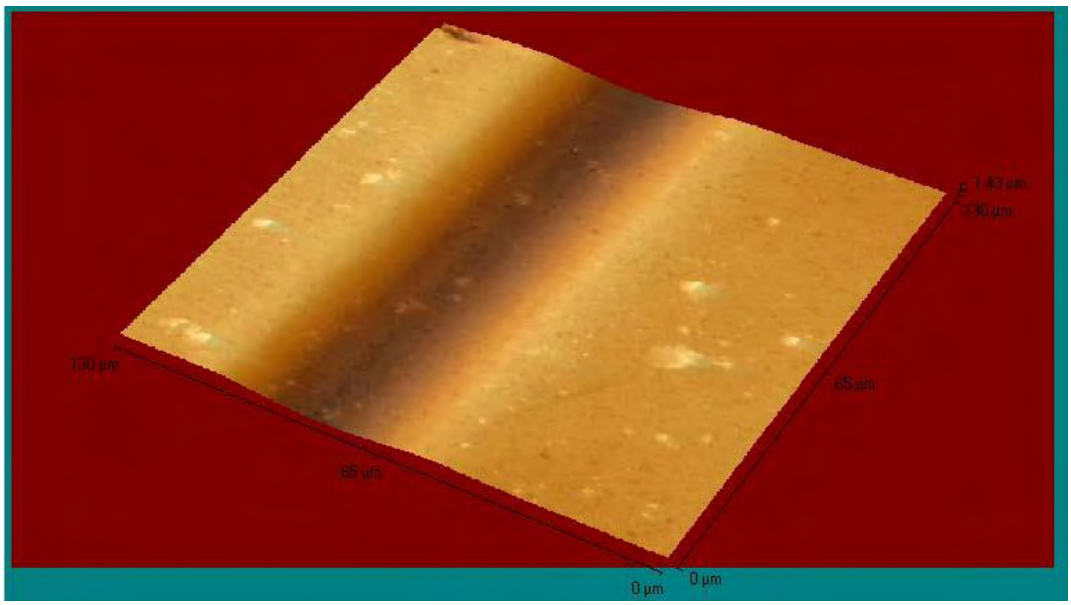

Fig. 66: The area before the point where the first coating failure occurred

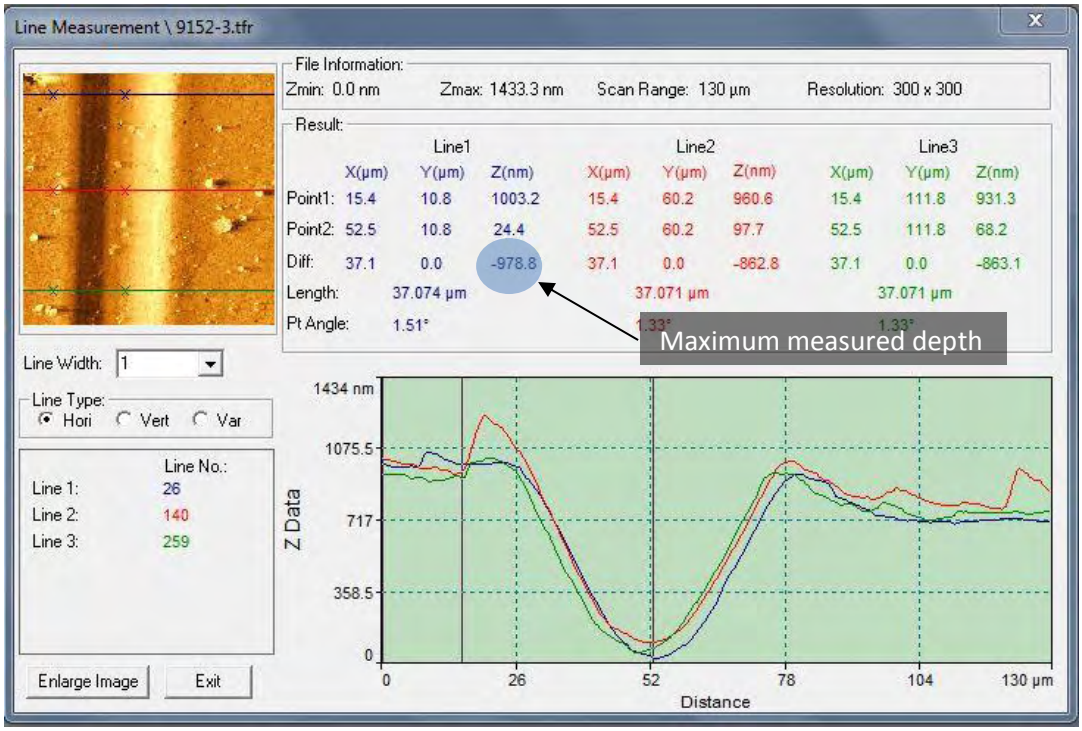

Fig. 67: Line scan measurements before the first coating failure occurred

The depth of the scratch was measured in order to find out if the coating was entirely detached from the spherical tip. As it is shown in Fig. 67, the maximum measured depth of the scratch in this area is 0,98µm, lower than the coating thickness (2µm).

A 3-D depiction of the area where the first coating failure occurred is provided in Fig. 68:

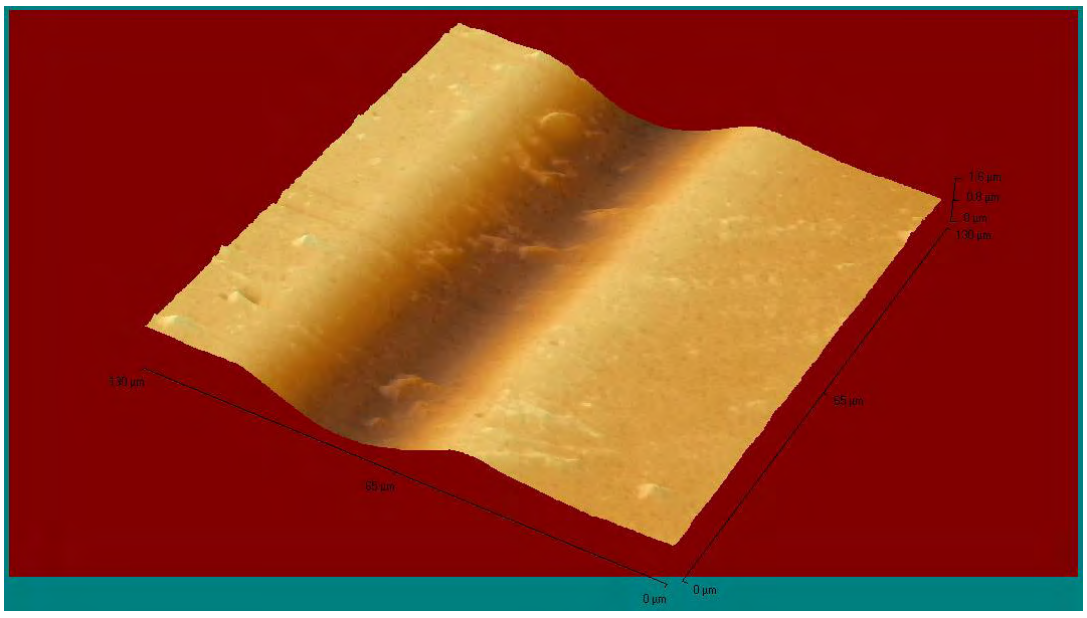

Fig. 68: The area where the first coating failure occurred

As it is shown in Fig. 69, the maximum depth of the scratch at this area is 1,18 µm, lower than 2µm, which corresponds to the coating thickness.

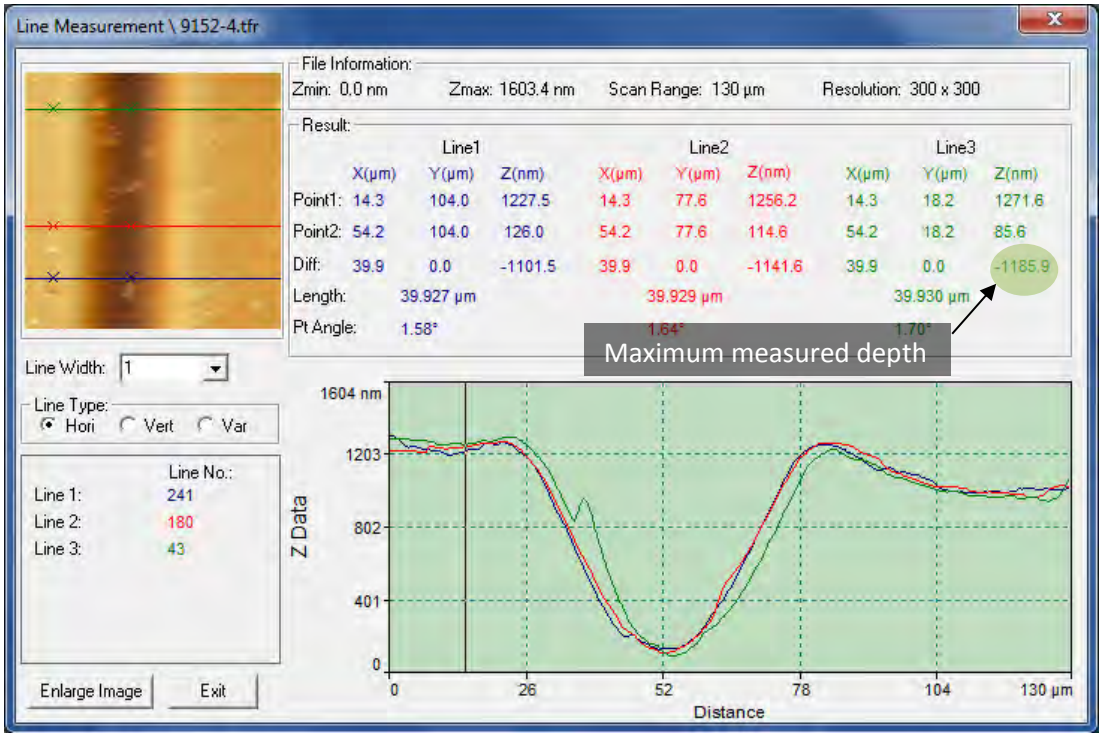

Fig. 69: Line scan measurements in the area where the first coating failure occurred

Therefore, it is concluded that, in the area where the first coating failure occurred, the coating has not entirely removed by the diamond tip.

The scratched area after the appearance of the first coating failure is provided in Fig. 70:

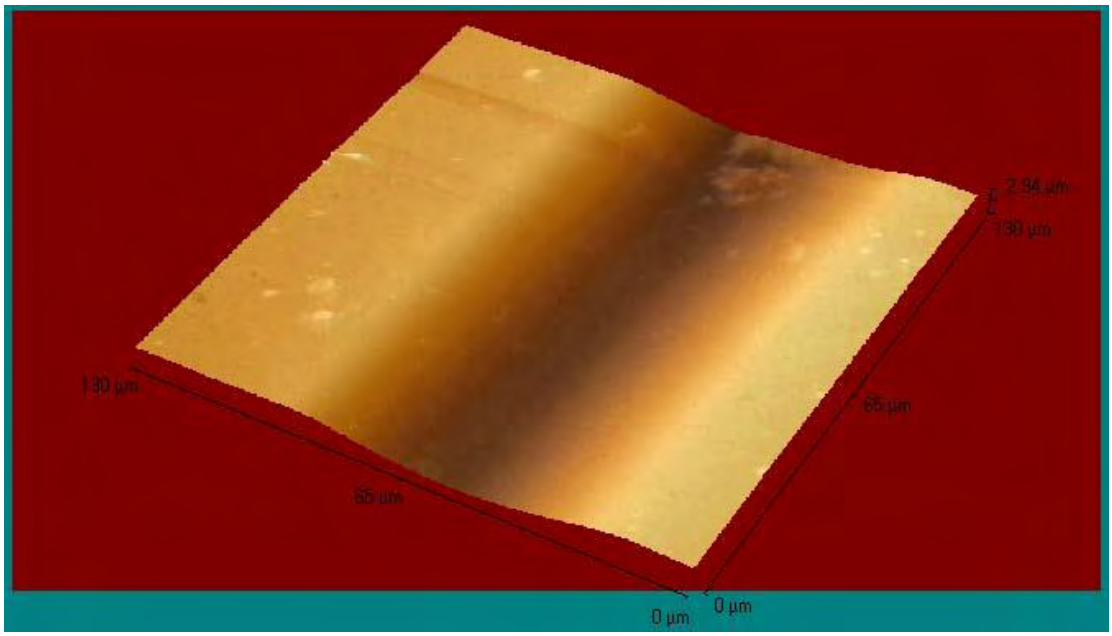

Fig. 70: The area after the appearance of the first coating failure

Line scan measurements in the current area (Fig. 71) provide useful information about the depth of the scratch.

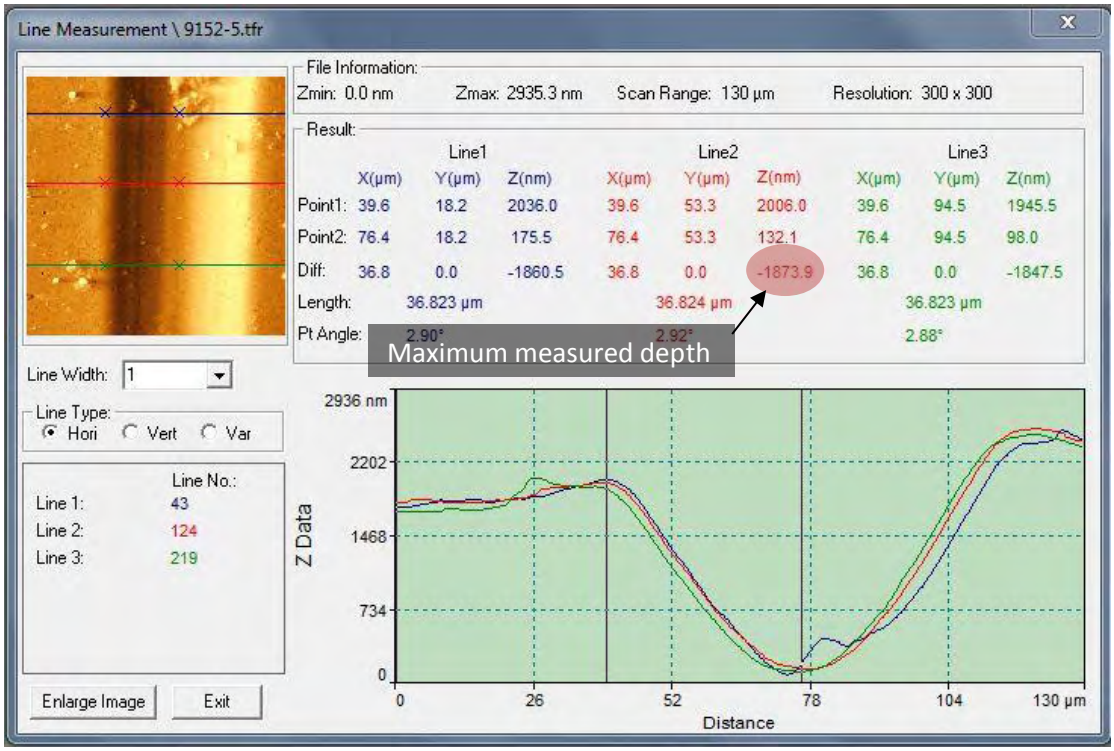

Fig. 71: Line scan measurements in the area after the appearance of the first coating failure

The maximum depth of the scratch in this area equals to 1,87µm. Thus, it is concluded that the coating has not been entirely removed by the spherical tip.

- <u>Test no. 2</u>

The initial stage of the analysis included a 3-D display of the scratch (Fig. 72) as well as line scan measurements (Fig. 73) before the point where the first coating failure occurred:

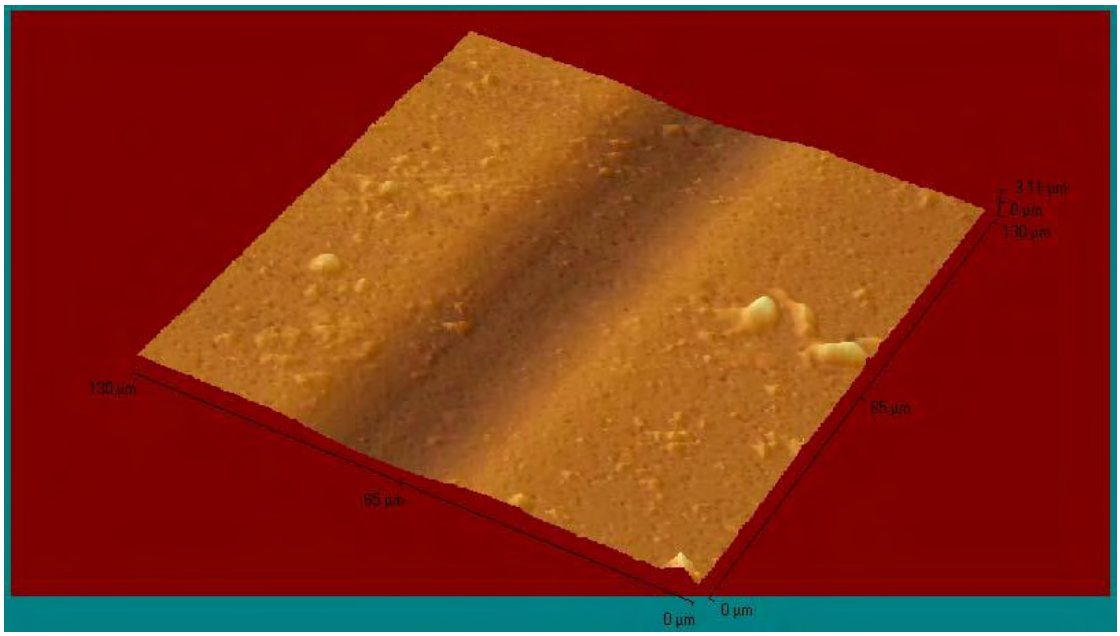

Fig. 72: The area before the point where the first coating failure occurred

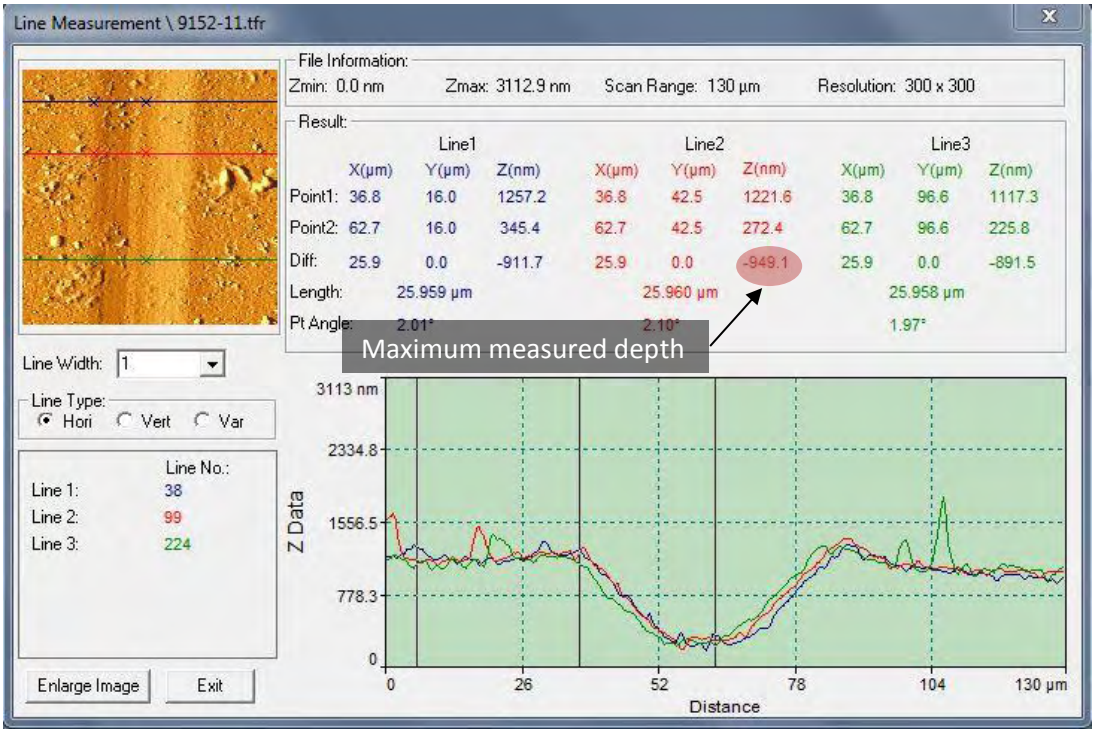

Fig. 73: Line scan measurements before the first coating failure occurred

In the current area, the maximum measured depth was found 0,95µm, fact that leads to the conclusion that the coating remains attached on top of the substrate.

A 3-D depiction of the area where the first coating failure occurred is provided in Fig. 74:

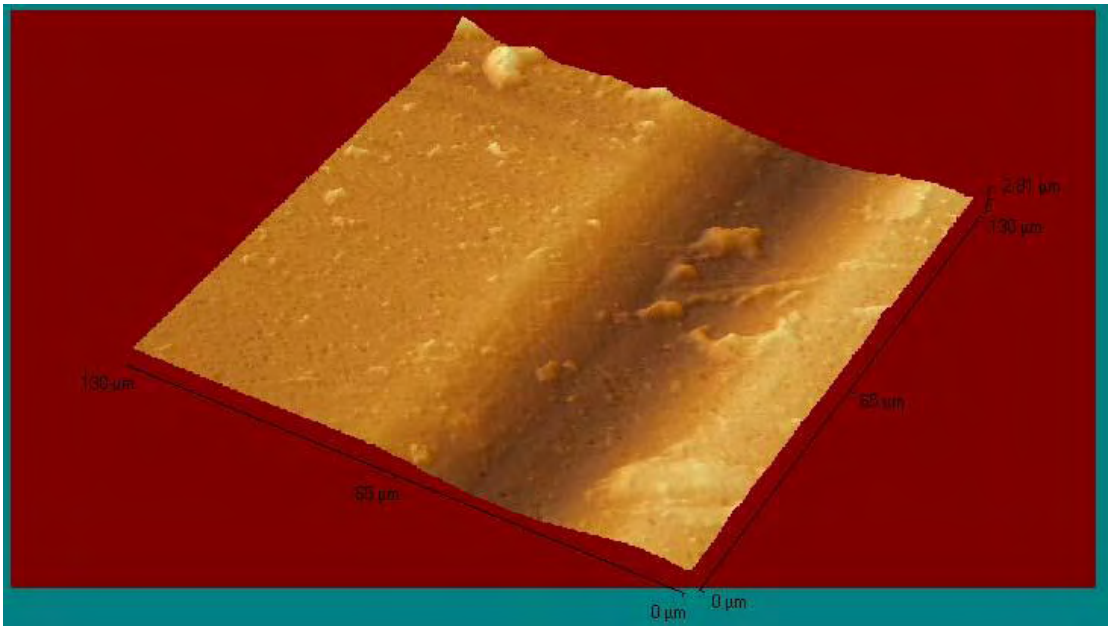

Fig. 74: The area where the first coating failure occurred

As it is shown in Fig. 75, the maximum depth of the scratch at this area is 1,31 μm, lower than 2μm, which corresponds to the coating thickness.

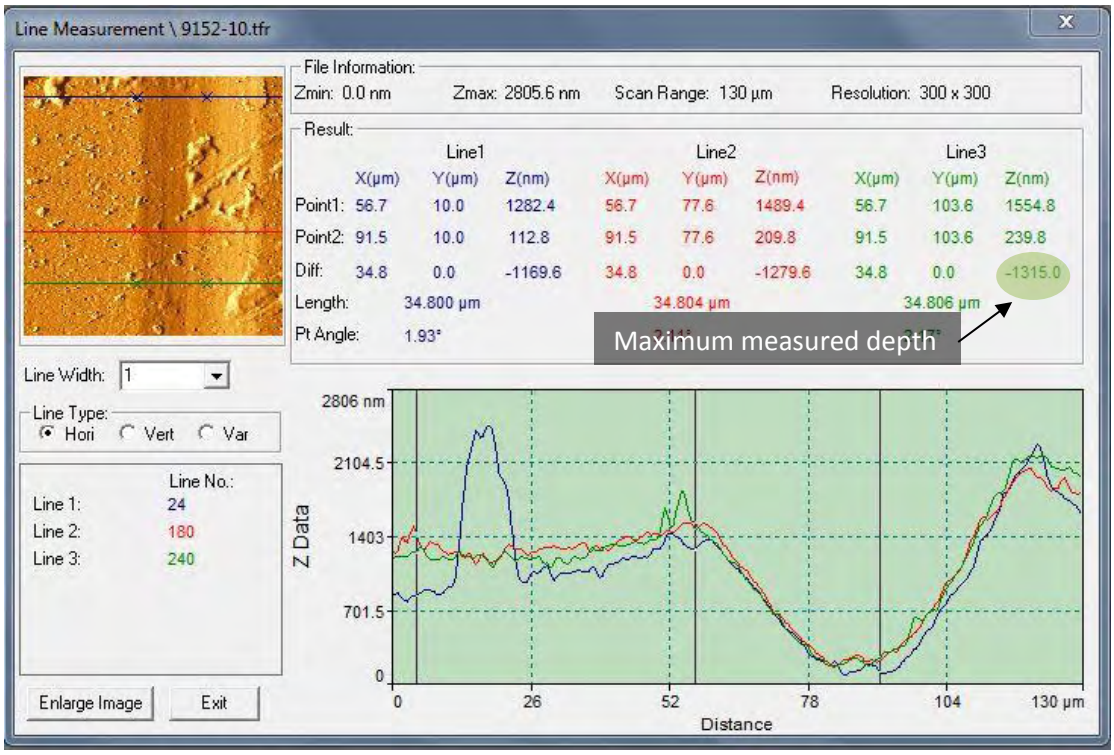

Fig. 75: Line scan measurements in the area where the first coating failure occurred

Therefore, it is concluded that, in the area where the first coating failure occurred, the coating has not entirely removed by the diamond tip.

The scratched area after the appearance of the first coating failure is provided in Fig. 76:

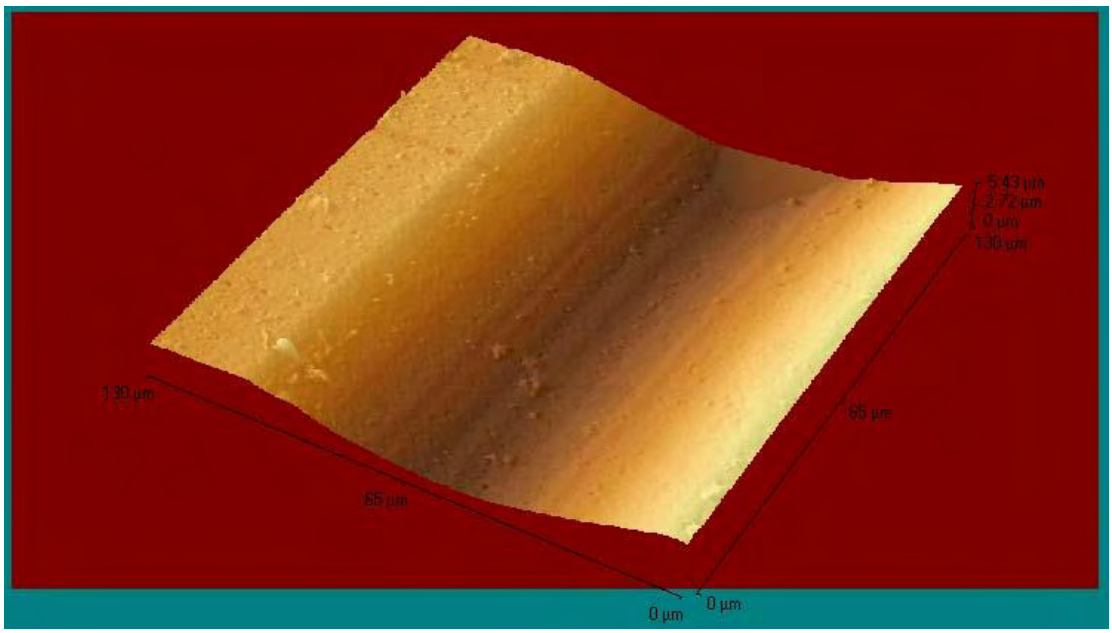

Fig. 76: The area after the appearance of the first coating failure

It is observed that the width of the scratch increases, compared to the previous stages of the analysis.

Line scan measurements in the current area (Fig. 77) provide useful information about the depth of the scratch.

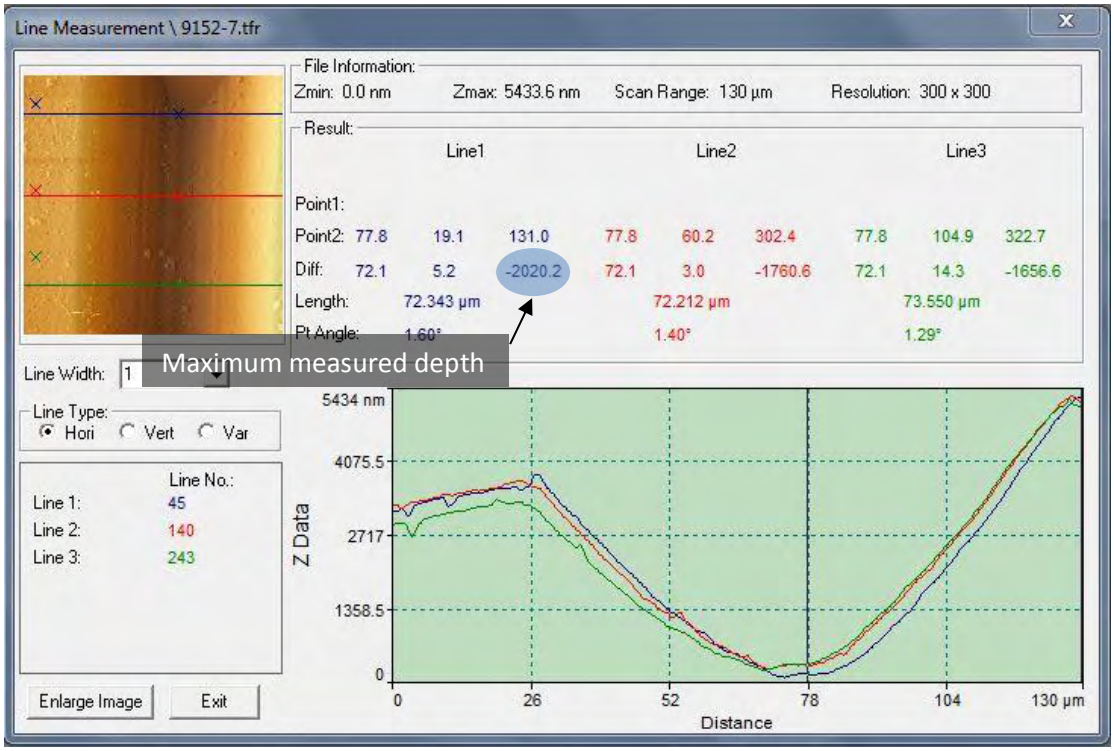

Fig. 77: Line scan measurements in the area after the appearance of the first coating failure

The maximum measured depth in the current area equals to 2,02µm while the coating thickness is 2µm. Therefore, it is concluded that, in the middle of the scratch track, the coating has been removed entirely by the diamond tip.

Chapter 5: Conclusions & Discussion

5.1 Coating Failure Analysis

Taking into consideration the results which presented in Chapter 4, the evolution of the failure pattern in each specimen during the scratch test is proposed in Table 15:

Table 15: Evolution of the coatings' failure pattern of each specimen

Material code	Treatment	Hardness ($HV_{0.01}$)	Coating failure pattern	Coating failure type
9101	AlTiN	1782±4	Buckling→ Chipping→ Microcracks	Adhesive
9102	CrN	1739±2	Angular cracks→ Semicircular cracks→ Buckling→ Chipping	Cohesive
9103	AlTiN+CrN	1940±3	Angular cracks→ Semicircular cracks→ Buckling→ Chipping→ Recovery spallation	Cohesive
9151	Nitrided+AlTiN	2167±2	Angular cracks→ Semicircular cracks→ Chipping	Cohesive
9152	Nitrided+CrN	2018±2	Angular cracks→ Semicircular cracks	Cohesive
9153	Nitrided+AlTiN+CrN	2272±1	Angular cracks→ Semicircular cracks→ Buckling→ Chipping	Cohesive

It is important to note that the information gathered on Table 15 present only some general facts about the failure mode that appeared when the L_c recorded. As a result, the influence of gas nitriding should be taken under consideration and examined separately.

5.2 The influence of Gas Nitriding

The gas nitriding process plays an important role on the specimen's performance during the conduction of scratch tests.

The comparison between the non-nitrided samples to the respective nitrided could provide remarkable information about their adhesion behavior.

In Fig. 78 below, the comparison between the AlTiN coated samples lead to the conclusion that the non-nitrided specimen failed under higher applied loads than the nitrided one.

On the contrary, it was observed that the coating layer was partially detached from the non-nitrided substrate while the nitrided specimen faced cohesion issues. As a result, in this case the process of nitriding did not offer increased performance as it concerns the scratch resistance of the AlTiN coated steels, except for slight variations at the failure mode of each coating.

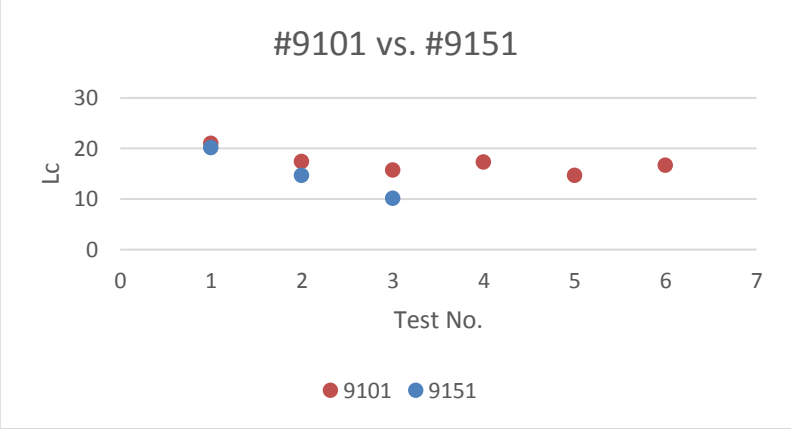

Fig. 78: Critical loads of AlTiN coated specimens

Moving on, in the case of the CrN coated samples, gas nitriding offers enhanced resistance to coating failure, as it is shown on Fig. 79. More specifically, during the conduction of scratch tests, the nitrided specimen faced a cohesive failure mode while on the surface of the non-nitrided sample both cohesive and adhesive failure modes were identified, notwithstanding the lower applied forces. Consequently, gas nitriding improved the performance of the CrN coated steel.

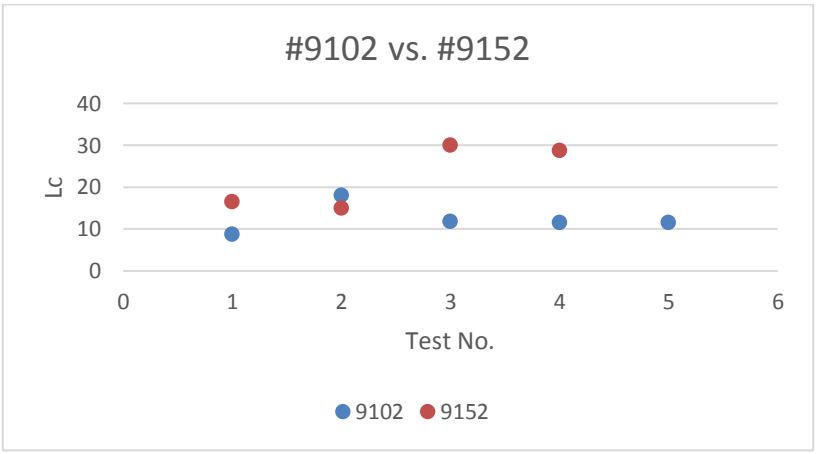

Fig. 79: Critical loads of CrN coated specimens

As concerns the double layer coated specimens, the conclusion that comes from the diagram in Fig. 80 is related to the nitrided sample's high resistance to fail. Thus, the gas nitriding process ameliorated the performance of the AlTiN/CrN coated DIN 1.2999 steel. A closer look to the failure modes that took place during the conduction of the scratch tests, lead to the conclusion that the nitrided specimen presented improved resistance to coating detachment, while in case of the non-nitrided steel recovery spallation was observed (AlTiN and CrN coatings were split).

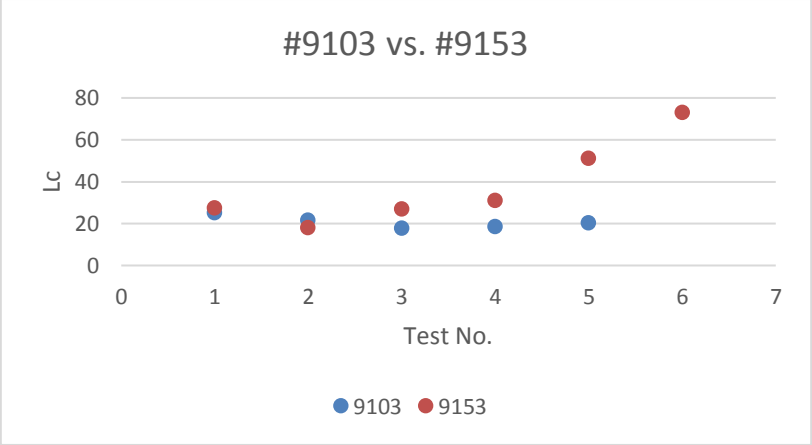

Fig. 80: Critical loads of the AlTiN+CrN coated specimens

5.3 Future Work Recommendations

The first stage of future work should be a complete AFM analysis of each specimen in order to acquire more data about the coatings' failure modes.

The study of the transverse cross-sections of each scratch could also provide additional information about the failure modes that occurred in every specimen.

Finally, the conduction of wear tests employing a pin on disc tribometer could provide useful results as it concerns the wear and friction resistance of each specimen.

References

[1] Holmberg K., Matthews A., *Coatings tribology, properties, mechanisms, techniques and applications in surface engineering*, 2nd ed., Elsevier, Oxford, 2009.

[2] Miyoshi K., *Solid lubrication: Fundamentals and Applications*, Marcel Deccer Inc., 2001.

[3] Jost P., *Tribology – Origin and future*, Wear, 136, 1 – 17, 1990.

[4] Communication with Kocaeli University (Research team: Gülşah Aktaş, Şeyda Polat, Ş. Hakan Atapek), Kocaeli, Turkey.

[5] Lapadatu D., Hambli R., Kobi A., Barreau., *Statistical investigation of die wear in metal extrusion processes*, International journal of advanced manufacturing technologies, 28, 272 – 278, 2006.

[6] Reggiani B., Donati L., Zhou J., Tomesani L., *The role of creep and fatigue in determining the high-temperature behaviour of AISI H11 tempered steel for aluminum extrusion dies*, Journal of Materials Processing Technology, 210, 1613-1623, 2010.

[7] Arif A.F.M., Sheikh A.K., Qamar S.Z., *A study of die failure mechanisms in aluminum extrusion*, Journal of Materials Processing Technology, 134, 318-328, 2003.

[8] Saha P., *Aluminum Extrusion Technology*, ASM International, Ohio, 2000.

[9] Heavens O. S., *Some factors influencing the adhesion of films produced by vacuum evaporation*, J. Phys. Radium, 11 (7), 355-360, 1950.

[10] Benjamin P., Weaver C., *Measurement of adhesion on thin films, Proccedings of the Royal Society*, 254, 163-176, 1960.

[11] Chalker P. R., Bull S.J., Rickerby D.S., *A review of the methods for the evaluation of coating-substrate adhesion*, Materials Science and Engineering, A140, 583-592, 1991.

[12] K.H. Lau, K.Y. Li, Y-W. Mai*, Influence of hardness ratio on scratch failure of coatings*, Int. J. of Surface Science and Engineering, 1,1, 3 – 21, 2007.

[13] Larsson M., Hedenqvist P., Hogmark S., *Deflection measurements as method to determine residual stress in thin hard coatings on tool materials*. Surf. Engineering, Vol. 12, No. 1, 43–48, 1996.

[14] Bull S. J., *Failure mode maps in the thin film scratch adhesion test,* Tribology International, Vol. 30, No. 7, 491 – 498, 1997.

[15] J.C.A. Batista, C. Godoy, V.T.L. Buono, A. Matthews*, Characterization of duplex and non-duplex (Ti, Al) N and Cr–N PVD coatings,* Materials Science and Engineering A336 (2002) 39–51.

[16] Birol Y., Yuksel B., *Performance of gas nitrided and AlTiN coated AISI H13 hot work tool steel in aluminum extrusion,* Surface & Coatings Technology 207 (2012) 461–466.

[17] DIN 1.2999 tool steel chemical composition:
http://www.steeldata.info/tempering/demo/html/1186.html

[18] Kuiry S*., Advanced scratch testing for evaluation of coatings*, Bruker Nano Surfaces Division, 2012.

[19] Batista J.C.A, Godoy C., Pintaudec G., Sinatora A., Matthews A., *An approach to elucidate the different response of PVD coatings in different tribological tests*, Surface and Coatings Technology 174 –175, 891–898, 2003.

Appendix: Acoustic Emission to Load Charts

A: Sample 9101

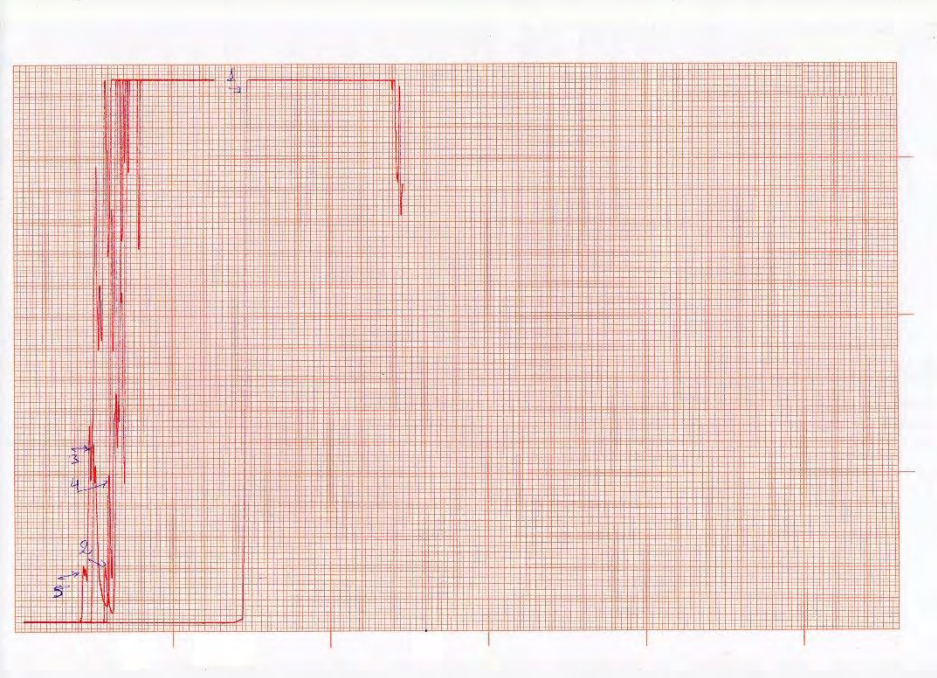

Fig. 81: Acoustic emission to load charts for tests no. 1-5

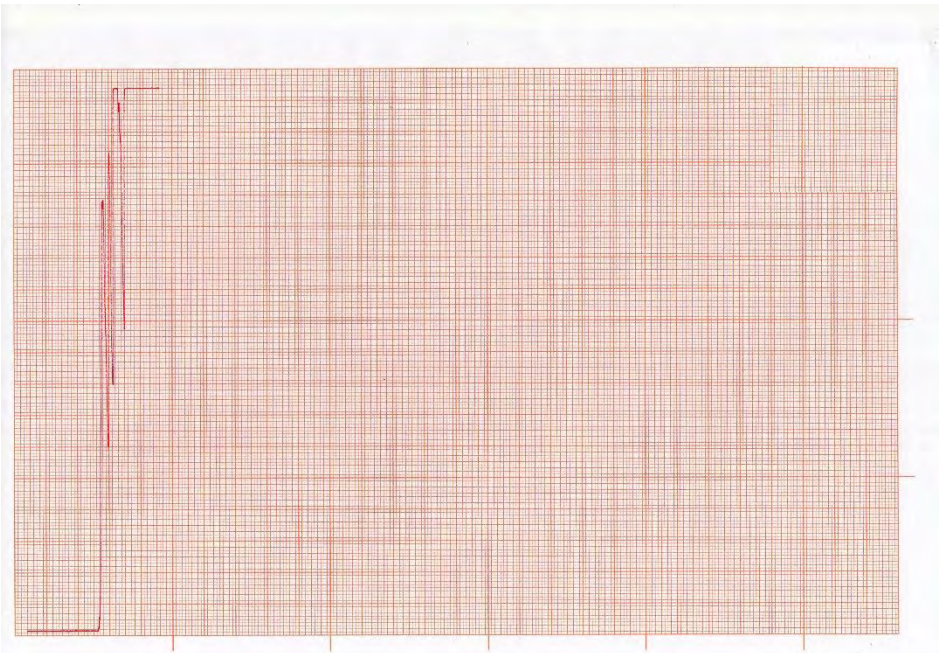

Fig. 82: Acoustic emission to load chart for test no. 6

B: Sample 9102

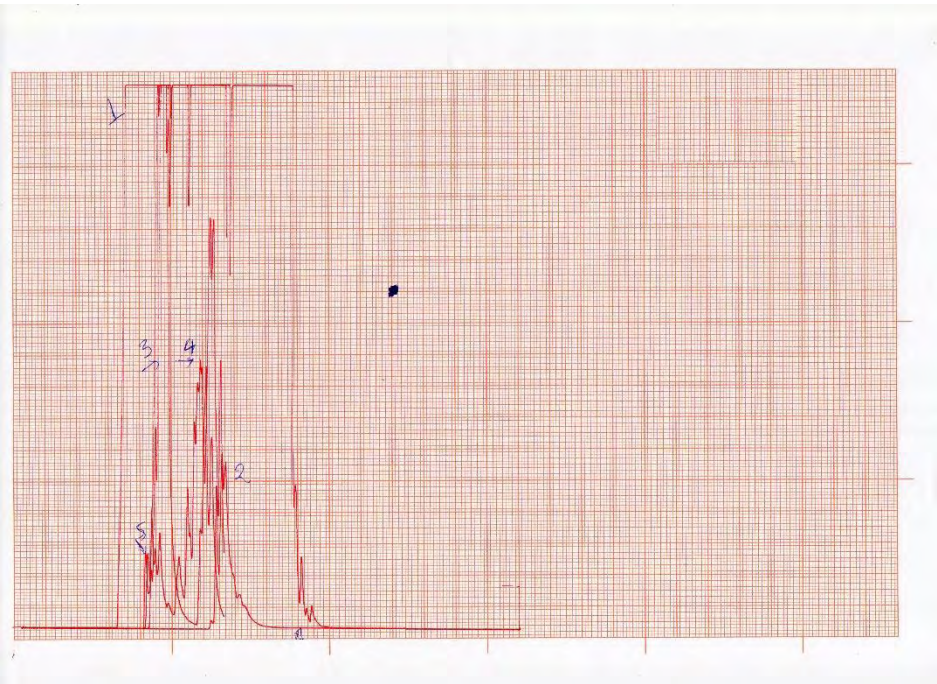

Fig. 83: Acoustic emission to load charts for tests no. 1-5

C: Sample 9103

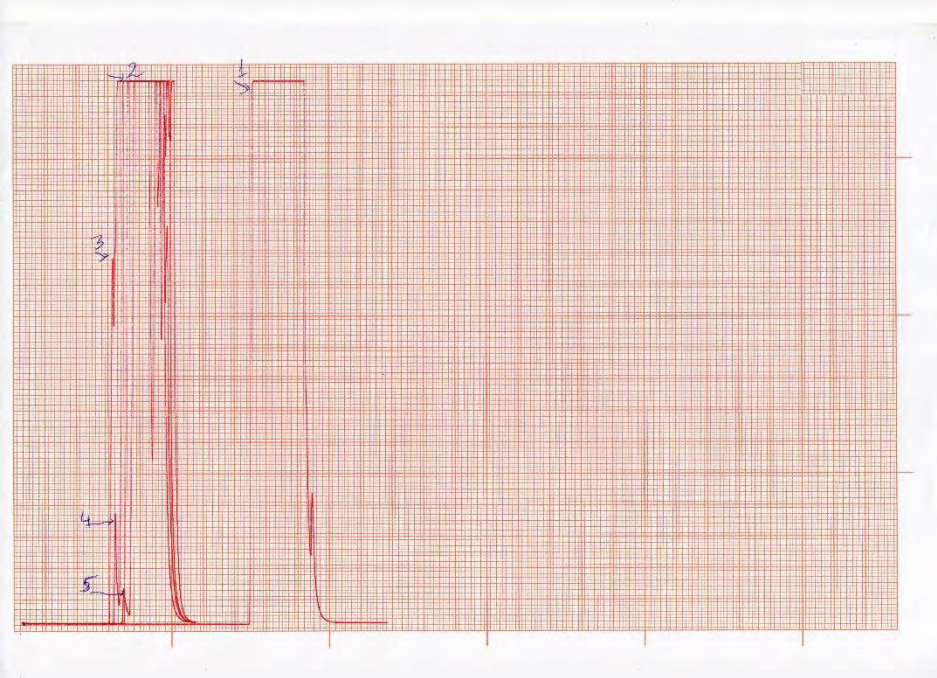

Fig. 84: Acoustic emission to load charts for tests no. 1-5

D: Sample 9151

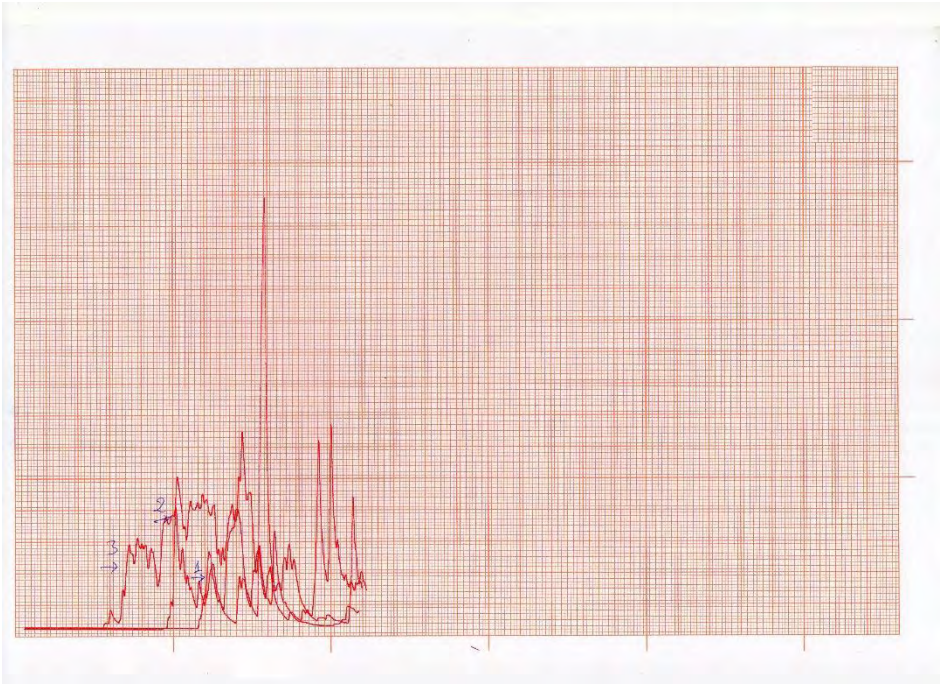

Fig. 85: Acoustic emission to load charts for tests no. 1-3

E: Sample 9152

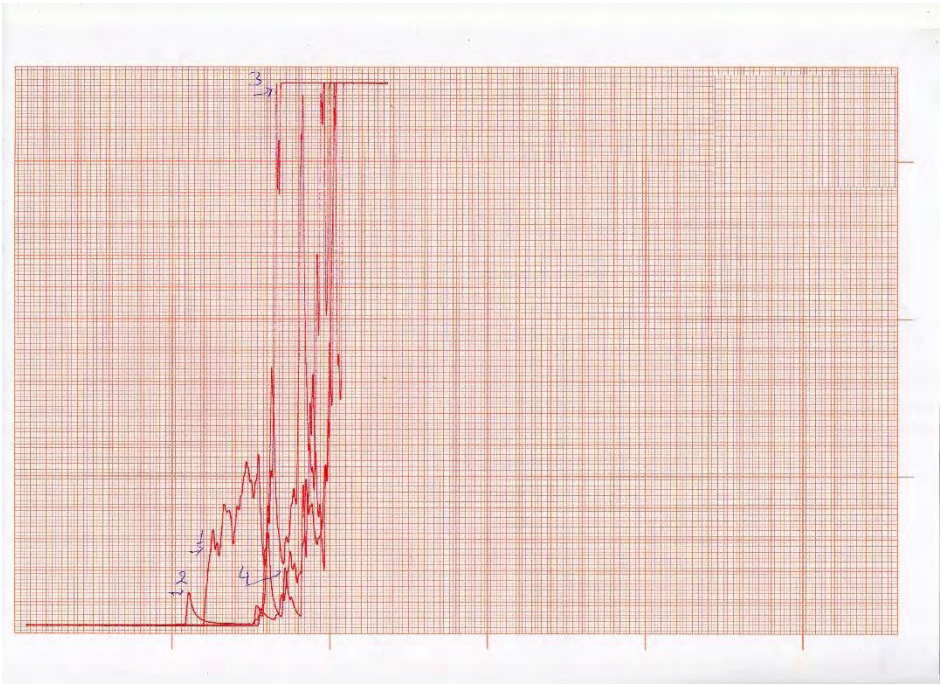

Fig. 86: Acoustic emission to load charts for tests no. 1-4

F: Sample 9153

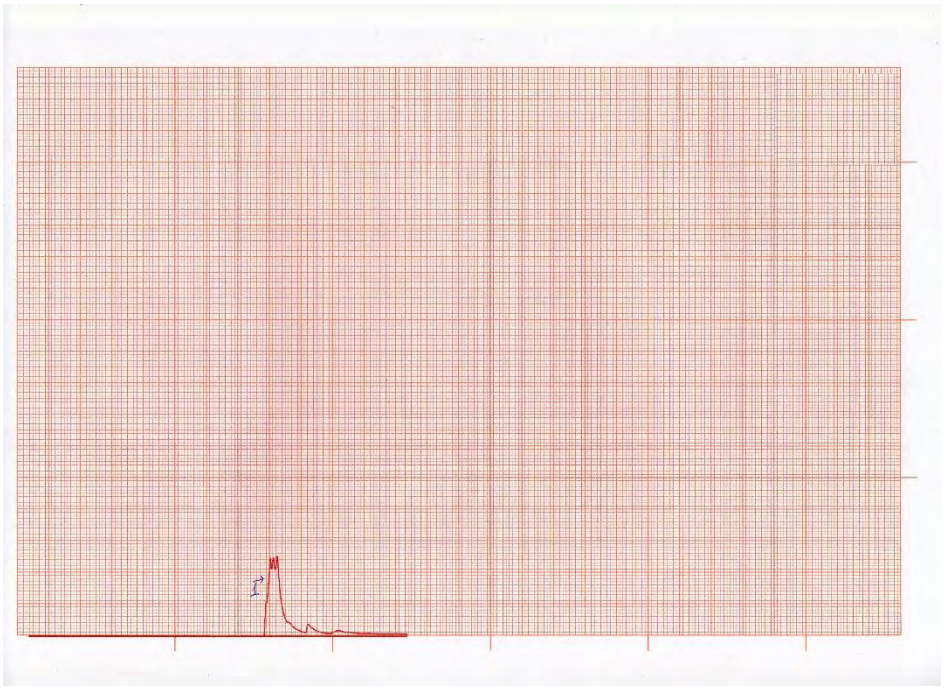

Fig. 87: Acoustic emission to load chart for test no. 1

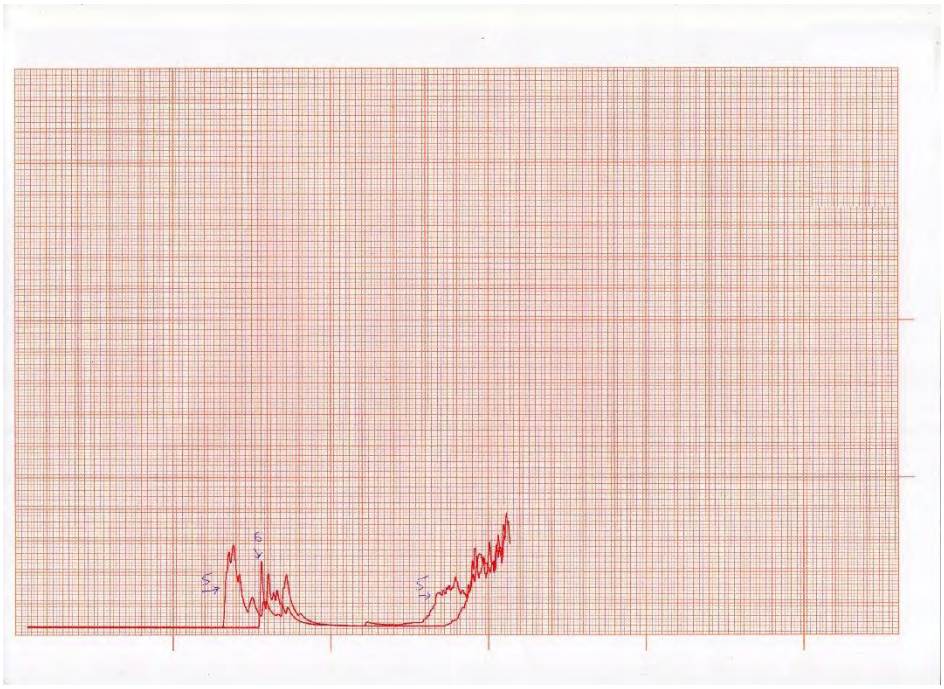

Fig. 88: Acoustic emission to load charts for tests no. 2,3

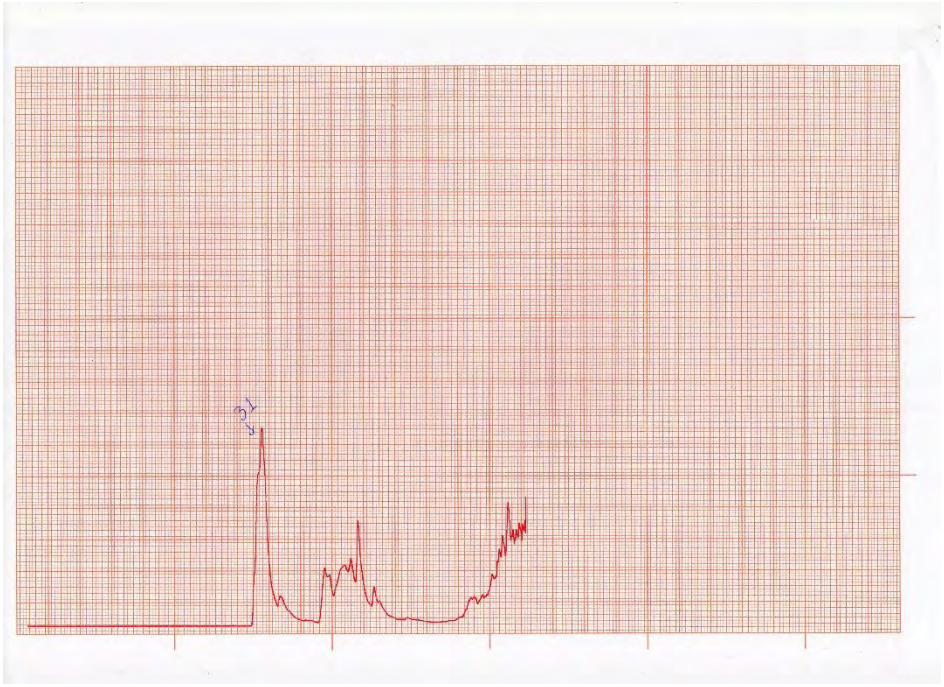

Fig. 89: Acoustic emission to load chart for test no. 4

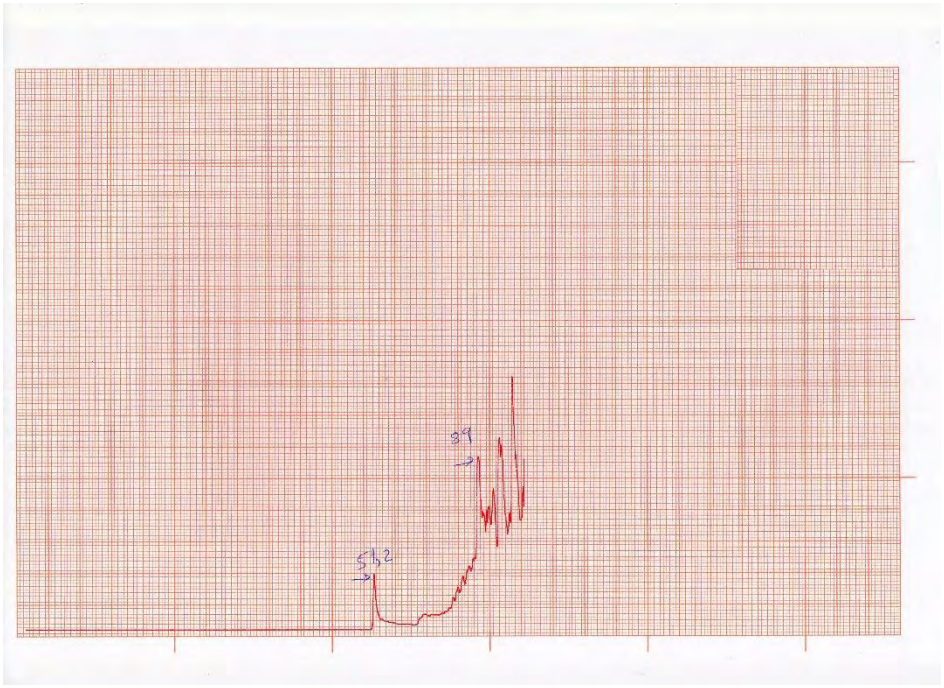

Fig. 90: Acoustic emission to load chart for test no. 5

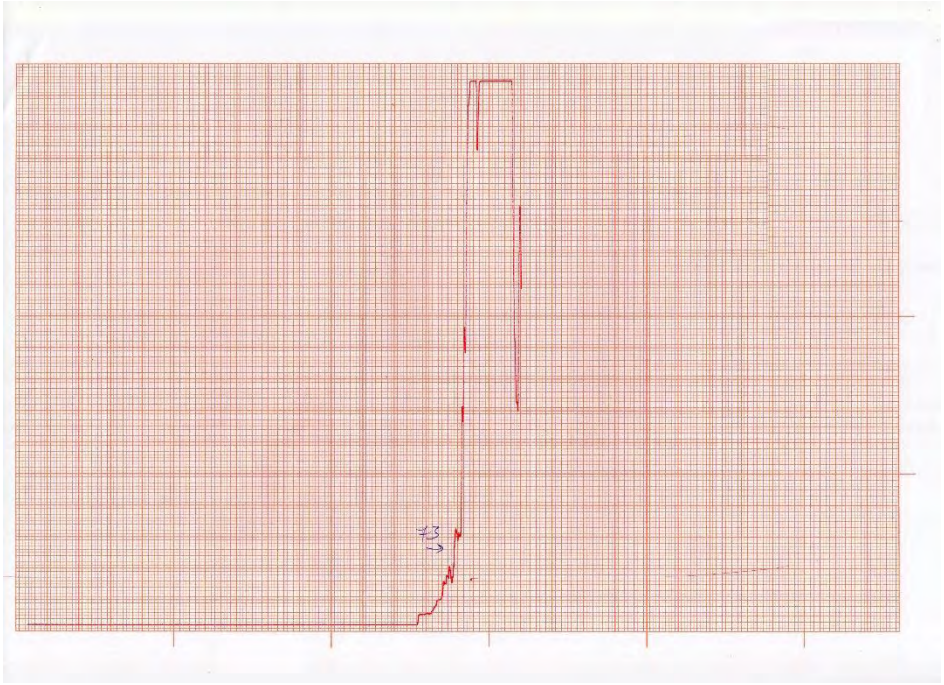

Fig. 91: Acoustic emission to load chart for test no. 6